Hydraulic performance of CoastaLock armour units

Auke Molenkamp

MSc thesis

TU Delft

ECONCRETE

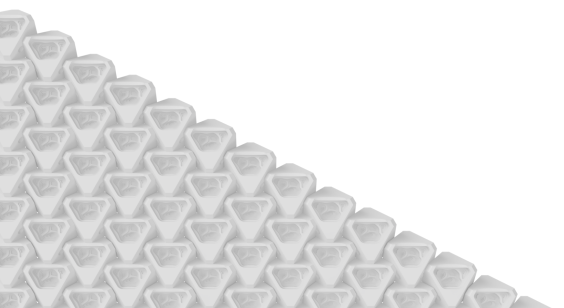

Hydraulic performance of CoastaLock armour units

by

Auke Molenkamp

to obtain the degree of Master of Science
at the Delft University of Technology,
to be defended publicly on Thursday, June 30th at 13:30.

Student number:	4548000	
Project duration:	October 1st, 2021 - June 30th, 2022	
Thesis committee:	Dr. ir. B. Hofland	TU Delft (chair)
	Ir. J. P. van den Bos	TU Delft
	Prof. dr. ir. M.R.A. van Gent	TU Delft
	J. Gutiérrez Martínez, MSc	ECOncrete Tech Ltd.

A digital version of this thesis is available via `repository.tudelft.nl`.

TU Delft

ECONCRETE

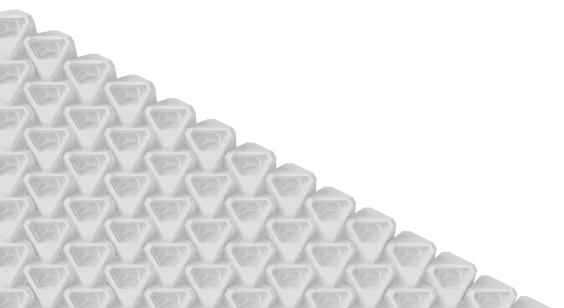

Preface

Before you lies the MSc thesis "Hydraulic performance of CoastaLock armour units", an exploratory research into the behaviour of a revetment constructed with the newly designed CoastaLock blocks. What started very small in a first meeting with a single supervisor and an introduction to ECOncrete as a company, ended up taking 9 months of planning, testing, analysing and writing, as well as almost 700 hand made armour units, to turn into the thesis that lies before you today. It is a thesis with which I finalise my six years as a student at the TU Delft, and of which I am very proud. I am now able to look back on a project that was challenging, educational and above all extremely interesting. There are a few people that made this project possible, and I would like to use this preface to thank them.

First of all, I would like to thank Bas Hofland, Jorge Gutiérrez Martínez and Jeroen van den Bos for their support, guidance and encouragement during the entire duration of this project. The diversity in backgrounds and perspectives of this committee meant that every member truly added a lot of value to the team. I would also like to extend my thanks to Marcel van Gent for joining the team last minute, ensuring an objective quality control of this thesis and for giving me some valuable advice.

I would like to extend a special thank you to the ECOncrete team for hiring me to conduct this research in the first place. More importantly though, Jorge, Ido, Maor, Andrew, Adi, Noa, Michal, Lior and Zeldy were always there to answer my questions, arrange technicalities or update designs whenever I needed. The ECOncrete team clearly went out of their way to support this research, for which I am very grateful.

I also want to express my gratitude towards Pieter, Chantal, Arie and Arno for facilitating the tests in the laboratory of the TU Delft, and helping me to equipment and repairs whenever the situation required those. You were a delight to work with and definitely made my days in the lab better.

I would like to end this acknowledgement with a thank you to all my friends and family who have supported and motivated me throughout my studies. This thank you concerns both my parents in particular, who supported me in every way they could and more. And finally, a big thank you Annick, who showed great patience over the last 9 months, as well as great skill in the (sometimes tedious) construction process of 700 CoastaLock units.

I hope you enjoy your reading.

Auke Molenkamp
Delft, June 23, 2022

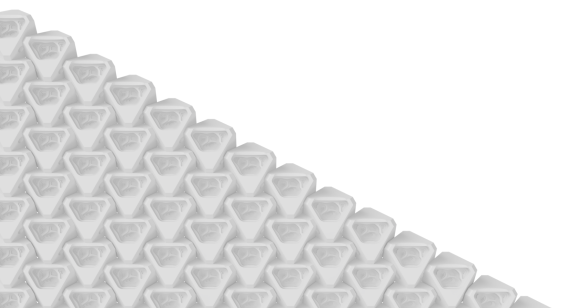

Summary

Due to advancing urbanisation and coastal populations, shorelines are becoming increasingly armoured and modified, often with damage to or the complete destruction of shallow water marine habitats. ECOncrete Tech Ltd believes that coastal-marine infrastructure (CMI) can be a viable habitat for marine life to thrive in, and they have developed multiple products that can be used in eco-friendly coastal structures. One of these products is the newly developed CoastaLock armour unit, on which this thesis is based. This research uses a literature study followed by physical model tests to answer the following research question:

What is the hydraulic performance with respect to stability, overtopping and wave reflection of CoastaLock armour on a deep water impermeable slope?

The literature study identifies the standard failure modes of a breakwater, and discovers that the mechanism of uplift is of particular interest when looking at interlocking placed block revetments. Uplift is an upwards force from under the armour layer, and is caused by large hydraulic pressure differences over the top layer of the structure. A measure for resistance over this top layer is the leakage length, which describes a fictional length of the path the water in the under layer has to travel in order to come out of the top layer.

Next to the uplift mechanism, a new failure mechanism for interlocking placed block revetments was also discovered with the literature study. Described by Van den Berg et al. (2020) during tests on the XblocPlus armour units, micro and macro-irregularities in the under layer were identified to have a significant destabilising effect on interlocking placed block revetments.

Consecutively, twenty-four different tests on a slope with a CoastaLock revetment were held in the wave flume of the Hydraulic Engineering Laboratory at the Delft University of Technology. These tests took place with different wave conditions, CoastaLock armour orientations, armour spacings and under layer thicknesses. From these tests, the coefficient of reflection, overtopping discharge and stability of the CoastaLock units were measured in order to answer the main research question.

One of the most important conclusions is that CoastaLock units are insufficiently stable compared to other units used in practice today when the total surface area of the under layer not covered by CoastaLock units (armour spacing) is smaller than 10%. When spacings of 10% or larger are applied, the CoastaLock units become stable on a level that matches or potentially exceeds that of other armour units.

Another important conclusion is that a mechanism that is seen across different types of placed block revetments, called breathing, should be defined as a failure mode. During breathing of the armour layer, the pressure differences over the top layer during wave run down are not large enough to break the chain of interlocking units, but they are large enough to lift the entire top layer off the slope. This cyclic motion of lifting up during wave run down and coming down during wave impact is the potential cause for a lot of damage on the under layer and armour units themselves. On top of that, the breathing motion of the top layer has been shown to cause the under layer to slide down and form a concave S-shape profile in the under layer, which is defined failure by Van den Berg et al. (2020). Deformations in the under layer should be prevented at all costs, as repair to the under layer requires complete removal of the interlocking armour layer. For these reasons this thesis advocates for the breathing mechanism to be designated as a failure mechanism.

The coefficient of reflection for CoastaLock armour is shown to be primarily dependent on wave steepness and secondarily on armour spacing. For wave steepnesses between 1.5% and 4.5%, the reflection coefficient drops from just under 0.8 to just under 0.5. For armour spacings with a constant wave steepness, the reflection coefficient goes from approximately 0.57 to just under 0.5. An equation is derived to describe this behaviour and compared to extra physical model tests.

The overtopping discharge of CoastaLock armour is shown to be mainly dependent on armour spacing. For spacings below 10%, failure of the layer occurred before the wave heights in the tests were large enough to induce significant overtopping. For spacings of 10% and higher, larger wave heights could be reached and therefore meaningful overtopping measurements could be made. The roughness factor γ_f is derived using the EurOtop (2018). The roughness factor is shown to be 0.732 for a spacing of 10%, and is reduced to 0.61 for a 25% spacing.

Furthermore, CoastaLock is a new concrete armour unit, with previously unknown hydraulic behaviour. The research for this thesis consists of the first physical model tests done on the CoastaLock units and therefore aims to gather many different data sets on different parameters, in order to give a first indication on the general behaviour of CoastaLock armour units. The results and conclusions should therefore be interpreted as an indication of the behaviour of the units, rather than a definitive description thereof.

Finally, the ecological CoastaLock armour units seem to have great potential to match or exceed the hydraulic performance of current armour units, once the porosity issue of CoastaLock at full packing is addressed. Fortunately, multiple people from the ECOncrete team have already expressed their views on improvements on the CoastaLock armour units. It is therefore recommended to update the design of the units, investigate the ecological and economical feasibility of these blocks and continue the research and development on CoastaLock units. Before the armour units are implemented, more physical model tests in different conditions (e.g. shallow water, permeable core, on a breakwater with a berm or toe) are required, as well as some 3D physical model tests focusing on more complex scenarios.

Contents

List of Tables

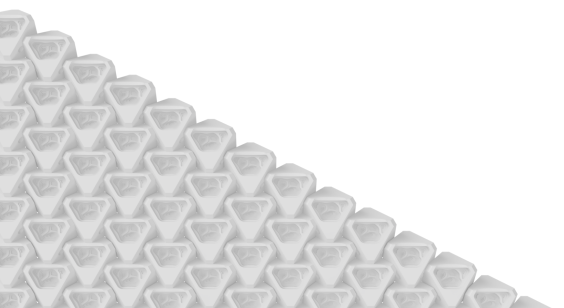

List of Figures

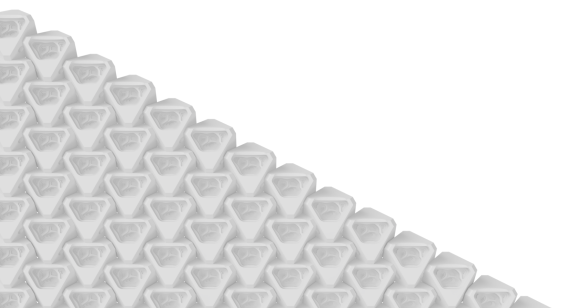

List of Symbols

Greek alphabet

Symbol	Description	Unit
α	Slope angle of a breakwater	degrees
α_R	Angle between simplified sets of blocks	degrees
β	Angle between a simplified set of blocks and the slope	degrees
γ_β	Influence factor for oblique wave attack	-
γ^τ	JONSWAP peak enhancement factor	-
γ_b	Influence factor for a berm	-
γ_f	Roughness factor for elements on a slope	-
$\gamma_{f,CL}$	Roughness factor for CoastaLock elements on a slope	-
γ_v	Influence factor for a wall at the end of the slope	-
γ^*	Geometric influence factor for wall, bullnose and promenade influences	-
Δ	Relative density, defined as $\Delta = \frac{\rho_{cl}-\rho_w}{\rho_w}$	-
Δp	Hydrostatic pressure difference over the layer	N
Λ	Leakage length	m
λ	Dimensionless scale factor between prototype and model	-
μ	Dinamic viscosity of water	Pa·s
ν	Kinematic viscosity	m^2/s
ξ	Irbarren breaking parameter	-
ρ	Mass density	-
ρ_{cl}	CoastaLock concrete density	kg/m^3
ρ_s	Density of sand particles	kg/m^3
ρ_{sw}	Density of salt water	kg/m^3
ρ_w	Density of fresh water	kg/m^3
σ	Standard deviation of a dataset	Unit of dataset
σ_s	Surface tension	N/m
ϕ_F	Water pressure under the armour layer	m
ϕ_T	Water pressure on top of the armour layer	m

Latin alphabet

Symbol	Description	Unit
A	Surface area	m^2
A_b	Cross-sectional area of an block	m^2
B	Crest width of a breakwater	m
b_f	Thickness of the filter layer	m
C_D	Drag coefficient	-
C_I	Inertia coefficient	-
C_L	Lift coefficient	-
C_a	Forchheimer viscosity coefficient	-
C_b	Forchheimer drag coefficient	-
C_c	Forchheimer inertia coefficient	-
C_r	General coefficient of reflection	-
$C_{r,CoastaLock}$	Coefficient of reflection for CoastaLock	-
$C_{r,M}$	Coefficient of reflection according to Muttray et al. (2006)	-
D	Thickness of the top layer	m
D_n or d_n	Nominal diameter of a block, defined as $D_n = \sqrt[3]{V_b}$	m
D_{under}	Thickness of the under layer	m
d	Height of a breakwater relative to the seabed	m
E	Elasticity	N/m^2
F_I	Inertia force on an object	N
F_L	Lift force on an object	N
F_d	Drag force on an object	N
F_f	Force as a result of internal flow	N
F_h	Horizontal forces on an object	N
F_p	Force as a result of internal pressure differences	N
F_v	Vertical forces on an object	N
g	Gravitational acceleration, constant. 9.81	m/s^2
H	Wave height	m
H_0	Deep water wave height	m
$H_{0,crit}$	Critical breaking wave height in deep water	m
H_i	Wave heights from a data set where the wave heights are ranked highest to lowest	-
$H_{m,0}$	Spectral significant wave height	-
H_{max}	Maximum wave height	m
H_s	Significant wave height	m
$H_{s,cr}$	Critical significant wave height	m
h	Total water depth	m
h_t	Water depth above the toe	m
i	Hydraulic pressure gradient	-
k	Permeability of a medium	m/s
k_f	Permeability of the filter layer or subsoil	m/s
k'	Permeability of the top layer	m/s
L	Characteristic length of a flow	m
L_0	Deep water wave length	m

Latin alphabet (continued)

Symbol	Description	Unit
L_1	Length of first schematised block	m
L_2	Length of second schematised block	m
L_e	Characteristic length of external load, (e.g. length of the wave front)	m
L_m	Length dimension of the model	m
L_p	Length dimension of the prototype	m
M	Rotational forces on an object	Nm
m_0	Zero moment of a wave spectrum	-
N	Number of individual wave heights	-
N_s	Stability number	-
$N_{s,c}$	Critical stability number, right before failing	-
$N_{s,r}$	Rocking stability number, right before the start of rocking	-
n	Porosity of core material	-
P	Empirical permeability of armour layer	-
p	Pressure	N/m^2
q	Overtopping discharge	l/s/m
Re	Reynolds number	-
R_c	Crest height of a breakwater	m
S	Spacing of CoastaLock concrete armour units	-
s	Individual wave steepness	-
T	Wave period	s
T_p or $T_{p,0}$	Peak wave period corresponding to the significant wave height	-
t	Time	s
t_a	Armour layer thickness	m
t_f	Thickness of the filter layer	
t_u	Thickness of the under layer	
U	Characteristic velocity of a flow	m/s
V_b	Volume of a block	m^3
v	Flow velocity	m/s
v_f	Filter velocity	m/s
x	Distance inside the armour or filter layers	m
x_{ij}	Horizontal distance from wave gauge i to wave gauge j	m
z	Depth of wave gauge below the still water line	cm

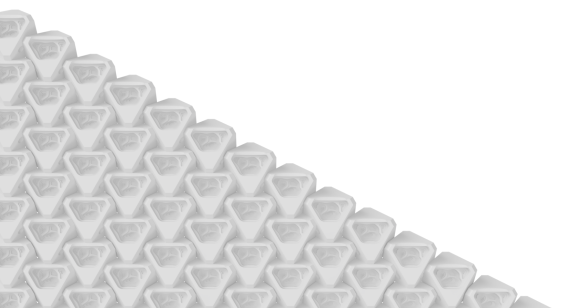

Chapter 1

Introduction

With increasing urbanisation over the last decades to a century, also comes an increase in the population of coastal cities, towns and settlements (Oxford University, 2018). According to Creel (2003), nearly two-thirds of the human population now lives in coastal areas. What also comes with this development is that shorelines are increasingly altered and armoured. This often leads to a partial or complete destruction of the natural shoreline, which is regarded to be the primary cause for the loss of shallow water habitats (Airoildi and Beck, 2007; Bulleri and Chapman, 2010). Israeli engineering company ECOncrete is now trying to change that trend by introducing a new concrete material that is not only CO_2 negative over its lifetime, but also boosts the biodiversity and water quality (Perkol-Finkel and Sella, 2014, 2015). Products of ECOncrete include nature-friendly quay walls, pile encasement, bottom protection and tidal pool additions to rip-rap rock armour. Now, they have come up with a new nature friendly armour unit, the CoastaLock, for the use on breakwaters, dykes or other slopes that require protection against incoming waves.

1.1 Revetments

A revetment is the protection layer applied to a man-made coastal defence, such as breakwaters, dykes, or any other man-made slopes in coastal zones. Nowadays, revetments are constructed with a series of different techniques, such as a grass or tarmac layer, a rubble mound slope with big natural rocks, artificial armour units like the Xbloc or Tetrapod, or placed block revetments like Basalton or XblocPlus blocks. ECOncrete's CoastaLock is a single-layer regularly placed armour unit, and belongs in the same category as XblocPlus. More theoretical information on these types can be found in Chapter 2.

1.2 CoastaLock

ECOncrete's CoastaLock armour units are specifically designed for use on breakwater or other shoreline protection systems, whilst pursuing ECOncrete's goals of enhancing the natural environment as well. CoastaLock is an octahedral block (see Figure 1.1) with a cavity that serves different ecological purposes depending on the orientation of the block. According to ECOncrete Tech Ltd. (2021), the blocks, when rotated "can create unique habitats such as water retaining tide pools, caves, and overhangs, providing niches critical to diverse marine species."

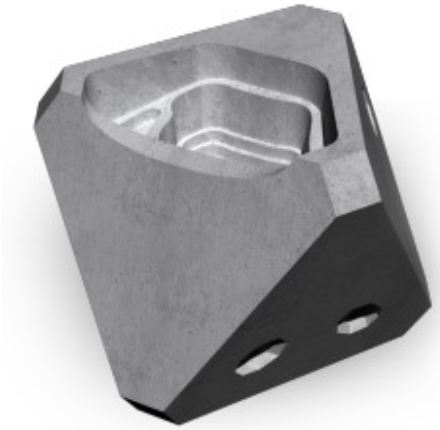

Figure 1.1: Artist's impression of the CoastaLock block (ECOncrete Tech Ltd., 2021).

The octahedral shape allows for stability, durability, easy placement and interlocking with other units. CoastaLock units are usually cast on site in steel CoastaLock moulds, improving their environmental efficiency. A pilot with CoastaLock units in San Diego is currently underway (Port of San Diego, 2021), and earlier experiments with ECOncrete's Admix (Perkol-Finkel and Sella, 2014, 2015, 2019) show promising results for enhancing marine life around these new blocks. However, a lot of knowledge on the hydraulic performance of these blocks is still missing.

1.3 Physical modelling

One way to determine the hydraulic performance of any armour unit, is to use computational fluid mechanics, which means using numerical models to solve for the flow conditions around the unit. However, calculating the behaviour of every single water particle around an armour unit requires enormous amounts of computing power, and for a proper representation of the real situation multiple units need to be involved. A supercomputer would take months or even years to solve this problem, or many simplifications need to be introduced to reduce the computing time of the model. On top of that, many assumptions need to be made on the boundary conditions of the model, making the model unreliable.

In hydraulic engineering, it is therefore very common to use physical scale models in order to determine these hydraulic specifications of the unit. Physical modelling requires no simplifications or assumptions and is much quicker and cheaper than using a super-computer with a numerical model. Also, numerical models require physical data to be calibrated and verified, so therefore directly using physical modelling is often the answer.

1.4 Problem definition

As stated in Section 1.2, the ecological properties of ECOncrete's Admix have been extensively tried and tested, not only on CoastaLock blocks but also on other armour blocks and pile reinforcements (Perkol-Finkel and Sella, 2015), quay walls (Perkol-Finkel and Sella, 2019) and tiles (Perkol-Finkel and Sella, 2014). However, little is known about the hydraulic properties of the CoastaLock armouring. An extra complicating factor for the CoastaLock blocks is the presence of the cavity, which could influence the hydraulic properties of the block depending on its orientation.

1.5 Scope

Due to this new and innovative design, there are many hydraulic aspects of the CoastaLock block to be researched and defined, but due to time limitations the scope of this thesis has to be limited to the most important hydraulic parameters of CoastaLock. Together with ECOncrete's Global Head of Engineering, Mr Gutiérrez Martínez, three parameters have been defined for this research. These are the stability, reflection and overtopping of CoastaLock armour units, for different wave steepnesses, block spacings, under layer thicknesses and block orientations. The primary focus is laid on the stability of the units. A detailed overview of the tests can be found in Chapter 4.

1.6 Objective

In other words, the main objective of this thesis is to determine some hydraulic properties of a CoastaLock armour layer. The main research question is therefore:

> What is the hydraulic performance with respect to stability, overtopping and wave reflection of CoastaLock armour on a deep water impermeable slope?

In order to be able to answer this main research question, the following sub-questions need to be answered first:

1. What are the failure mechanisms of CoastaLock concrete armour units on a deep water impermeable slope, and when do they occur?
2. What is the influence of wave steepness, block spacing, under layer thickness and block orientation on the stability of CoastaLock units?
3. What is the influence of wave steepness, block spacing, under layer thickness and block orientation on the wave reflection of CoastaLock units?
4. What is the influence of wave steepness, block spacing, under layer thickness and block orientation on the overtopping of CoastaLock units?

1.7 Approach

The research on the performance of the CoastaLock blocks is done through a combination of literature studies and physical modelling. Firstly, the former, as it provides the theory required for answering the research questions, as well as the basis needed for the understanding of the behaviour of CoastaLock and the physical model tests. Physical model tests are done due to their many advantages as described in Section 1.3, and due to the fact that very little input values for a numerical model, such as drag and lift coefficients of CoastaLock, are known. For this physical model test, the 2D wave flume in the Hydraulic Engineering laboratory of the Delft University of Technology is used. The physical model test consists of multiple test runs with different wave heights, steepnesses, block spacings and CoastaLock orientations, which are elaborated on in Chapter 4.

The physical model test takes place on an impermeable slope in deep water, as this provides solid results for many basic structures, like shoreline slopes, dikes and impermeable breakwaters. Some theory behind slopes and revetments can be found in Chapter 2 and Appendix A.

1.8 Reading guide

This thesis aims to answer the research questions, firstly by introducing the main elements in Chapter 1, after which a more in-depth theoretical overview with the required knowledge for this research follows in Chapter 2. Then, the set-up of the physical model is described in Chapter 3, before the testing process itself is outlined in Chapter 4. The data processing method is then elaborated on in Chapter 5. After that, Chapter 6 reports and analyses the results. From this, a conclusion is drawn in Chapter 8, preceded by a discussion in Chapter 7 and followed by a recommendation in Chapter 9.

Chapter 2

Theoretical framework

In order to understand the physical processes that are described in this thesis, some background knowledge is required. This chapter contains some information on stability, reflection, and overtopping and defines failure mechanisms for breakwaters and revetments. For more extensive theoretical background information on revetments and/or breakwaters, please refer to Appendix A. A theoretical basis on waves can be found in Appendix B, and the JONSWAP spectrum is described in Appendix C. Some background information on scaling effects is provided in Appendix D.

2.1 Introduction to revetments and breakwaters

Breakwaters are structures protecting ports, coasts, land reclamations or any other type of coasts or coastal activities from the harsh environment of the sea. A revetment forms an integral part of any breakwater, consisting of an armour, under and filter layer, being the first line of defense of the breakwater for the incoming wave attack.

2.1.1 Revetment types

Revetments for mound breakwaters can be classified into three different types. Firstly, rubble mound armour. Rubble mound armour consists of large randomly placed armour units or large natural rocks and and are usually thick and very permeable. Placed block revetments are mostly regularly placed and traditionally consist of thinner layers of concrete armour units when compared to rubble mound layers, but are also less permeable. Single-layer placed block revetments with interlocking concrete armour are among some of the most used revetments in modern breakwaters, as they offer significant technical and economical advantages compared to other armour types (Reedijk and Muttray, 2009). Impervious revetments are completely impermeable and normally come with an asphalt or concrete top layer. The permeability and shape of the units determine their response to wave attack and the leakage length of the top layer. This will be elaborated on in Section 2.3.2. Examples of three different revetment types are shown in Figure 2.1.

(a) Rubble mound armour with Xbloc (Allaway, 2011).

(b) Placed block revetment with Shed concrete armour (Reedijk and Muttray, 2009).

(c) Impervious asphalt revetment (Rijkswaterstaat, 2019).

Figure 2.1: Examples of different types of revetments.

2.2 Armour stability

The armour layer is crucial in protecting the breakwater core and filter material from the wave attack, and takes the largest impacts. But, if the armour layer itself is not stable, blocks might get damaged, displaced or completely washed away.

2.2.1 Stability number

The stability of a block is defined with its stability number, as shown in Equation (2.1) (Van den Bos and Verhagen, 2018). Please refer to the List of Symbols for the definition of the symbols.

$$N_s = \frac{H_s}{\Delta \cdot D_n} \tag{2.1}$$

So in words, the stability of an armour unit depends on the relation between the significant wave height on the one side, and the relative density of the block to the water and the size of the block on the other side. In this thesis, two stability numbers will be researched. The first, the critical stability number $N_{s,c}$, is the stability number of the block right before failing. The second, the rocking stability number $N_{s,r}$, is the stability number of the armour units once they start rocking.

2.2.2 Failure mechanisms

In order to understand the stability and behaviour of breakwaters, their failure modes need to be identified. Burcharth (1997) defined a number of these for a standard breakwater, which are shown in Figure 2.2, and briefly described below. Two other failure mechanisms that are specifically related to breakwater armour and that are not described by Burcharth (1997), settlement and extraction of armour units, are also elaborated on in this section. The failure mechanism of overtopping is treated seperately in Section 2.6.

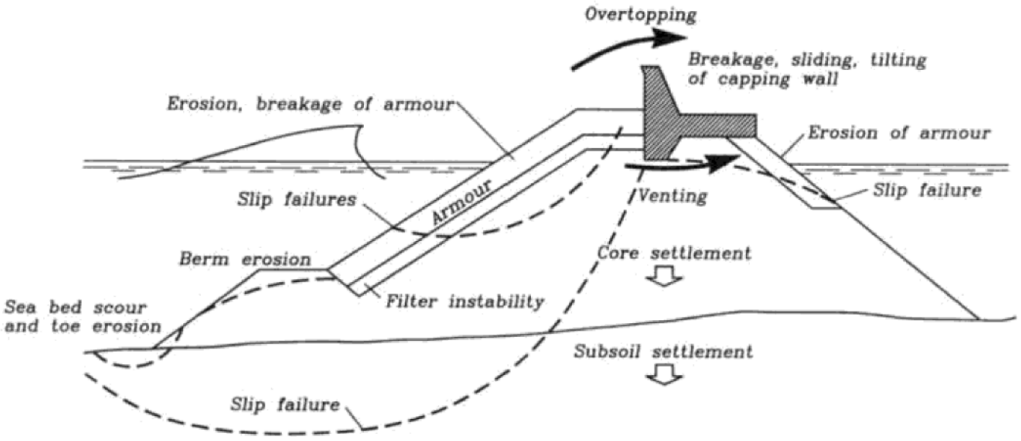

Figure 2.2: Failure modes of a breakwater with toe and overtopping wall, as described by Burcharth (1997).

Geotechnical failures

Some of the failure mechanisms described by Burcharth (1997), are slip failures and settlements of the core material or the subsoil. These failures are geotechnical failures, and therefore usually slow failures that are not caused by wave loading. Settlements are usually caused by weak compressible subsoils like clay or peat or due to liquefaction of the subsoil as a result of extreme loads such as an earthquake. Settlement of the core material or the subsoil does not immediately need to be classified as a failure, as some settlement can be accounted for in the design. However, once settlements become so large that it leads to deformation of the breakwater or other failure modes to occur, it becomes a failure mechanism itself.

Slip failures usually occur due to a lack of cohesion in the core or subsoil material, and will cause a large part of the breakwater to slide down in a circular motion, along the so-called slip circle. Geotechnical failures can usually be predicted, calculated and therefore accounted for in the design phase through programmes similar to GSTABL or Plaxis (Van Alboom et al., 2018) or D-Settlement and D-Geo stability by Deltares.

Erosion inner slope

Another failure mechanism as described by Burcharth is the erosion of the inner slope of a breakwater. This is mainly dependent on excess overtopping and the material of the rear slope. Van der Meer et al. (2010) found that the rear slope of reinforced grass dikes can stay damage free up to overtopping volumes of 75 l/s/m, and Elastocoast rear slopes up to 125 l/s/m, whereas clay rear slopes could only sustain a maximum of 10 l/s/m (Van der Meer et al., 2010).

Venting

Venting is a mechanism that often occurs in very permeable filters simultaneously with heavy overtopping. It can lead to erosion of the layers under a crown wall, destabilising it. Burcharth (1987) also described venting to cause sand blowouts and sinkholes in a land reclamation behind the Tripoli breakwater in Lybia. According to the same paper, venting cannot be studied in physical model tests due to scale effects (Burcharth, 1987).

Toe erosion and scour

Both scour and erosion are failure modes that occur on the seaward side of the breakwater near the bed. Scour is the erosion of the seabed in front of the toe (potentially leading to toe instabilities), whereas toe erosion is the erosion of the toe itself. These mechanisms may cause the toe of the breakwater to lose its function of supporting the armour and filter materials, resulting in them sliding down and exposing the breakwater. "The key mechanism of scour is the steady streaming in the vertical plane caused by the action of partially standing waves in front of the breakwater" (Sumer and Fredsøe, 2000) and such wave conditions should therefore be accounted for in the design of the breakwater.

Crown element damage or displacement

Another possible failure method is the displacement or damage of crown elements. In breakwaters with an overtopping wall, as illustrated in Figure 2.2, this wall may become damaged or fully removed, reducing the effectiveness of the breakwater.

However, this failure mechanism can also occur in breakwaters with regular crown elements, rather than overtopping walls, as these top elements can also be damaged and washed away. The reason that this is also considered a separate failure mechanism for breakwaters without overtopping walls, is that the underlying principles for failure are different compared to those belonging to the extraction of a unit.

Crown element displacement is mostly caused by the forces induced on the block by wave run up, rather than the wave impact or pressure differences themselves. Therefore, the destabilising forces on the crest elements are more directed parallel to the slope than with other elements in the layer and displacement of the units is also more often in parallel direction to the slope. Also, crest elements in revetments are normally the weakest, as these elements are not stabilised by the weight and interlocking effects from higher rows. Sometimes the design crest elements even needs to be adapted to fit the requirements, as was done for the XblocPlus by Ruwiel (2020). It is for these reasons that the failure of crest elements needs to be regarded separately.

2.2.3 Armour layer failures

The armour layer itself can fail in multiple ways. Figure 2.2 lists 'erosion, breakage of armour' as a failure mechanism of a mound breakwater, but this is a relatively general term. Depending on the type of revetment, multiple failure mechanisms of the armour layer can occur. Some of these are elaborated on in this section.

Rocking

Armour units themselves can be damaged. This erosion or complete breaking of the unit is usually caused by rocking of the units and is seen in rubble mound armour layers. Under rocking, the unit moves only briefly and then returns to its original position, often in a repetitive pattern. This process, or other minor movements in and of itself are not necessarily considered to be failure of the structure (Kamali and Hashim, 2009). However, if extensive rocking takes place, units might break into multiple pieces and rocking can then be classified as a reason for potential damage (Yagci and Kapdasli, 2003). The breakage of armour units in scale model tests is not representative for the real situation, though, as the strength of the concrete cannot be scaled (CIRIA, CUR and CETMEF, 2007). Therefore it is important to identify rocking in scale model tests, as this might indicate breaking of the units on the final prototype.

Extraction of armour units

Armour units can also fail by being extracted from the armour layer, as is described by Vieira et al. (2020) and Garcia et al. (2013). This can happen for any type of armour layer, but for single layer revetments, this can be considered as failure of the entire layer, as the under layer is exposed and therefore in danger of being eroded away. For interlocking or friction-based revetments, it also means that a part of the stabilising effect is lost, with the danger of greater damage to the breakwater. Block displacement is caused by disturbing the balance between the vertical, horizontal and rotational forces on the block, either due to excess pressure in the under layer or due to wave impact. For more information on forces acting on armour units, please refer to Appendix A.3.

Armour settlement

Settlements in the armour layer can also occur, as is shown by Vieira et al. (2020), Van Gent and Van der Werf (2017) and Garcia et al. (2013). This sliding down of individual blocks can change the packing density of armour units on the slope. After sliding down, the low packing density of armour units on the top of the slope can significantly reduce stability if it comes below recommended values (Medina et al., 2014), and potentially even expose the core of the structure. Also, packing densities that are too large reduce the porosity of the layer and increase the leakage length through the armour layer, which reduces the stability of the layer (Pilarczyk, 2003).

Armour layer sliding

For steep slopes with tightly packed revetments, sliding of the entire armour layer over the filter layer is possible too (Bosch et al., 2002). On these slopes, due to their inclination, the along slope gravitational component is much larger than the gravitational component perpendicular to the slope. As a result of this, the along slope pull is large and the friction between the two layers is small. During wave down rush, the retracting flow can exert downward drag forces parallel to the slope on the armour layer, causing it to slide down if not properly supported with a toe construction. Once sliding of a large part of the armour layer occurs, it loses its structural integrity and may expose the breakwater core.

2.3 Leakage length and its effects on stability

What has not been considered in the theory on failure mechanisms in Section 2.2.2, is the different armour types that are used on breakwaters, specifically rubble mound armour and placed block revetments. Both may exhibit the same damage mechanisms as discussed in Section 2.2.2, but the underlying principles for failure modes such as erosion or breakage of armour, extraction of armour units or armour settlement might be different.

This will be elaborated on in this section by introducing the concept of leakage length first and then highlighting the differences between rubble mound armour and placed block revetments.

2.3.1 Leakage length theory

The principle of leakage length, and how it can be calculated, is explained in detail by Pilarczyk and Klein Breteler (1998) and Pilarczyk (2003). In short, the leakage length factor is a factor that contains "nearly all physical parameters that are relevant to the stability" of revetments on filter layers (Pilarczyk and Klein Breteler, 1998). It is an empirical factor that describes the resistance to the flow between two layers. The leakage length is the main factor that determines the magnitude of the hydrostatic pressure differences that cause the uplift mechanism as described in Section 2.3.2. The leakage length of a revetment on a filter can be described according to Equation (2.2) (Pilarczyk and Klein Breteler, 1998).

$$\Lambda = \sqrt{\frac{b_f \cdot D \cdot k_f}{k'}} \tag{2.2}$$

Pilarczyk (2003) subsequently describes the relation of the leakage length to the stability of armour on a filter in Equation (2.3).

$$\frac{H_{s,cr}}{\Delta \cdot D_n} = f \cdot (\frac{D}{\Lambda \cdot \xi})^{0.67} \tag{2.3}$$

With the following parameter ranges and limits (Pilarczyk, 2003):

- $\frac{D}{\Lambda} = 1$ for $\frac{D}{\Lambda} > 1$
- $\frac{D}{\Lambda} = 0.01$ for $\frac{D}{\Lambda} < 0.01$
- $5 < f < 15$, with:
  - $f = 5$ for static stability of loose blocks (no friction)
  - $f = 7.5$ for static stability of a system (friction between the blocks)
  - $f = 10$ for when movement of the units at design conditions is acceptable.

Moreover, it must be noted that Equation (2.3) is valid for placed block revetments where $0.01 < \frac{k'}{k_f} < 1$ and $0.1 < D/b_f < 10$. One of the conclusions that Pilarczyk draws from Equation (2.3) is that when the leakage length Λ is reduced by 30%, the critical significant wave height H_s is increased by 20%. This can be achieved by reducing the thickness of the filter layer by 50%, or by increasing the $\frac{k'}{k_f}$ ratio with a factor 2. Some methods for achieving the doubling of the $\frac{k'}{k_f}$ ratio include halving the grain size of the filter layer or increasing the absolute block spacing by 50% (Pilarczyk, 2003).

2.3.2 Leakage length effects by armour type

As stated in Section 2.3, different armour types have different underlying principles for the same failure modes, and these can be linked back to the concept of leakage length as described in Section 2.3.1.

When looking at rubble mound layers, it can be stated that the leakage length is very short compared to characteristic length of the external force, such as the length of the wave front. This condition, $\Lambda << L_e$, means that there is no head difference across the top layer of the revetment and that uprush and downflow velocities cause drag forces on individual stones (Schiereck and Verhagen, 2019).

On the contrary, impervious protections like asphalt where the leakage length is much larger than the characteristic length of the external force ($\Lambda >> L_e$) will see large head differences over the top layer and no drag effects, with a net lifting force as a result.

Placed block revetments, however, have a leakage length in the same order of magnitude as the characteristic length of the external load ($\Lambda \approx L_e$) and therefore neither the drag nor uplift mechanisms can be neglected according to Schiereck and Verhagen (2019). Nonetheless, as the drag forces during wave run-up and run-down are exerted parallel to the slope, they are less problematic for placed block revetments and may only cause some sliding (Pilarczyk, 2003).

The problematic mechanism for placed block revetments is that of uplift, which is shown in Figure 2.3. Uplift is caused by the large differences in hydraulic head that reach their maximum during maximum wave run-down. In other words, incoming and breaking waves will induce a high phreatic level in the filter, and then during the wave run-down the leakage length of the top layer is long enough to provide enough resistance to the outward directed flow to sustain the high phreatic level to a certain degree.

The maximum uplift pressure will occur when the head difference over the layer is the largest, which means that it will occur at the front of a wave during maximum wave run-down, as is shown in Figure 2.3b. When this uplift pressure is large enough to counter the stabilising forces on the blocks (gravity and friction, for example. See Appendix A.3.1 for more information), the units will move. This movement will then lead to either extraction, settlement, breakage or damage of the units.

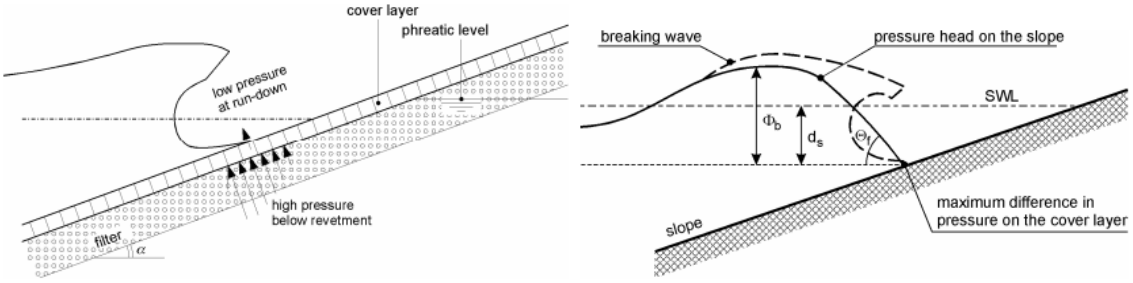

(a) Incoming wave (b) External pressure gradient

Figure 2.3: The uplift mechanism on a placed block revetment (Pilarczyk, 2003).

Run-up induced uplift

Klein Breteler et al. (2014) introduces a second phenomenon that induces uplift on block placed revetments, which is not described by Pilarczyk and Klein Breteler (1998) or Pilarczyk (2003). According to Klein Breteler et al. (2014), a secondary uplift pressure is generated during wave run-up due to irregularities in the armour positioning. This can occur when blocks are not placed correctly, or when they are already slightly displaced by other processes. This means that once other forces deform the armour layer or displace armour units enough in order for the run-up induced uplift to occur, it can significantly amplify the damage already done.

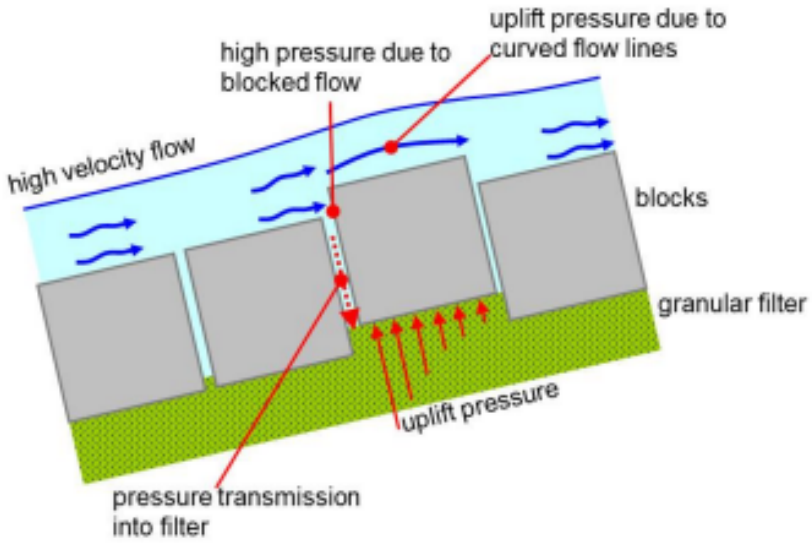

Figure 2.4: Run-up induced uplift mechanisms (Klein Breteler et al., 2014).

The secondary uplift pressure has two contributing factors, which are shown in Figure 2.4. The first being pressure transmission into the filter, as high velocity flow hits an armour unit and builds up pressure there. This pressure is then partially transmitted downwards into the filter. The second factor contributing to the run-up induced uplift pressure is the curvature of flow lines over the exposed block. For revetments that can usually withstand high parallel flow velocities, the uplift force associated with curved flow lines is significant. Curvature of flow lines over displaced blocks creates a drop in pressure over the block, sometimes even reducing the pressure to values below atmospheric pressure (Klein Breteler et al., 2014).

2.4 Under layer variations

On top of the theory of placed block revetments it must be noted that some of the most popular modern revetment types, those of single layer interlocking concrete armour units, are susceptible to irregularities in the under layer (Van den Berg et al., 2020). Van den Berg et al. researched and quantified this influence and concluded that micro-irregularities as shown in Figure 2.5a reduce the interlocking capabilities of concrete armour layers, but that these revetments also show maximum sensitivity for convex deformations of the slope in the cross-shore direction, such as shown in Figure 2.5b.

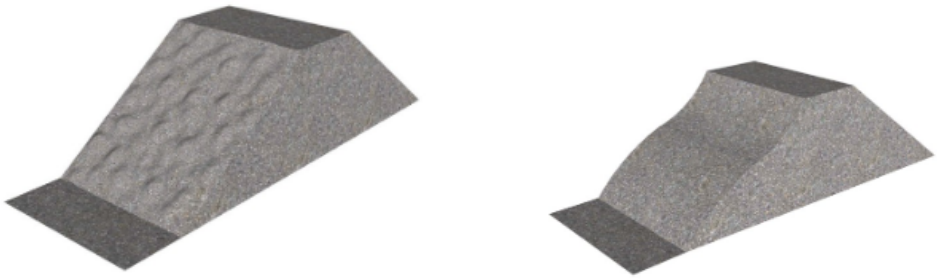

(a) Micro-irregularities (b) Concave S-profile

Figure 2.5: Impression of irregularities in the under layer of a revetment (Van den Berg et al., 2020).

2.4.1 New failure mechanism for interlocking armour units

The sensitivity of armour units to this concave S-profile was even so large, that Van den Berg et al. defined a new failure mechanism for the start of damage with interlocking armour units. This mechanism has not previously been observed or described, but "during wave run down the armour layer at this location is pushed outward by a combined effect of the weight of the upper armour and the hydraulic pressure of the remaining water under the top layer" (Van den Berg et al., 2020). This effect can then even be magnified by the change in steepness of the slope below the water line.

In their analysis, Van den Berg et al. derive Equation (2.4), which describes the expected stability number of the XblocPlus concrete armour units used in the tests as a function of micro and macro-irregularities in the under layer.

$$N_s = -0.1 \cdot (\alpha_R + \beta) + 5.7 \tag{2.4}$$

α_R and β depend on each other in a linear relation, which is quantified in Equation (2.5) (Van den Berg et al., 2020).

$$\alpha_R \approx \beta \cdot (1 + \frac{L_1}{L_2}) \tag{2.5}$$

An impression of these micro (angle between the blocks, α_R) and macro-irregularities (deviation of the block angle from the slope, β) is displayed in Figure 2.6.

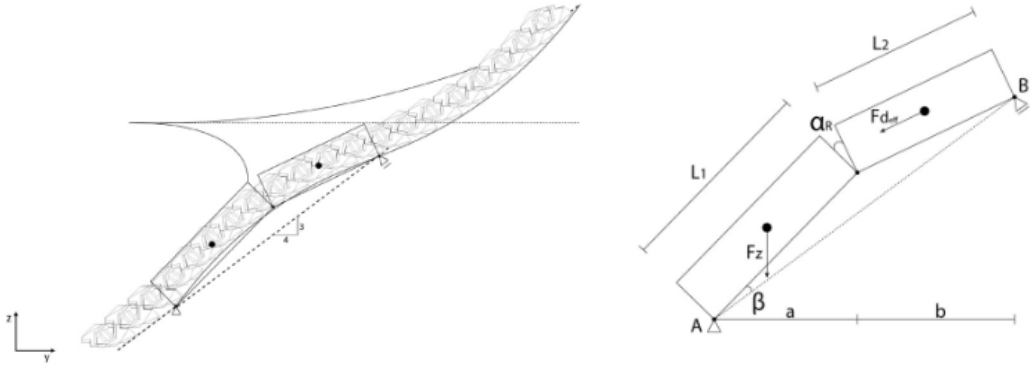

(a) Schematised S-profile (b) Simplified model

Figure 2.6: Schematisation of irregularities in the under layer for interlocking concrete armour units (Van den Berg et al., 2020).

To summarise, the theory behind this new failure mechanism is that once blocks are slightly displaced and $\beta > 0$, the leverage arm of stabilising force F_z around point A decreases, whereas the horizontal component of the effective force $F_{d,eff}$ of the second block in the simplified model will increase. At the same time, the interlocking capabilities of the armour layer are reduced, with all this making the situation less stable. It is for this reason that Van den Berg et al. (2020) classify these under layer deformations as a new failure mechanisms for single layer interlocking concrete armour units.

2.5 Wave reflection

The coefficient of reflection, C_r, is the parameter that describes the ratio between the square root of the incoming wave energy and square root of the outgoing wave energy after collision with a structure (Van der Meer, 1992). The coefficient of reflection contains multiple physical processes and is calculated by dividing the reflected significant wave height by the incident significant wave height at a structure. These significant wave heights can be derived by performing a spectral analysis and decomposition, as described in Section 5.2.3.

Muttray et al. (2006) summarise multiple methods and equations to predict the reflection coefficient. One of those is Equation (2.6) by Van der Meer (1992), which bases reflection on the permeability of the armour layer and a breaking parameter.

$$C_r = 0.07 \cdot (P^{-0.08} + \xi) \qquad \text{for:} P \geq 0.1 \tag{2.6}$$

This equation, however, has a relative standard deviation of 37%. It does also not consider the porosity of the armour layer, rather the permeability of the layers directly under the armour. It is, however, one of the only pieces of literature that considers reflection as a function of porosity. A more accurate method that does not include the porosity of a layer (with a mean error of 0.99 and relative standard deviation of 5%) is derived in Muttray et al. (2006). This equation is shown in Equation (2.7).

$$C_r = \frac{1}{1.3 + 3h\frac{2\cdot\pi}{L_0}} \tag{2.7}$$

However, Equation (2.7) does assume a porous rubble mound breakwater, whereas Equation (2.8), as taken from Muttray and Oumeraci (2003), has been derived for impermeable slopes.

$$\begin{aligned} C_r &= 1 - (\frac{H_0}{H_{0,crit}})^{3/2} \cdot (1 - \frac{2}{\pi}) && \text{for:} \quad \frac{H_0}{H_{0,crit}} < 1 \\ C_r &= \frac{2}{\pi} \cdot \frac{H_{0,crit}}{H_0} && \text{for:} \quad \frac{H_0}{H_{0,crit}} \geq 1 \end{aligned} \tag{2.8}$$

With:

$$H_{0,crit} = L_0 \cdot \sqrt{\frac{2 \cdot \alpha}{\pi}} \cdot \frac{\sin^2 \alpha}{\pi} \tag{2.9}$$

2.6 Overtopping

The overtopping parameter, defined in litres per metre per second (l/m/s), is a parameter that standardises the volume of water that comes over a hydraulic structure per unit of time and per unit of distance along the entire length of the structure. Failure due to overtopping is usually limited by objective demands, defined by the activities behind the breakwater. For example, the maximum allowable overtopping discharge for a breakwater where trained professionals work with water passing below knee levels, can be set to 10 l/m/s. When pedestrians are present on the breakwater, this limit is lowered to 0.1 l/m/s, and can even be reduced to 0.03 l/m/s if these pedestrians have no view of the incoming waves (Besley and Michel, 2009). However, too much overtopping can also damage the rear slope of a dyke or a breakwater itself, destabilising the structure as a whole.

All in all, the overtopping parameter is a parameter with significant impact on the performance and design of a revetment, but the maximum allowable overtopping varies with every revetment design and with every situation, and can therefore not be defined in physical model testing. Instead, all overtopping is measured and reported so that this can be taken into account in the design phase of a project. Consequently, an optimisation of the crest level can be carried out to create an economically efficient design that stays within the allowable overtopping limits.

2.6.1 Overtopping discharge calculation

The overtopping discharge calculation was described in a simplified form by Van der Meer and Bruce (2014) in Equation (2.10). It is derived from early Dutch research from the 1970s and consists of a Weibull-distribution with three parameters a, b and c that can be easily fitted to test data. According to Van der Meer and Bruce (2014), $c = 1.3$ and b is equal to 2.7 for breaking waves, and 1.5 for non-breaking waves. If this information is known, parameter a can then be fitted to the test data to give an indication of the roughness factor of the armour layer.

$$\frac{q}{\sqrt{g \cdot H_{m0}^3}} = a \cdot \exp\left(-(b\frac{R_c}{H_{m0}})^c\right) \qquad \text{for} \quad R_c \geq 0 \tag{2.10}$$

The problem with this approach, even tough it is simple, is that the parameter a becomes a 'residual' factor that contains many different parameters and effects. The overtopping manual EurOtop (2018) gives a more detailed version of Equation (2.10), which splits out different factors such as the slope inclination, Irbarren breaking parameter and situational effects in terms of different gamma symbols. For the definitions of the symbols used in this equation, please refer to the List of Symbols.

$$\frac{q}{\sqrt{g \cdot H_{m0}^3}} = \frac{0.023}{\sqrt{\tan(\alpha)}} \cdot \gamma_b \cdot \xi_{m-1,0} \cdot \exp\left(-(2.7\frac{R_c}{\xi_{m-1,0} \cdot H_{m0} \cdot \gamma_b \cdot \gamma_f \cdot \gamma_\beta \cdot \gamma_v})^{1.3}\right) \tag{2.11a}$$

With a maximum of:

$$\frac{q}{\sqrt{g \cdot H_{m0}^3}} = 0.09 \cdot \exp\left(-(1.5\frac{R_c}{H_{m0} \cdot \gamma_f \cdot \gamma_\beta \cdot \gamma^*})^{1.3}\right) \tag{2.11b}$$

In practice, Equation (2.11a) is used for situations with breaking waves, and Equation (2.11b) is used in situations with non-breaking waves.

For deep water breakwaters without a berm, with normally incident waves and without a wall or promenade on top of the slope, their respective effects are not present and their influence factors are set to 1. This means that $\gamma_b = \gamma_\beta = \gamma_v = \gamma^* = 1$.

Chapter 3

Physical model setup

In this chapter, the setup of the physical model is discussed. Firstly, a practical model size for the CoastaLock blocks is determined. The test conditions, bound by the availability of materials and equipment in the testing facility, are then based on the CoastaLock model size. Then, the test conditions define the composition of the breakwater and the positioning of wave gauges in the flume. Next, the wave gauges are calibrated and finally, other measuring equipment used during the test is described.

The physical model test is set up with the aim to simulate a breakwater in deep water conditions, in order to assess the behaviour of the CoastaLock units without bottom or toe effects. An impermeable core is chosen in compliance with the industry standard for placed block revetments.

3.1 CoastaLock model units

The size of the CoastaLock model units is determined and set to a d_n of 3cm, which means that they are a factor $\frac{1}{\lambda} = 0.02675$ smaller than the blocks as described by ECOncrete Tech Ltd. (2021). Blocks of this size are expected to be small enough to definitely allow for damage with the largest waves that are practically possible in the TU Delft wave flume ($H_s \approx 18$cm), and large enough to prevent laminar flow scale effects at smaller wave heights, as at an H_s of 5cm the blocks will still have a Reynolds number of $Re \approx 21000$.

The units are constructed to represent the real-world conditions as accurately as possible. According to ECOncrete Tech Ltd. (2021), the density of the real CoastaLock units is around 2400 kg/m^3. Assuming a density of salt water of 1030 kg/m^3, the ideal relative density of CoastaLock to water is $\Delta = 1.33$.

After construction of the blocks, they are weighed and measured according to the Archimedes principle. Their final properties are listed in Table 3.1.

As can be derived from Table 3.1, the achieved relative density Δ for the CoastaLock model units is 1.30, which is 2.25% lower than the ideal relative density of 1.33.

Property	Symbol	Quantification	Unit
Nominal diameter	d_n	0.0298	m
Density	ρ_{cl}	2299.44	kg/m^3

Table 3.1: Measured properties of the CoastaLock armour units after production.

3.2 Test conditions

This section will elaborate on the hydraulic test conditions used in the physical model tests. For some theoretical background on waves and the JONSWAP wave spectrum, please refer to Appendices B and C.

3.2.1 Wave spectrum

The aim of this thesis is to determine the hydraulic properties of the first design of the CoastaLock armour units, so standard wave spectra with standard settings are chosen to keep the research focussed on the blocks, and to make the block properties easily comparable with the specifications of other units.

The wave spectrum chosen for the tests is a JONSWAP wave spectrum, as it resembles 'young' or not fully developed sea states, which are common coastal sea states used in physical model testing. The standard peak enhancement factor γ of 3.3 is applied.

3.2.2 Significant wave height

According to ECOncrete (Gutiérrez Martínez, 2021), the expected stability number of the CoastaLock units N_s, should lie around 2.5. With $N_s = \frac{H_s}{\Delta \cdot d}$, this corresponds to failure at an expected significant wave height of $H_s = N_s \cdot \Delta \cdot d = 2.5 \cdot 1.30 \cdot 0.0298 = 0.097$m. The most extreme expected stability of CoastaLock is $N_s \approx 4$, which leads to an expected H_s of 0.16m for the most extreme tests.

3.2.3 Wave steepness

Different wave steepnesses are used in the tests, which are 1% increments in a range from 2% to 6% steepness. This range then contains the standard and realistic wave steepness of 4%, which makes the results of the test realistic and easily comparable with other armour units. The 2% and 3% wave steepnesses are added to the test programme, as they are expected to do more damage to the CoastaLock armour units. 5% and 6% steepness is added to the schedule to get a complete idea of the response of the CoastaLock units to different wave steepnesses. For the full test programme, please refer to Chapter 4 and Table 4.1.

3.3 Flume configuration

The tests are executed with a constant water depth of 0.6m. This is the water depth for which the largest deep water waves can occur in the flume, without spilling over the top.

The flume has an internal length of 42 metres from begin to end, with an effective length (excluding the wave maker) of 40 metres. At 22.25 metres from the wave generator, the flume has a 1 metre long glass window in the bottom. As this window allows for visual observations from below the waves, the slope is placed just after the window, at 23.25 metres. A cross section of the flume is displayed in Figure 3.1.

(a) Side view

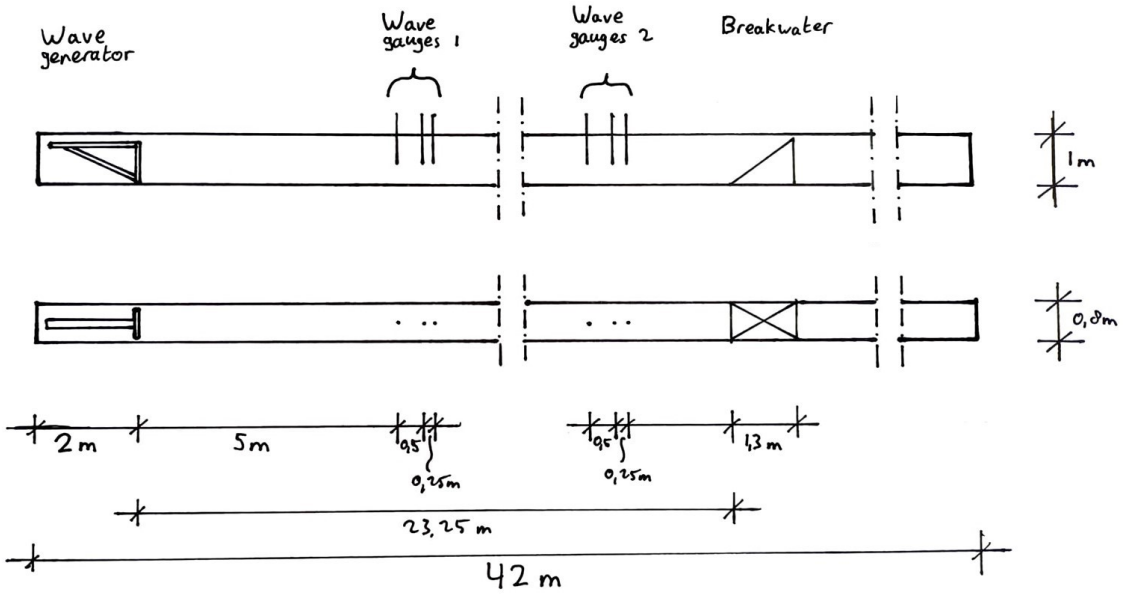

(b) Top view

Figure 3.1: Cross-section of the wave flume and test setup.

3.3.1 Wave generator

The wave generator in the wave flume of the TU Delft Hydraulic Engineering Laboratory is a piston-driven wave paddle that can generate both regular and irregular waves. The movement of the paddle is purely horizontal and has a maximum stroke length of 2 metres. The wave generator is fitted with sensors on the wave paddle, which feed hydrostatic pressure information to the Active Reflection Compensation (ARC) software. The ARC system uses this to actively compensate the water elevation of the waves reflected on the breakwater, minimising reflection off the wave paddle.

3.4 Breakwater composition

The composition of the slope is that resembling a deep water breakwater with impermeable core, and consists of many elements, some of which are described below. The layout of the breakwater itself is shown in Figure 3.2.

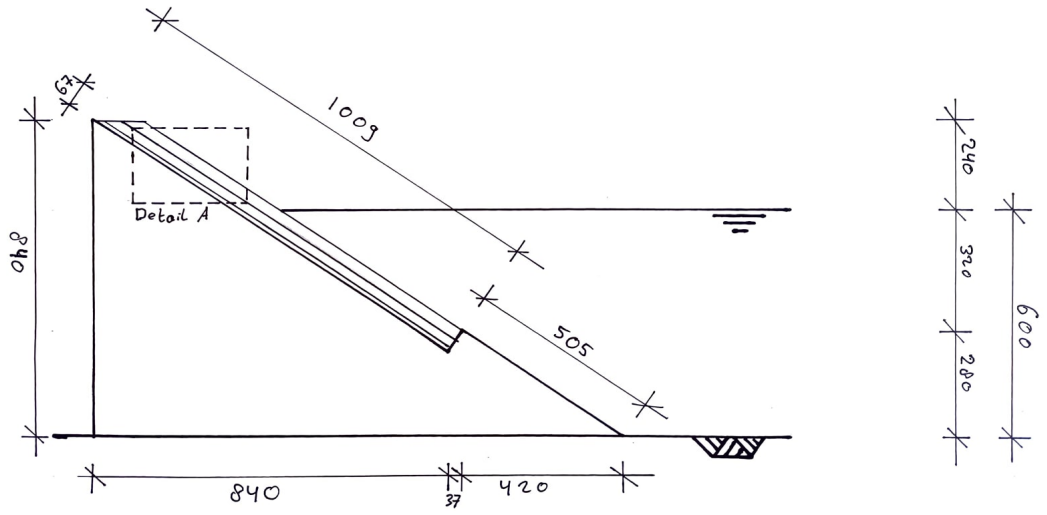

Figure 3.2: Cross-section of the breakwater test setup. Dimensions in mm.

3.4.1 Slope

The core is represented by a wooden board under a standard 2V:3H inclination, which, in combination with a wave steepness of 4%, will lead to the Irbarren breaking parameter shown in Equation (3.1).

$$\xi = \frac{\tan \alpha}{s_{op}} = \frac{\frac{2}{3}}{0.04} = 3.33 \tag{3.1}$$

The Irbarren parameter of 3.33 means that a mix between collapsing and surging waves can be expected for the standard test with 4% wave steepness. For more information on the Irbarren parameter, please refer to Appendix B.

3.4.2 Vertical dimensions

The board does not have a toe structure, as to mimic deep-water conditions. Instead, the armour layer is be held in place by a wooden elevation at 2 times a maximum expected H_s of 0.16m below the still water level, as is shown in Figure 3.2. This 2 $H_{s,max}$ below the water line follows directly from Appendix B.2.2, in which the maximum wave attack zone was determined to be between 2 $H_{s,max}$ above and below the water line.

The crest of the structure is placed at 1.5 $H_{s,max}$, to represent a more realistic application of the CoastaLock blocks. The lower crest height also reduces the weight on the lower blocks, weakening them and therefore making for a more critical test. On top of that, the more realistic crest height also tests the performance of CoastaLock as crest element.

3.4.3 Under and filter layers

The filter layer is glued into the wooden board, and represents the core material. The main goal of this filter layer is to provide the slope with enough roughness to prevent the under layer from sliding down, and consists of fine gravel with $d = 2$mm.

The chosen material for the under layer is 'Japanese Split 8-11mm', and calibrated according to the Archimedes principle to have a d_{n50} of 8.34mm. This material has a relatively steep grading of $\frac{d_{85}}{d_{15}} = 1.22$ and a ratio $\frac{d_{n,armour}}{d_{n50,under}} = 3.6$. The under layer is constructed with three different thicknesses over different tests, expressed as a factor of the d_{n50}. These thicknesses are 0 (no under layer), 2 (standard) and 3.4 (extra thick) times the d_{n50}. A detail of the layers on the breakwater can be seen in Figure 3.3.

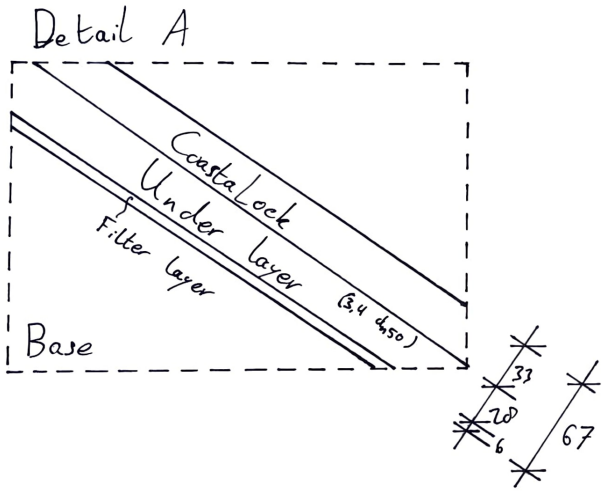

Figure 3.3: Detail A of breakwater test setup, showing the CoastaLock armour layer, under layer and filter layer for the maximum under layer thickness. Dimensions in mm.

3.4.4 Armour layer

The armour layer consists of the CoastaLock units with the specifications as defined in Table 3.1, in various orientations and packing densities.

Orientations

The standard orientation of the CoastaLock armour units is named the 'San Diego' orientation, after the full scale pilot with CoastaLock blocks in San Diego, California. This orientation consists of units above the still water level with their cavity facing forwards, and units below the still water level with their cavities facing sideways to the right. The San Diego orientation is considered the standard, as that is the design orientation and the most probable application of the blocks for environmental reasons.

In order to distinguish the effects of the two different orientations present in the San Diego setup, a test where all blocks have their cavity facing forwards and one where all blocks have their cavity facing sideways will also be committed.

Examples of the different orientations are shown in Figure 3.4.

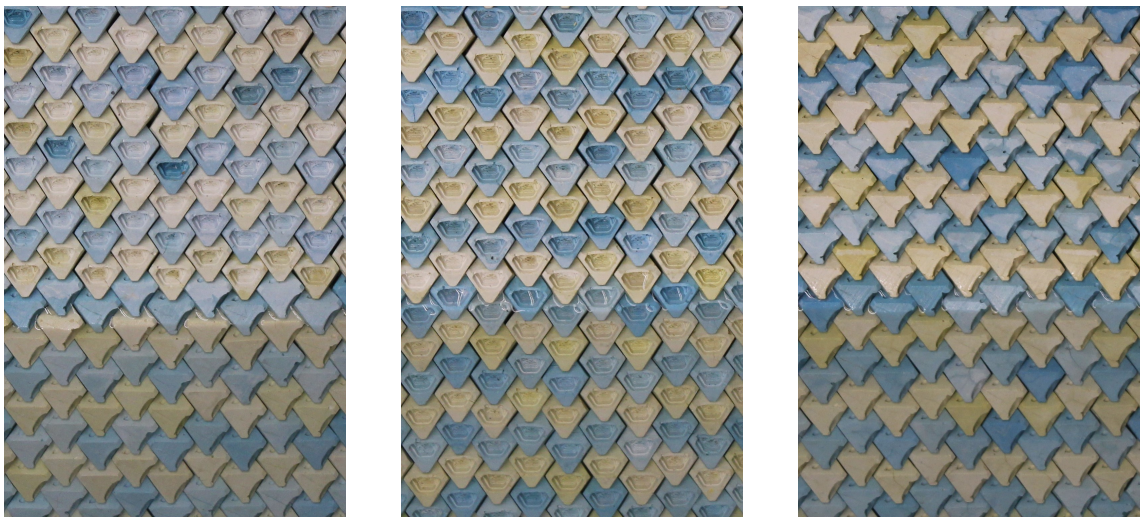

(a) San Diego (b) Cavity forward (c) Cavity sideways

Figure 3.4: The three different orientations of CoastaLock used in the physical model tests.

Spacing

In the standard San Diego case, the units are placed against each other and packed as tightly as possible, to form one uniform layer. During later tests, the blocks are spaced further apart to reduce the leakage lengths and the number of blocks used per unit of surface area of the slope, leading to a more ecological solution.

The spacings used are simple spacings; the blocks are moved apart only horizontally, up until a maximum spacing of 25%, which leaves just individual columns of CoastaLock on the slope, and completely removes the horizontal interlocking effect of the blocks.

This is not representative for the practical application, but will give a good indication of the sensitivity of CoastaLock to the leakage length for when a design with integrated spacers in all directions is made. An overview of the different spacings is shown in Figure 3.5.

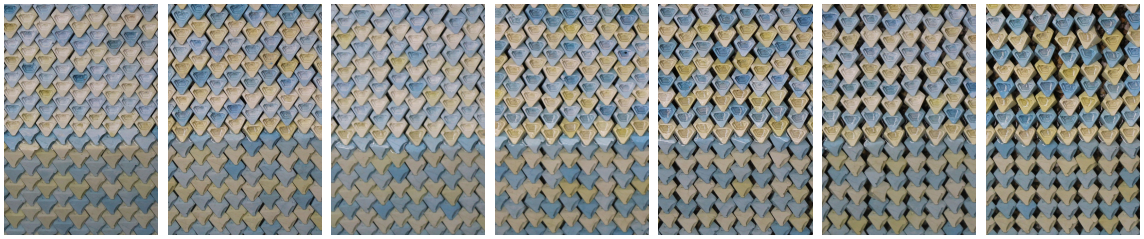

(a) 0% (b) 5% (c) 7.5% (d) 10% (e) 15% (f) 20% (g) 25%

Figure 3.5: The different spacings of CoastaLock used in the physical model tests.

Side elements

To simulate an infinitely wide breakwater, side elements are 3D printed to slot in between the last CoastaLock units and the glass of the flume. This will lead to a realistic situation where the leakage length is not shortened by gaps in the side of the structure. The 3D printed plastic elements come with two negative side effects: their low density makes them highly buoyant compared to the CoastaLock blocks, which suffer an upward directed force from these side elements as a result.

Secondly, due to the shape of the side elements and the presence of the glass wall, the interlocking capabilities of the side elements are lower than that of full CoastaLock units. Due to these two effects, the conditions at the sides of the flume are unstable and not realistic. Therefore, these effects are countered by placing two chains over these side elements along the glass wall, as shown in Figure 3.6.

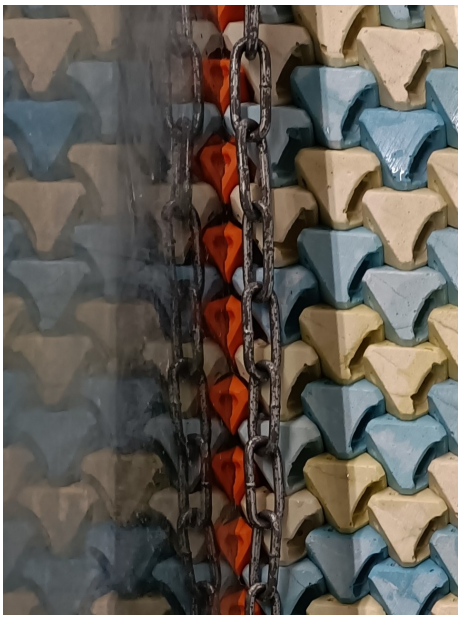

Figure 3.6: 3D printed side elements and metal chains.

3.5 Wave gauge positioning

Two sets of three wave gauges are placed in the wave flume to measure the wave characteristics that occur during the tests. One set of gauges is placed five metres from the wave machine, in order to measure the waves produced by the wave generator. The second set is placed two metres from the test structure, in order to measure the incident and reflected waves just before and after impact on the structure. The two metres distance is based on the wave lengths expected in the flume, and is equal to 0.4 times the maximum expected wave period L_p, rounded up to 2 metres.

The internal spacing of the wave gauges is based on the Mansard and Funke 3a method as described by Wenneker and Hofland (2014). The maximum expected wave length equals 5 metres, and is based on a wave height of 0.1m at a steepness of 2%.

The minimum expected wave length is the 1.25m belonging to the so-called shakedown test, which has a projected H_s of 0.05m at 4% steepness.

These wavelengths lead to the demand of $0.2 < x_{12} < 1.2$, and a ratio $\frac{x_{12}}{x_{23}} = 2$. The wave gauges are placed at a spacing x_{12} of 0.5m and x_{23} of 0.25m, as previously shown in Figure 3.1. One wave gauge is also placed inside the overtopping basin, where it can be used to measure the change in water level elevation over the duration of the test.

3.6 Wave gauge calibration

After the wave gauges are positioned, they are calibrated, and the scale factor of voltage output to metres is calculated, as this is required for the analysis of the wave signal (see Chapter 5). For the calibration, the flume is filled with 0.6m of water, as this is the water depth used in the actual tests as well. The wave gauges are positioned just below the water line (at depth $z = 0$), with the voltage outputs manually set close to zero. The wave gauges are then all lowered by 2 centimetres, and their output voltages are recorded again. This process is repeated until the maximum output of 10 volts is reached for every wave gauge. Readings of exactly the maximum of 10.00 volts are then omitted out of the results.

Then, the measured outputs can be plotted versus the depths at which these measurements were taken. This is shown in Figure 3.7. According to the manufacturer, the wave gauge output voltages increase linearly with the depth, but due to some minor measurement inaccuracies this is may not be precisely true. Therefore, a linear line is fitted through the data and also displayed in Table 3.2.

The slope of the linear fitted lines through the wave gauge data is then reported in Table 3.2. The reciprocal of the slope is then equal to the scale factor of voltage to metres of water depth above the wave gauge, as required for the data processing in Chapter 5.

Please note that there is no correlation between the names of the wave gauges and their position in the flume. The names correspond with the labels already present on the gauges and the gauges are presented in the order in which they appear in the flume.

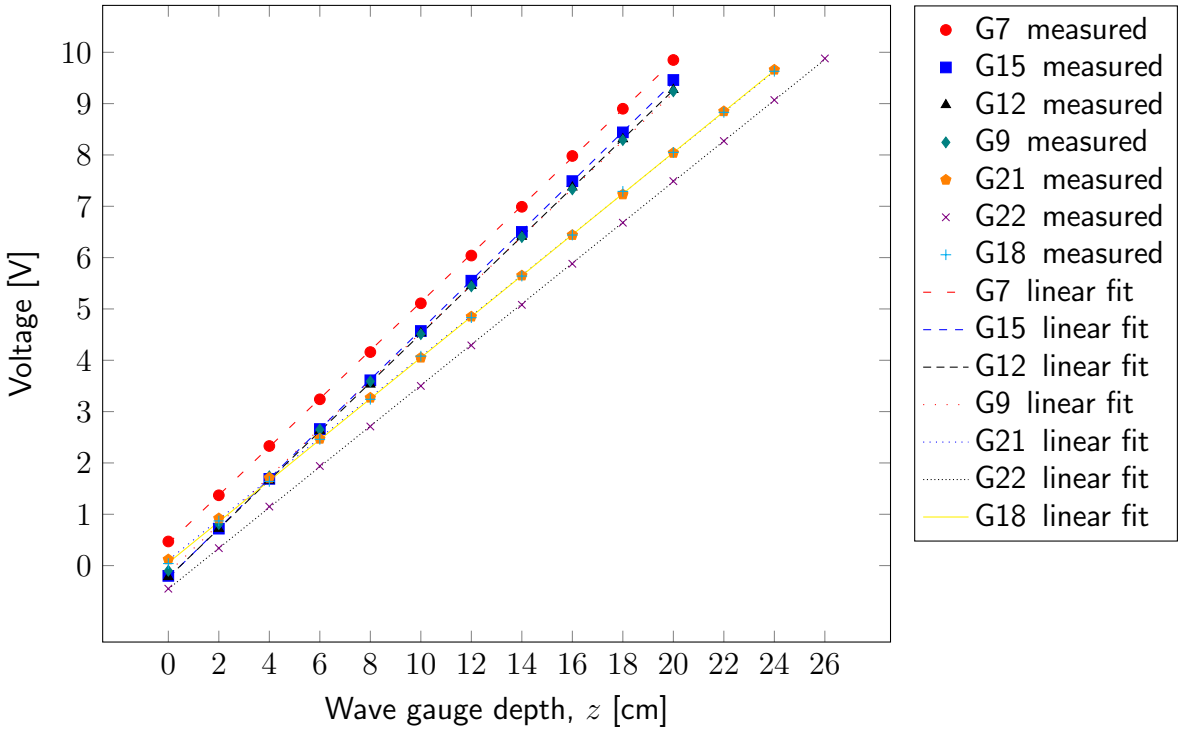

Figure 3.7: Wave gauge calibration data with linear fits.

That means that wave gauge G7 is located closest to the wave generator, gauge G12 is the last gauge in set 1, gauge G9 is the first gauge in set 2, gauge G22 is the gauge closest to the structure and gauge G18 is placed in the overtopping basin.

Wave gauge	Slope [-]	Scale factor to m [-]
G7	46.97727	0.021287
G15	48.27273	0.020716
G12	47.46364	0.021069
G9	46.70000	0.021413
G21	39.67857	0.025203
G22	39.67363	0.025206
G18	39.95330	0.025029

Table 3.2: Wave gauge calibration results

3.7 Visual measuring equipment

The tests are recorded with two individual cameras placed around the flume. A Canon EOS 550D is fixed at 2.5 metres above the centre of the slope and is connected to a laptop by the side of the flume through USB cable. This laptop is then used to control the camera settings and take a picture of the slope before and after every test run. These pictures are then used to determine the change in position of the CoastaLock armour units during the test.

A SONY AX33 4K Handycam video camera is placed by the side of the flume, fully recording all tests from the side of the breakwater. This video footage is then used in a later stage to validate visual observations and notes made during testing.

3.8 Overtopping basin

Behind the breakwater, an overtopping basin is created to catch any overtopping water during the test. This water is then pumped out using a Watson-Marlow 704S/R IP55 peristaltic pump, and weighed in a bucket on a KERN KXP 150V20M scale with a KFS-T monitor. This scale returns weights under 60 kilograms with an accuracy of 1 gram. For tests where the overtopping discharge is too large for the peristaltic pump, a Kärcher WD6 P Premium vacuum is used to pump the overtopping basin dry. For these larger overtopping volumes, weighing the water is not possible anymore, but the Kärcher vaccum has an internal volume of 70 litres, so an estimation of the total volume of overtopped water is made based on the amount of times the Kärcher vacuum is filled and emptied during a test.

An extra wave gauge is also placed in the overtopping basin, as it can accurately determine the water level (and therefore water volume) increase in the overtopping basin over the duration of the test. An overview of the equipment inside the overtopping basin is displayed in Figure 3.8.

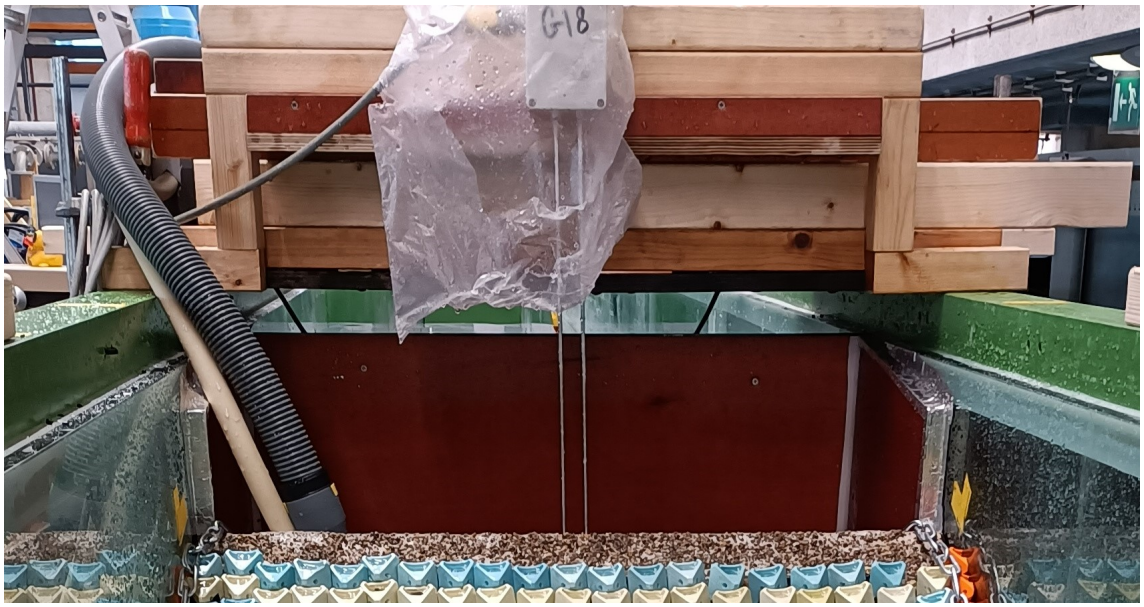

Figure 3.8: The overtopping basin behind the test slope, with wave gauge G18 and the hoses of the two pumps inside it.

Chapter 4

Test information

This chapter describes the practicalities of testing. First, the test procedures are explained, and then the different tests committed are elaborated on.

4.1 Test procedure

The CoastaLock scale model tests consist of test series containing different test runs. Every individual series aims to test a certain parameter of the CoastaLock armour units and starts with a short standard shakedown test to settle the blocks. Then, different runs with increasing wave heights are executed until the test is finished.

4.1.1 Test series

Preparation

Before one test series is conducted, the under layer is constructed. It is important that the under layer is rebuilt, so that effects and displacements from previous series are not present anymore and every test series starts with a newly constructed under layer. The desired thickness of the under layer is marked on the glass along the sides of the slope, so the under layer material is laid out on the slope and then levelled with a wooden plank. Afterwards, the CoastaLock units are placed on top of the under layer in the desired orientation and with the desired spacing.

With 0% spacing, the blocks are laid out diagonally from the bottom left corner of the slope, so that the blocks always support a few blocks around them and the interlocking effect already keeps them in place during construction. Once the diagonal reaches the right side of the flume, the layer is finished from the bottom upwards. This process is shown in Figure 4.1.

When spacing is required, the bottom layer of blocks is first measured out and laid out carefully with the desired spacing. Then, the layer is finished from the bottom up. This process is shown in Figure 4.2.

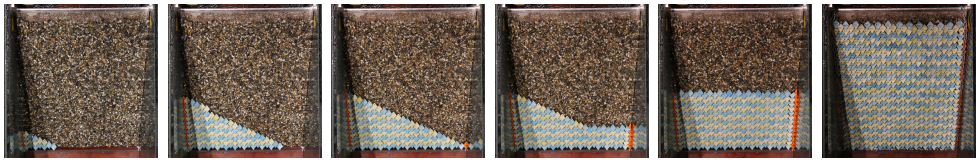

Figure 4.1: Construction process of a layer with 0% spacing.

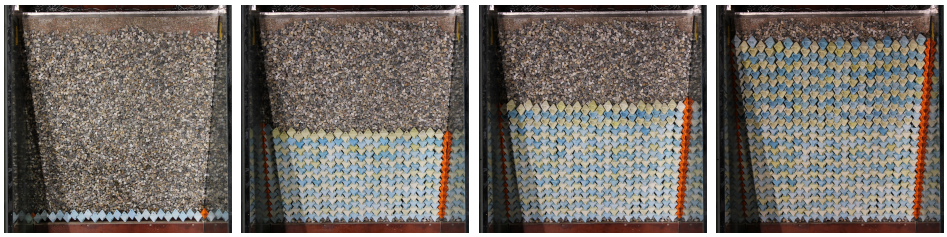

Figure 4.2: Construction process of a layer with spacing.

After construction of the armour layer, the flume is filled carefully to the desired water depth of 0.6m.

Individual test runs

The individual test runs will be executed with the standard test procedure described below.

1. Take a picture of the breakwater with the Canon EOS 550D fixed directly above the breakwater.
2. Start the wave gauge measurements in DASYlab and trigger the SONY AX33 4K Handycam video camera fixed by the side of the flume.
3. Check whether the settings of the wave generator are correct and start the test.
4. Observe the test, and write down any abnormalities witnessed during the test, such as 'breathing' of the layer or rocking of individual armour units.
5. Stop the wave generator once the test duration has elapsed, or when more than one CoastaLock element is extracted from the layer, whichever comes first. Do not disable the Automatic Reflection Compensation (ARC) feature.
6. Stop the wave gauge measurements in DASYlab and stop the SONY AX33 4K Handycam video camera fixed by the side of the flume.
7. Pump out any water from the overtopping basin, weigh this and register the weight. Meanwhile, wait for the waves in the flume to settle.
8. Take a picture of the breakwater with the Canon EOS 550D fixed directly above the breakwater.

The test duration as mentioned in item 5 varies per test and is calculated according to Equation (4.1).

$$D = T_p \cdot N_{waves} \tag{4.1}$$

The peak period T_p depends on the wave steepness and wave height used in every test, those can be found in Table 4.1. The number of waves also depends on the type of test. The 'shakedown' tests that are used just after construction of the layer to settle the blocks consist of 500 waves, all other tests consist of 1200 waves.

End of test series

A test series has ended when a test run with the maximum possible wave height in the flume has been conducted, or when a test run is stopped due to extraction of CoastaLock units from the layer (item 5 in the procedure for individual test runs). Once the test procedure for individual runs is completed, the wave flume is drained carefully and the CoastaLock units are removed from the layer. If not done before, all the data from the cameras and wave gauges are saved, labelled and organised. Then, the preparation for the next test series can start.

4.2 Test programme

The test programme consists out of 24 series, which individually consist of multiple test runs. These are elaborated on below. The full programme for the CoastaLock scale model tests is described in Table 4.1.

4.2.1 Test series

24 different test series are executed. The first tests aim to research the effect of the under layer thickness on the behaviour on the CoastaLock units, and afterwards different wave steepnesses are tested. Then, different spacings are researched and the baseline test is validated. Afterwards, tests with sideways or forwards cavities are executed, as well as extra tests with medium-short and medium-long waves and combinations between earlier tests. The full programme can be found in Table 4.1.

In short, the parameters that are varied over the test series are the wave steepness s_0, which is a function of the wave length and wave height, the orientation of the units, the under layer thickness D_{under} and the armour spacing S. These parameters are visualised in Figure 4.3.

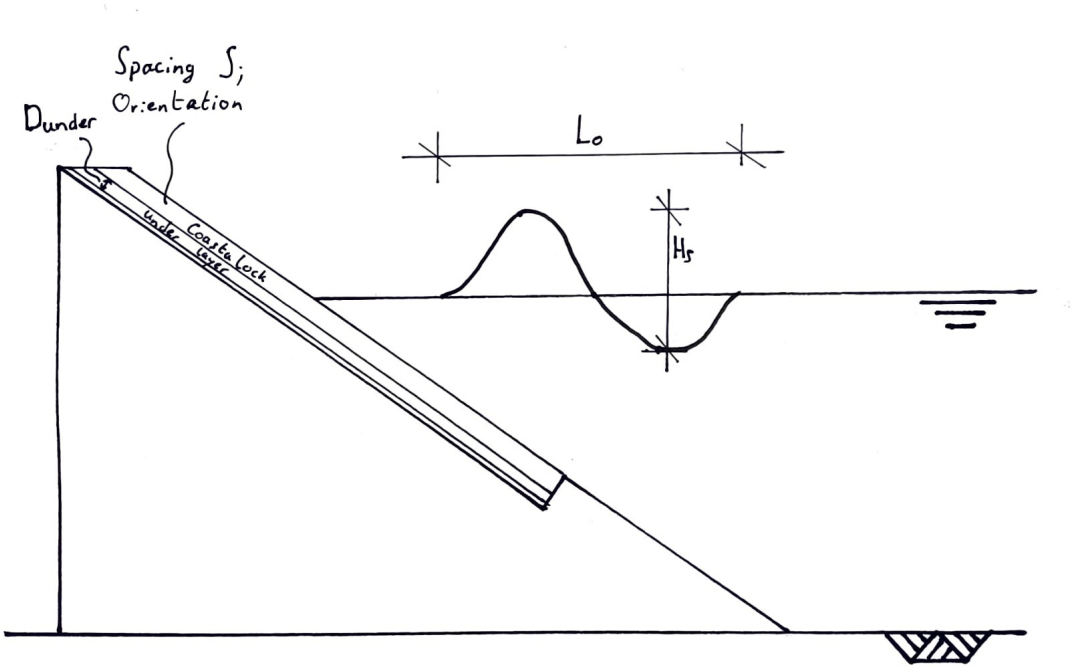

Figure 4.3: Variables for the CoastaLock physical model tests, visualised. The waves are not to scale.

4.2.2 Test runs

The test series mentioned above all consist of multiple individual test runs according to the procedure listed in Section 4.1.1. The first run after construction is a shakedown test of 500 waves, which aims to let the blocks settle into place before starting the real tests.

The following test runs then start at $H_s = 0.07$m, and increase with 0.01m per test run. This means that the resolution around the projected point of failure ($H_s = 0.1m$, (Gutiérrez Martínez, 2021)) is 10%. For test series that have not achieved extraction of an armour unit by $H_s = 0.13$m, the H_s step size will increase to 0.015m per consecutive test run until the end of the test.

Test series	Description	Wave steepness s_0 [-]	Spacing S $[A_{slope}]$	Block orientation	Under layer thickness D_{under} $[d_{n50,under}]$
01	Extra thick under layer	0.04	0.00	San Diego	3.4
02	Extra thick under layer	0.04	0.00	San Diego	3.4
03	No under layer	0.04	0.00	San Diego	0
04	No under layer	0.04	0.00	San Diego	0
05	Baseline test	0.04	0.00	San Diego	2
06	Baseline test	0.04	0.00	San Diego	2
07	Short waves	0.06	0.00	San Diego	2
08	Short waves	0.06	0.00	San Diego	2
09	Long waves	0.02	0.00	San Diego	2
10	5% spacing	0.04	0.05	San Diego	2
11	10% spacing	0.04	0.10	San Diego	2
12	10% spacing	0.04	0.10	San Diego	2
13	15% spacing	0.04	0.15	San Diego	2
14	20% spacing	0.04	0.20	San Diego	2
15	25% spacing	0.04	0.25	San Diego	2
16	Validate baseline	0.04	0.00	San Diego	2
17	Cavity sideways	0.04	0.00	Cavity sideways (right)	2
18	Sideways, 20% spacing	0.04	0.20	Cavity sideways (right)	2
19	7.5% spacing	0.04	0.075	San Diego	2
20	Cavity forwards	0.04	0.00	Cavity forwards	2
21	Forwards, 10% spacing	0.04	0.10	Cavity forwards	2
22	Medium-long waves	0.03	0.00	San Diego	2
23	Long waves, 10% spacing	0.02	0.10	San Diego	2
24	Medium-short waves	0.05	0.00	San Diego	2

Table 4.1: Test programme for the test series used in the CoastaLock physical model test.

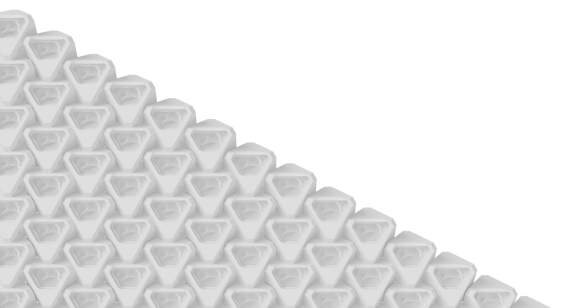

Chapter 5

Data processing

This chapter gives a brief overview of the data processing methods used. From securing and storing visual measurements during the tests, to converting the wave gauge outputs into workable files, before decomposing the wave signal into spectral significant wave heights and finally writing all the converted data into a single `.csv` file.

5.1 During testing

During testing, the images and videos from the two cameras are processed and stored directly into designated folders on an external hard drive connected to the laptop besides the flume. The videos are labelled with a three digit labelling system. The first two digits stand for test number 01 to 24 (as shown in Table 4.1), the third digit stands for the test run corresponding to that video. For example, video 173 corresponds with test 17, run 3. The DASYlab data file with the output of all seven wave gauges is also stored according to the same system.

The photos are stored with a four digit system, where the first three digits are identical to the videos, and the fourth digit will be either a 0 (taken before the test run) or a 1 (taken after the test run). This means that photo 1730 corresponds to test 17, run 3, and was taken before the test.

In the end, 24 tests with 135 runs have resulted in a sum total of 270 test photos, 135 videos and 135 wave gauge data files.

5.2 After testing

The largest part of data processing comes after the tests, and consists of several steps in order to convert the data into a type that can be used in the results and analysis. Firstly, the DASYlab files with the raw wave gauge data are converted using a Python script so that they are suitable for MATLAB input. Then, the required depth and parameter files are created with a Python script for the signal decomposition with `decomp.m`, with which the final processing step is taken.

5.2.1 DASYlab conversion using Python

DASYlab is the software that records the wave gauge outputs every 0.1 second and writes them to an `.ASC` file with `ASCII` encoding. DASYlab files have 8 columns with data; a time stamp and the output of 7 wave gauges. Depending on the duration of the test, DASYlab files can have up to 27000 rows of data. An example of the first few rows of a DASYlab file is shown in Appendix G.

The DASYlab files have two aspects that make them unusable for `decomp.m` in MATLAB. Firstly, the output contains decimal commas whereas MATLAB requires decimal points, and secondly, the time stamp has a format of hours, minutes and seconds, whereas `decomp.m` requires a time stamp in seconds. Therefore, a Python script is written that replaces all decimal commas with decimal points and converts the time stamp to seconds in all 135 DASYlab files. The code of this script can be found in Appendix H.

5.2.2 Parameter file preparation

The MATLAB script `decomp.m` requires three inputs to perform the decomposition of the wave gauge signals. Firstly, the converted DASYlab file as created in Section 5.2.1. Secondly, a parameter file containing the parameters for the test, such as an estimation of the wave period, which is equal to the wave period entered in the settings of the wave generator for every test. The parameter file also requires the scale factor of voltage to metres for the wave gauges in question, as derived in Section 3.6, as well as the positions of the wave gauges compared to the first wave gauge of the set (reference point $x = 0$).

As two sets of wave gauges have been used, two parameter files need to be created; one for every set of wave gauges. This is done through a Python script, which takes the `.txt` template file as shown in Appendix I, copies, updates and saves it accordingly for every DASYlab file. This Python script can be found in Appendix J.

Finally, a depth file is required by `decomp.m`, which is the same for all tests and test runs. This file contains a simple bottom profile by reporting the bottom elevation on four points along the flume. The points are chosen such that they correspond with the position of the three wave gauges; the location of the first wave gauge of a set is the reference distance $x = 0$. The fourth point is located just outside the set of wave gauges. The depth file is illustrated in Figure 5.1 below.

```
pos (m),  diepte (m)
0.0       0.60
0.50      0.60
0.75      0.60
0.90      0.60
```

Figure 5.1: Contents of the `.txt` depth file used as input for decomposition with `decomp.m`.

5.2.3 Signal decomposition using `decomp.m`

Finally, the converted DASYlab files, the parameter files for every specific test run and the depth file are entered into the MATLAB script `decomp.m`.

`decomp.m` is a MATLAB script as created by Bakkenes (2002) and Klaasman (2005), which is specifically designed for wave signal decomposition in the wave flume of the Delft University of Technology. It uses a collection of 60 different MATLAB functions in separate scripts to perform a full spectral analysis of the wave signal and exports those as a `.txt` file.

As two sets of wave gauges are used, the `decomp.m` is run twice for every DASYlab wave gauge file; once for the first wave gauge set with the parameter file for wave gauge set 1, and once for wave gauge set 2 with the parameter file for wave gauge set 2. This results in 270 manual runs of `decomp.m`, with the same number of `.txt` output files.

These output files are then saved and labelled according to a four digit labelling system, where the first three digits correspond to the test and test run, as used for saving the DASYlab files in Section 5.1. The fourth digit is either a 1 or a 2 and corresponds to the wave gauge set used for this signal decomposition. For example, output file `1192.txt` corresponds with test 11, run 9, wave gauge set 2.

Finally, another Python script is written to collect the incident and reflected spectral significant wave height H_{m0} and calculate the reflection coefficient and wave length, before compiling all this data into a single `.csv` file. This script is shown in Appendix K.

5.2.4 Data selection

The decomposition process is done twice, once for three wave gauges per set (the Mansard and Funke 3a (MF3a) method (Wenneker and Hofland, 2014)) and once for two wave gauges per set (Goda and Suzuki (GS) method (Wenneker and Hofland, 2014)). The reason for this is that the Mansard and Funke 3a method itself is superior to the Goda and Suzuki one, but that there are doubts about the `decomp.m` MATLAB software with this method. The GS method is therefore used to verify the MF3a method.

After inspection of the data generated with the Mansard and Funke 3a method, it is discovered that approximately 10% of the data shows physically impossible values, with either reflection coefficients $c_{ref} > 1$, or significant wave heights of several metres. Another 15% of the data shows improbable values, with reflection coefficients $0.85 \leq c_{ref} \leq 1$ or significant wave heights around a factor 10 higher than visual estimates of the wave heights from the test videos.

Inspection of the data generated with the Goda and Suzuki method does not reveal any such anomalies. Moreover, it resembles the MF3a data at points where it is realistic. Therefore, it is decided to omit all the Mansard and Funke 3a data on the basis of unreliability due to a software issue. The Goda and Suzuki data is then exclusively used in the results and analysis of this thesis.

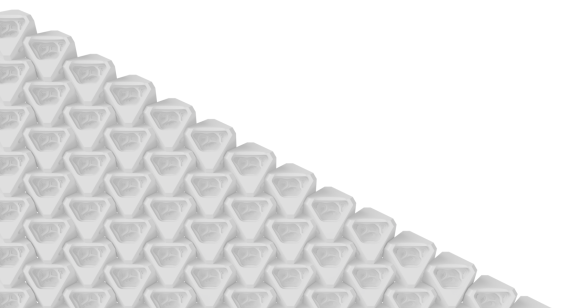

Chapter 6

Test results and analysis

In this chapter the main results are represented and compared with expected values from literature. In Section 6.1 a new failure mechanism is defined and consequently the results regarding stability are presented in Section 6.2. In Section 6.5, the reflection results are presented. Section 6.6 contains the overtopping results, as well as the derivation for the roughness parameter of CoastaLock and a comparison to literature.

6.1 Failure mechanism: breathing

This section describes the mechanism of 'breathing', which is not specific for CoastaLock, but common in all placed block revetments. However, it has never properly been described. This section aims to do so, and advocates for listing it as a failure mechanism of placed block revetments.

In Section 2.4.1 Van den Berg et al. (2020) describe a new failure mechanism, which are under layer deformations either on a micro scale (for individual blocks) or on a macro scale, where the layer is deformed in a concave S-shape. These under layer irregularities lead to instabilities in the armour layer and were classified as a failure mechanism.

In the physical model tests for this thesis, a process causing these under layer deformations has been registered that has been observed in other tests with other placed block revetments, but which has not been described before. This mechanism has been dubbed 'breathing' of a placed block revetment layer. Breathing occurs before unit extraction and consists of extensive and repeated movement of the entire layer perpendicular to the slope on which it rests. It is clearly visible with the naked eye, and the movement resembles that of a human chest moving up and down under breathing, hence the name. Breathing is caused by a large pressure difference between the under layer and the outside of the armour layer, resulting in an unbalance of the forces on the layer and the subsequent movement. This pressure difference is the largest during the run down of a wave and when the leakage length is long; this causes the pressure to be 'trapped' in the under layer.

Once the next wave arrives, the pressure levels are restored and the layer is pushed back onto the slope. This is then repeated with every critical wave and results in the layer 'breathing'.

In the observations made for this thesis, the centre of the armour layer was estimated to have a maximum displacement away from the slope of 1.5 to $2D_{n,armour}$ before being pushed back by the next wave. This displacement is the cause of multiple unwanted effects in an armour layer and should therefore be defined as a failure mechanism.
The first effect that takes place during the extensive and repetitive movement of the layer, is that the interlocking blocks continuously rub against each other, undergoing large pressure and frictional forces. The blocks do not collide as they do during rocking (see Section 2.2.2), since they are already in contact. However, there still is substantial movement of the blocks relative to each other, see Figure 6.1. This rubbing and rotating of the units is potentially powerful enough to break or damage prototype units, which is the first reason why breathing should be designated as a new failure mechanism.

Figure 6.1: Breathing of the CoastaLock armour layer, with layer in raised position.

Secondly, the repeated impact of the armour units as the layer is placed back onto the under layer is also a potential cause for many problems. This repeated contact between the armour and under layer can cause erosion of the under layer material, damage or breakage of the armour units or potentially even geotechnical failures like settlement of the subsoil.

Finally, and most importantly, breathing of the armour layer causes the under layer to slide and deform, with micro-irregularities and either a local or global concave S-shape in the under layer as a consequence. An example of this is shown in Figure 6.2, where the filter layer and breakwater core is even exposed (highlighted in green) due to the under layer material sliding down (highlighted in red).

This mechanism can have large impacts, as large deformations in the under layer need to be repaired (they are a failure mechanism, see Section 2.4.1). This reparation does not only require fundamental restructuring of the under layer, it also requires the armour layer to be taken off entirely, as the interlocking nature of the blocks does not allow for them to be removed or placed back individually. In practice, this is an expensive and time consuming operation. It is for this reason, together with the potential damage or breakage of armour units as described before, that breathing of the armour layer needs to be classified as a new failure mechanism for interlocking concrete armour units.

Figure 6.2: Displacement of under layer material due to breathing of the armour layer. Exposure of the core material highlighted in green, accumulation and formation of concave S-profile highlighted in red.

6.2 Stability

The results of the stability performance of are shown in Figure 6.3. Three plots are depicted, those for the extraction failure mechanism, the breathing mechanism and those for no failure. The stability number reported for no failure is the highest stability number measured for that test. The stability number for breathing and extraction is reported with an error bar: the top of the error bar resembles the measured stability number for the test run where the failure first occurred, the bottom end of the error bar resembles the measured N_s corresponding to the last test where this failure did not occur. The plotted stability number is then the average between the two.

What stands out from these results is that breathing always closely precedes failure. This means that breathing, next to being a failure mechanism itself, can also be seen as a warning that armour units are about to be extracted.

Additionally, the stability behaviour shows similar traits as that of the overtopping parameter. The values are very low for almost all cases where the armour spacing is smaller than 10%, but are high where the armour spacing is larger than 10%. But most of all, armour spacing (and with it the permeability of the top layer) seems to have a dominant influence on the stability of the unit until a certain threshold is reached where the leakage length is short enough for the pressure gradients to even out. More information on the influence of the leakage length can be found in Section 6.2.1.

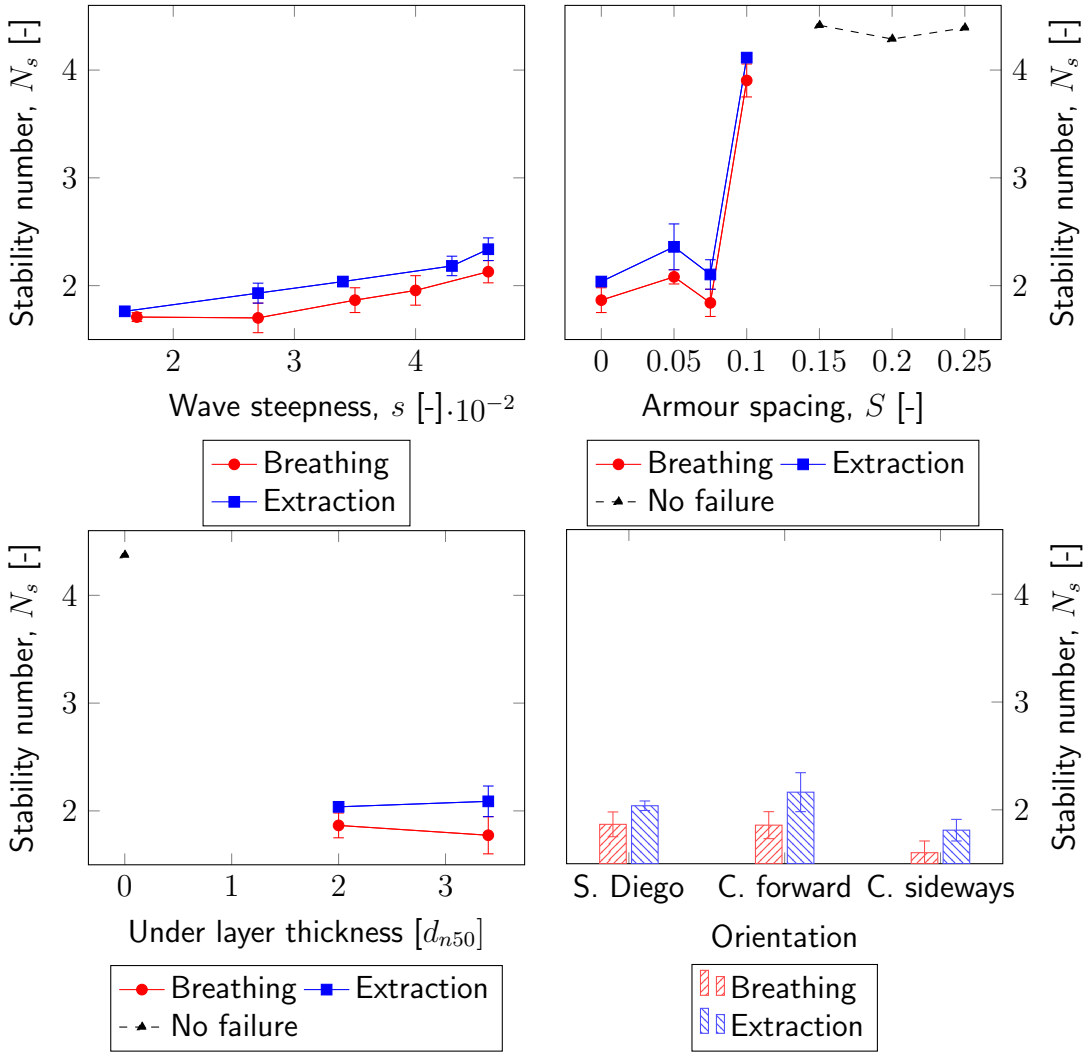

Figure 6.3: The influence of four different parameters on the stability of CoastaLock armour. The tests were executed with $s = 0.035$, $S = 0$, under layer thickness 2 d_{n50} and orientation San Diego, unless stated otherwise.

The results can be interpreted such that for all tests where the armour spacing is smaller than 10% and where there is an under layer present, the stability of the armour units is insufficient as it does not score as high as other blocks in use today. For example, a seaward slope with regular Xblocs does not test below $N_s = 3.2$ (Reedijk et al., 2005), whereas its minimum design value is $N_s = 2.2$ (Van den Bosch et al., 2012). This means that if CoastaLock already produces these test results for armour spacings below 10% on structures with an under layer, the design value for those conditions will not be able to match that of other blocks in use today.

A second interpretation of the results is that the stability of CoastaLock is sufficient or requires further research for spacings of 10% and larger and for a situation without an under layer.

For those situations, failure was not achieved and $N_s > 4$, which is comparable to other single-layer interlocking armour units like the XblocPlus, where a stability number $N_s > 3.8$ was found for its crest elements (Ruwiel, 2020) and no damage was observed to the slope for $N_s = 4.1$ (Reedijk et al., 2018). CoastaLock not showing damage for $N_s = 4$ for armour spacings of 10% and above can therefore be interpreted as a proof of concept, but more research would be needed in order to assess how competitive and promising CoastaLock actually is.

6.2.1 Comparison with literature and leakage length

As described in Section 2.3.1, Pilarczyk (2003) predicts the stability based on the leakage length of a breakwater. Similarly, when the stability number is known, an estimation of the leakage length can be made. This is done in this section, and the parameters used for calculating the leakage length based on Equations (2.2) and (2.3) can be found in Table 6.1.

Parameter	Value	Unit	Source
f	7.5	-	Assumed from Pilarczyk (2003)
D	0.034	m	Measurement
ξ	3.33	-	Section 3.4.1
b_f	0.01668	m	Section 3.4.3
k_f	0.45	-	Assumed from CIRIA, CUR and CETMEF (2007)

Table 6.1: Parameters used for estimating layer permeability and leakage length of CoastaLock armour.

Consecutively, Equations (2.2) and (2.3) are fitted to the data for every spacing individually using a Least Squares Error method and keeping k' as variable. This returns the values for k' and Λ as shown in Table 6.2.

Spacing	k' [m]	Λ [m]	Spacing	k' [m]	Λ [m]
0.00	0.023	0.106	0.10	>0.221	<0.034
0.05	0.043	0.077	0.15	>0.221	<0.034
0.075	0.060	0.065	0.20	>0.221	<0.034
			0.25	>0.221	<0.034

Table 6.2: Derived values for top layer permeability and leakage length.

The values for the small spacings represent the expectations from the stability tests: the permeability is small and the leakage length is relatively long. As blocks are spaced further apart, the leakage length decreases and the permeability increases. These changes happen more or less proportionate to the spacing increase.

For full packing of the armour layer, the leakage length was determined to be 10.6cm, which is roughly three times the D of the block. For a spacing of 7.5%, the leakage length becomes roughly twice the D of the block at 6.5cm.

The k' and Λ values for spacings of 10% and larger could not be derived using this method, as the leakage length becomes smaller than the block size for this case. Equation (2.3) is limited to a maximum $\frac{D}{\Lambda} = 1$. This means that the permeabilities for spacings 10% and above are larger than 0.221, and the leakage lengths smaller than 3.4cm (one D of a block), but that for the exact derivation of these parameters a different method needs to be used.

6.3 Theoretical prediction of stability

As shown in Table 6.2 and Figure 6.3, the point of failure of large armour spacings is still unknown. From the leakage length theory, a model can be built in order to make an estimate of the theoretical stability numbers of the CoastaLock armour unit.

The theoretical situation can be schematised as shown in Figure 6.4. Figure 6.4 resembles the top of the armour layer with the wave loading and pressure difference over the top layer drawn in as well. It is important to realise that the moment where the layer fails first is during the maximum wave run down of the largest wave. For this reason, the wave height in Figure 6.4 is defined as $H = H_{max}$.

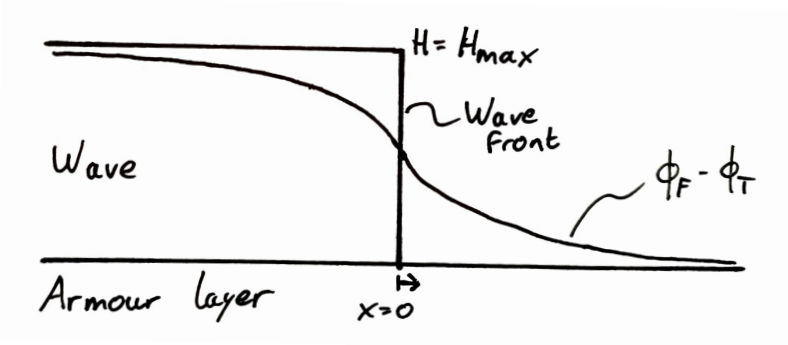

Figure 6.4: Schematisation of the pressure difference over the armour layer under wave loading, not to scale.

6.3.1 Pressure differences as a function of leakage length

According to Schiereck and Verhagen (2019), the pressure differences over the top layer can be described according to the second order differential equation as shown in Equation (6.1).

$$\phi_F - \phi_T = \Lambda^2 \frac{d^2\phi_F}{dx^2} \tag{6.1}$$

In the schematisation of Figure 6.4, it is assumed that the pressure difference over the top layer, $\phi_F - \phi_T$, is of the shape ae^{bx} for both sides of $x = 0$, and that both equations have the value $\phi_F - \phi_T = H_s$ at $x = 0$. It is also assumed that the pressure differences converge to $\phi_F - \phi_T = H_{max}$ at $x = -\infty$ and $\phi_F - \phi_T = 0$ at $x = \infty$.

With these assumptions and Equation (6.1), Equation (6.2) can be derived. For the full derivation, please refer to the step-by-step solution in Appendix F.

$$\phi_F - \phi_T = H_s \; e^{-\frac{x}{\Lambda}}, \qquad \text{for } x \geq 0 \tag{6.2}$$

6.3.2 Linking leakage length to armour stability

For critical stability, the forces on the armour units need to be exactly in balance. Once the forces are not in balance, movement of the blocks will occur. Failure, in the form of breathing, of the armour layer starts once the upward force on the blocks is just larger than the downward force on the blocks. The upward force consists of the uplift force caused by the pressure differences over the top layer (see Equation (F.5)). The downward force is the gravitational component perpendicular to the slope.

The point where breathing starts to occur is therefore when:

$$F_{down} = F_{up}$$
$$D \; (\rho_{CL} - \rho_w) \; \cos(\alpha) \; g = (\phi_F - \phi_T) \; \rho_w g$$

With Equation (F.5), taking the critical situation one block length away from the wave front ($x = D$):

$$D \; (\rho_{CL} - \rho_w) \; \cos(\alpha) \; g = H_s \; e^{-\frac{D}{\Lambda}} \; \rho_w g \tag{6.3}$$

This can then be rewritten into an expression for N_s based on the slope α, block diameter D and leakage length Λ, as shown in Equation (6.4).

$$\frac{H_s}{\Delta D} = \frac{\cos(\alpha)}{e^{-\frac{D}{\Lambda}}} \tag{6.4}$$

6.3.3 Linking leakage length to armour spacing

With Equation (6.4), N_s is now a function of the leakage length Λ for real leakage lengths of zero metres and larger. In order to predict the stability of the armour units, a relation between the leakage length Λ and the armour spacing S needs to be drafted.

According to Klein Breteler (2007), the leakage length can be described with Equation (6.5).

$$\Lambda = \sqrt{\frac{b_f \cdot D \cdot k_f}{k'}} \tag{6.5}$$

With b_f, D and k_f known constants, the permeability of the top layer k' can be derived using Darcy's Law (Atangana, 2018), which is shown in Equation (6.6).

$$Q = \frac{kA}{\mu L} \Delta p \tag{6.6}$$

This can be rewritten in terms of k':

$$k' = \frac{Q\mu L}{A\Delta p} \tag{6.7}$$

With parameter μ known, and the other parameters derivable from the physical model tests, k' can be calculated for every test and the theoretical stability can be calculated. This can then be used to predict the actual stability of the armour units during physical model testing.

When superimposed on Figure 6.3, the theoretical stability of the units is then expected to resemble Figure 6.5 (not to scale).

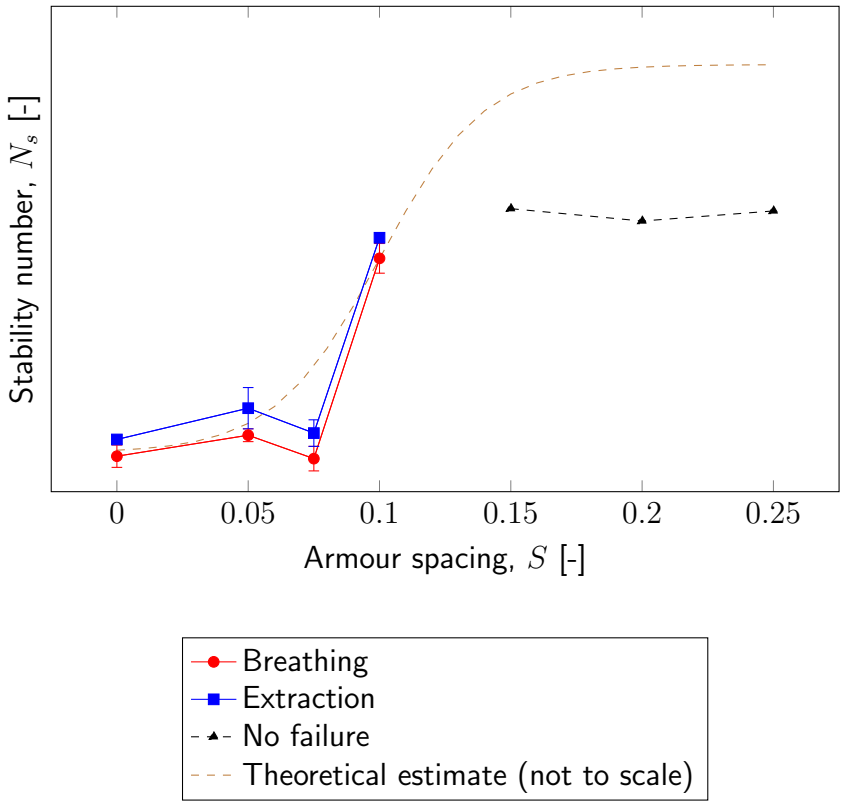

Figure 6.5: The influence of armour spacing S on the stability of the CoastaLock armour, with the theoretical estimate not to scale.

6.4 Stability with 3D Elevation Models

Since the deformations in the under layer are of such a large influence on the stability and failure of a structure, al Hanati (2022) wrote a separate BSc thesis in addition to this MSc thesis. The aim of the BSc thesis by al Hanati is to determine whether it is possible to measure under layer deformations with simple digital techniques and whether these techniques are able to register these variations before they can be seen with the naked eye.

For this research, al Hanati used 15 different photo sets of 60 photos, taken between the five test runs in the last test series conducted for this thesis (test 24 in Table 4.1). For every individual photo set, the photos were combined into a 3D point cloud using Autodesk ReCap Photo, scaled and translated in MeshLab and finally compared using a self made Python script.

Figure 6.6 below shows the first results of al Hanati (2022). From left to right, it contains a 30 centimetre wide central section from the models of the situation after test runs 0 up to and including 4. These simulations show a clear image of the CoastaLock armour layer and progressive deformation of the armour layer over the different runs. The first conclusion of al Hanati is therefore that it is possible to identify deformations in the under layer with a digital photographic technique like this.

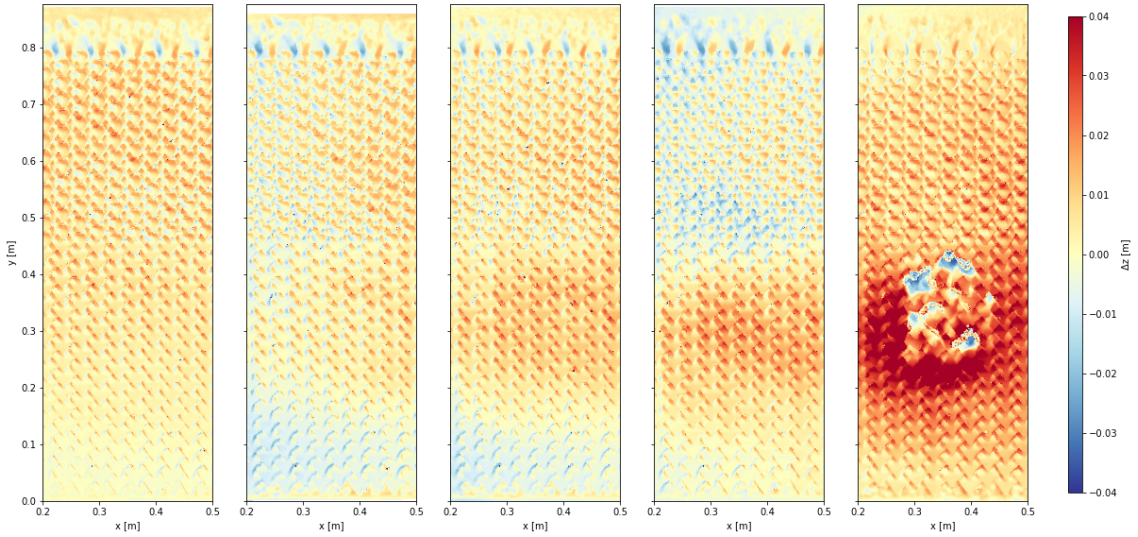

Figure 6.6: 3D elevation models relative to a fictional reference plane, generated after every run of test 24. From left to right: run 0 up to and including run 4.

Around the first run, the shakedown run, three digital models were made to assess the accuracy of the model. The mean of these models was calculated, and used as the fictional plane that served as the reference position for the armour units. Deformations shown in Figure 6.6 are relative to this fictional plane and the average deformations and visual observations from this thesis are listed in Table 6.3 below.

Run	Avg. deformation [mm]	Visual observation
0	0.37	-
1	0.34	-
2	2.11	Start breathing
3	3.08	Heavy breathing
4	12.06	Extraction

Table 6.3: Average deformations relative to the fictional reference plane and visual observations made during the tests conducted for this MSc thesis.

By comparing the relative distance of the three models made around the shakedown test to the fictional plane, al Hanati (2022) showed that this digital photographic method has a standard deviation σ of around 1mm. The maximum deviations were estimated to be around 3mm. The conclusion is therefore that the estimates were not yet accurate enough in order to detect deformations of the armour layer before they were noticed with the naked eye. However, as the error was largest around the boundaries of the model, it was suggested that the accuracy of the model could be improved if the photo sets were expanded, in particular with more photos of the boundaries, and if better reference markers were applied. For more information, please refer to the BSc thesis by al Hanati (2022).

6.5 Reflection

Figure 6.7 below shows the measured coefficients of reflection for the different tests performed. These reflection coefficients are the average of all measured reflection coefficients for tests with $0.058 \leq H_s \leq 0.078$ ($1.5 \leq N_s \leq 2$), as these significant wave heights were used in all tests and therefore allow for comparison under similar circumstances.

6.5.1 Differences between wave gauges

The first feature that stands out is the difference between wave gauge set 1 (WG1) and wave gauge set 2 (WG2). As described in Chapter 3, wave gauge set 1 is placed near the wave generator and wave gauge set 2 is placed near the structure. The measurements with WG1 consistently produce a lower coefficient of reflection throughout all tests, and this effect can be explained by making the assumption that some wave energy is lost (e.g. due to friction or wave breaking) in the flume between the two sets of wave gauges.

As wave gauge set 2 is placed close to the structure and little energy dissipation has occurred before the measurement, the reflection data from wave gauge set 2 can be considered 'true' and the data from wave gauge set 1 can be used as validation.

6.5.2 Influence of hydraulic parameters on reflection

The second feature that stands out is the fact that the reflection coefficient depends the most on wave steepness. This theory has widely been described before, and as can be seen in Muttray et al. (2006), all 10 considered reflection formulae derived between 1974 and 2006 are dependent on the wave steepness through a breaking parameter that includes wave steepness.

The armour spacing also appears to be of influence on wave reflection, as when the spacing (permeability and macro-roughness) of the layer increases, the reflection coefficient goes down. This is also described by Van der Meer (1992), but Figure 6.7 shows that its influence on the total reflection coefficient of the layer.

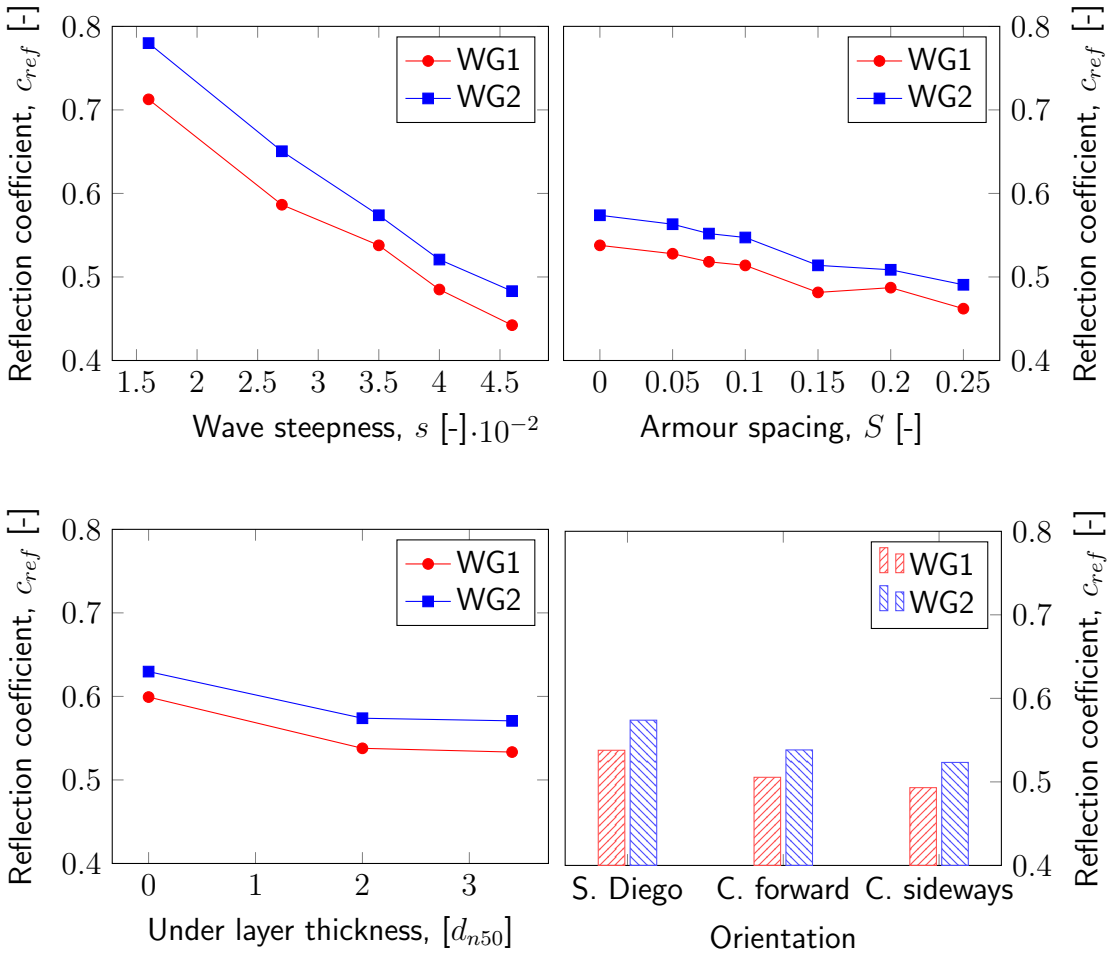

Figure 6.7: The influence of four different hydraulic parameters on the coefficient of reflection of CoastaLock . The tests were executed with $s = 0.035$, $S = 0$, under layer thickness 2 d_{n50} and orientation San Diego, unless stated otherwise.

Furthermore, the under layer thickness does not seem to be of influence on the reflection coefficient of a CoastaLock armour layer as long as there is one. When the under layer is removed, the units rest directly on an impermeable slope and reflection increases.

Finally, the orientation of the unit (micro-roughness) and the position of the cavity seem to be of minor influence on the coefficient of reflection of the structure. However, these results are unexpected. The cavity facing sideways was expected to yield the highest coefficient of reflection, as the smoothest side of the units faces forward in this orientation. The cavity forward orientation was then expected to be the least reflective, with the San Diego orientation being somewhere in between.

The unexpected results for this parameter could potentially be explained by small unintended variations in wave steepness or armour spacing between the tests, as minor disparities in these parameters of major influence will probably cause larger variations in the results than the orientations will.

6.5.3 Comparison with literature

In this section, the results of the wave steepness and unit spacing tests will be compared with earlier literature studies that are described in Section 2.5.

Wave steepness

Firstly, the two equations that are not dependent on armour permeability can be drawn into the graph for the reflection coefficient based on the wave steepness. These are Equations (2.7) and (2.8), taken from Muttray et al. (2006) and Muttray and Oumeraci (2003). As stated in Section 2.5, the former was designed for porous rubble mound breakwaters, which is why it underestimates the amount of reflection coming from the CoastaLock placed block revetment with impermeable core. The latter equation, Muttray and Oumeraci (2003), is applicable to impermeable slopes and therefore overestimates the amount of reflection induced by the CoastaLock structure.

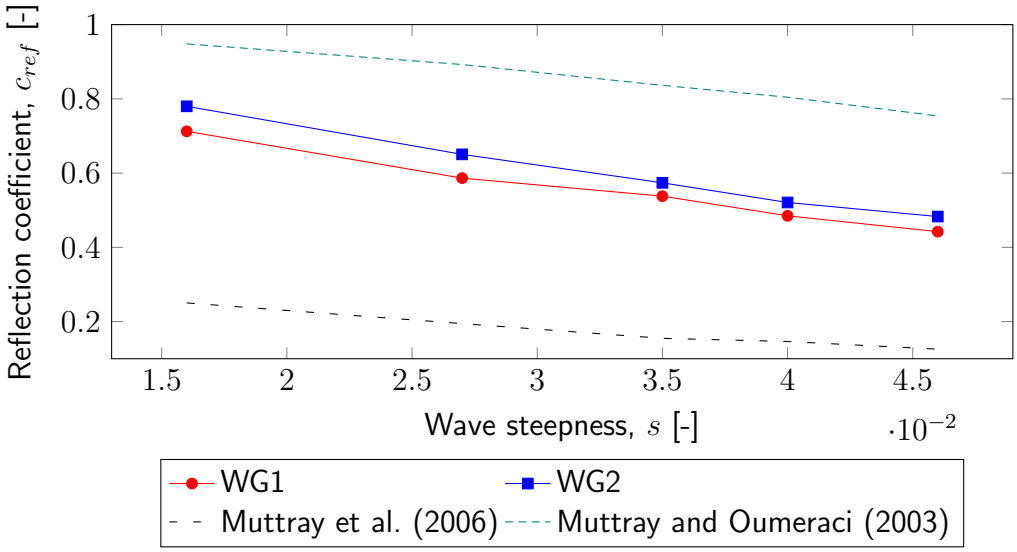

Figure 6.8: Comparison of the wave steepness results to literature. The tests were executed with $S = 0$, under layer thickness 2 d_{n50} and orientation San Diego.

Unit spacing

Secondly, the Van der Meer (1992) equation (Equation (2.6)) can be drawn into the graph with the results for spacing of armour units. It must be noted that the permeability P as used in the Van der Meer equation does not equal the spacing of the armour units, as the former is an empirical parameter for the permeability of an armour layer, and the spacing of armour units as used in this thesis is an indication of the proportion of slope surface not covered by CoastaLock units.

Due to this difference it can also be seen that Equation (2.6) is a conservative, but not an accurate estimate of the reflection coefficient of CoastaLock armour units with different spacings.

In Figure 6.9 below, the Van der Meer equation is portrayed using $P = 0.1$ for armour spacings smaller than 10%, as values for P smaller than 0.1 are not allowed, and $P = 0.1$ therefore gives the largest possible value for the coefficient of reflection. P is assumed to be equal to the armour spacings for spacings larger than 10%.

This is because the permeability of the layer will increase with more spacing, and the reflection coefficient should go down too, making the behaviour of the coefficient of reflection of Van der Meer slightly more realistic.

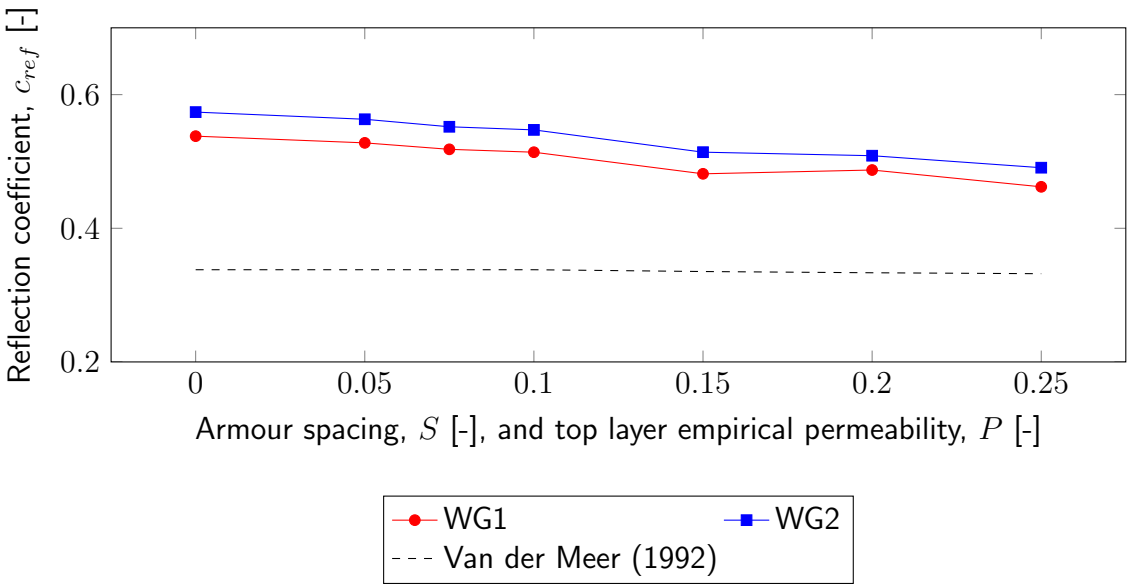

Figure 6.9: Comparison of unit spacing results to literature. The tests were executed with $s = 0.035$, under layer thickness 2 d_{n50} and orientation San Diego.

6.5.4 Derivation of equation for reflection

Finally, a single equation is fitted through the steepness and spacing results. The under layer thickness is not taken into account, as it is assumed that its effect is negligible for armour layers with an under layer.

An orientation factor could be introduced for the different orientations used, but as was theorised in Section 6.5.2, the influence of the micro-roughness of these blocks is potentially also negligible compared to the macro-roughness of the layer (unit spacing). It is for that reason, for simplicity and practicality of the formula that it was decided to focus only on wave steepness and armour spacing.

For the contribution of the wave steepness, Equation (2.7) (Muttray et al., 2006), is chosen as it matches the slightly convex shape of the reflection coefficient, and Equation (2.8) (Muttray and Oumeraci, 2003) shows some slightly concave behaviour. Also, (Muttray and Oumeraci, 2003) is a less practical and less applicable equation as it is designed for impermeable structures, which is not the case for CoastaLock armour with some degree of spacing.

The contribution of the armour spacing can be quantified with a straight linearly fitted line, as this is more accurate than Equation (2.6) (Van der Meer, 1992). A line with slope -0.37 and intercept 0.58 will have a mean error of $4.1 \cdot 10^{-3}$ with a standard deviation of $\sigma = 3.16 \cdot 10^{-3}$. Van der Meer (1992) also has multiple physical and theoretical imperfections when used to quantify the influence of armour spacing on the coefficient of reflection.

The two contributing factors are added up and their parameters are optimised by performing a weighted Least Squares Error method, ultimately coming to Equation (6.8), which describes the measured data optimally and therefore gives a good estimate of the influence of wave steepness and block spacing on the reflection coefficient associated with the CoastaLock armour unit.

$$C_{r,CoastaLock} = 0.2 + 2.34 \cdot C_{r,M} - 0.25 \cdot S \tag{6.8}$$

With S the armour unit spacing and $C_{r,M}$ the reflection coefficient according to Muttray et al. (2006) (Equation (2.7)).

Equation (6.8) has a mean error of 0.6% and a standard deviation of that error of 0.46%. It is visualised in Figure 6.10. The connecting lines between the measurements of WG1 and WG2 are left out for clarity reasons.

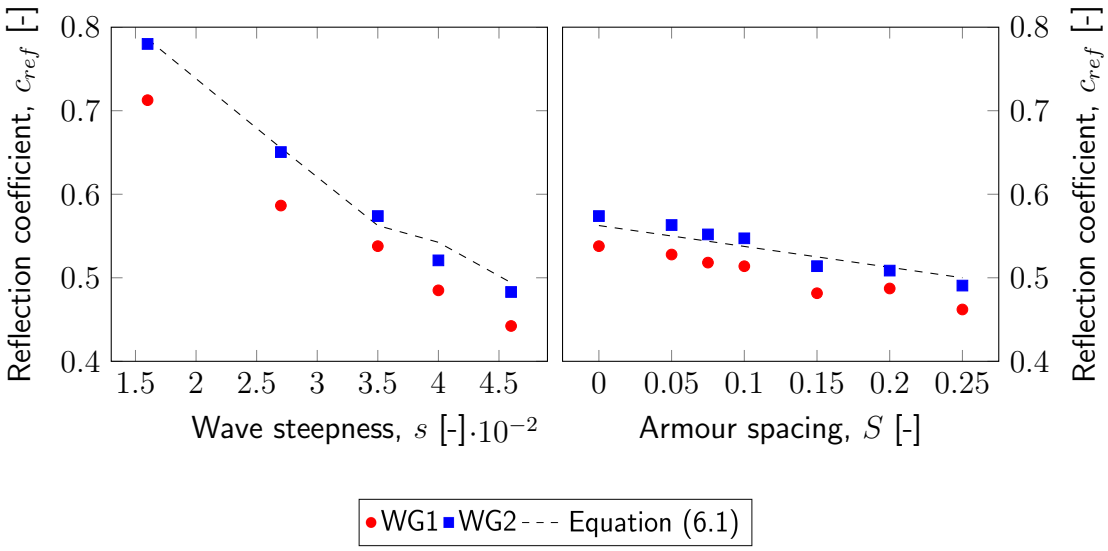

Figure 6.10: Comparison of Equation (6.8) to the test data. The tests were executed with $s = 0.035$, $S = 0$, under layer thickness 2 d_{n50} and orientation San Diego, unless stated otherwise.

Equation (6.8) can also be validated against tests 18, 21 and 23 from the test programme (see Table 4.1), as these tests are combinations of block orientations, armour spacings and wave steepnesses and will therefore serve as a first indication towards the accuracy of Equation (6.8) outside the dataset that it was based upon.

Figure 6.11 shows the measured reflection coefficients from these tests versus the calculated reflection coefficient with Equation (6.8). It must be noted that the tests in Figure 6.11 were not part of the dataset used to derive Equation (6.8).

What is interesting to see about Figure 6.11 is that Equation (6.8) makes a reasonably accurate estimate of the real reflection coefficient, albeit slightly higher than the measured coefficient of reflection. It must be noted though that this validation is only done on these three data points, which may have errors of their own. An example of this is the fact that the reflection coefficient at WG1 for test 23 is larger than that for WG2, suggesting that the wave spectrum gained energy whilst travelling away from the structure. It is therefore recommended to do some further research into validating Equation (6.8).

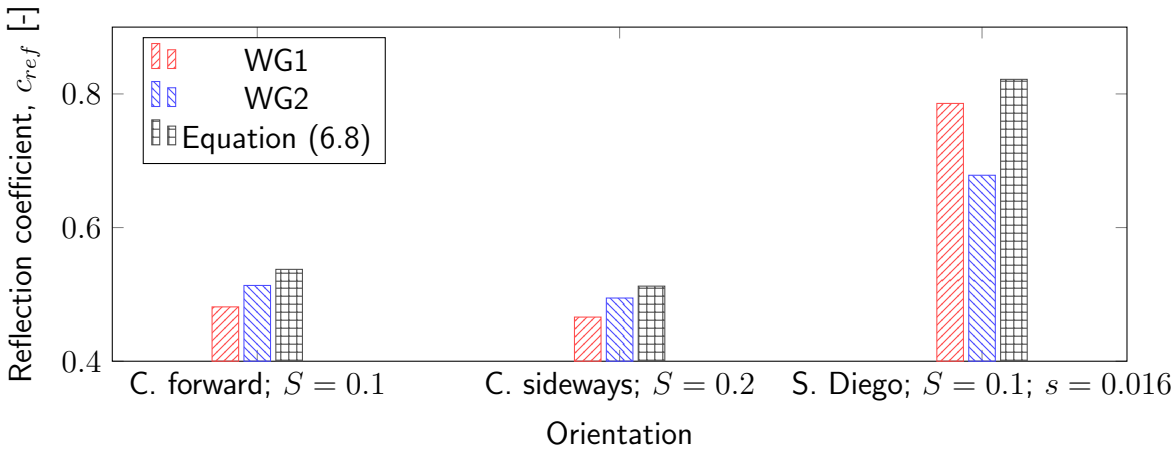

Figure 6.11: Validation of Equation (6.8) against tests 18, 21 and 23. The tests were executed with $s = 0.035$, $S = 0$, under layer thickness 2 d_{n50} and orientation San Diego, unless stated otherwise.

6.6 Overtopping

The first results of the overtopping performance of the CoastaLock armour units is displayed in Figures 6.12 and 6.13, after which the results are analysed and compared to Equation (2.11) (EurOtop, 2018) in Section 6.6.2.

6.6.1 Influence of hydraulic parameters on overtopping

The first thing that stands out is that the overtopping data for unit spacings of 10% and above have to be ommitted from Figure 6.12, since they require a different scale to be viewed (see Figure 6.13). Secondly, the values of the overtopping discharge for all tests with block spacings smaller than 10% are very small, in the order of 10^{-2} l/m/s. According to the Froude scaling theory from Frostick et al. (2011), the overtopping discharge can be scaled according to Equation (6.9).

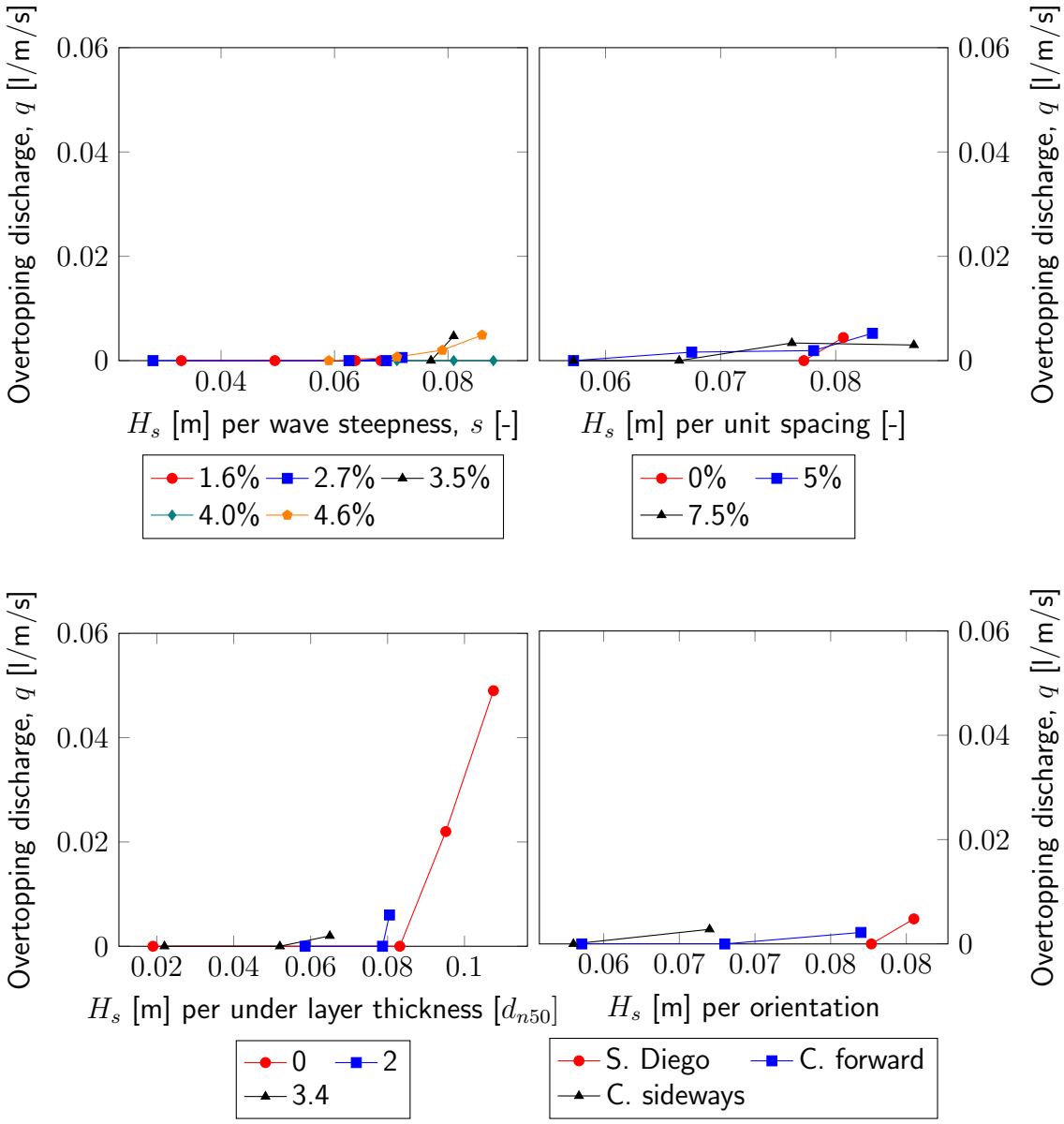

Figure 6.12: The influence of four different parameters on the overtopping volumes of CoastaLock armour. The tests were executed with $s = 0.035$, $S = 0$, under layer thickness 2 d_{n50} and orientation San Diego, unless stated otherwise.

$$\frac{L}{m \cdot s} \propto \frac{\lambda^3}{\lambda \cdot \lambda^{\frac{1}{2}}} = \lambda^{\frac{3}{2}} \tag{6.9}$$

Equation (6.9) would mean that an overtopping discharge in the order of 10^{-2} l/m/s in the model ($\lambda = \frac{1}{0.02675}$ as compared to ECOncrete Tech Ltd. (2021)) would mean a discharge in the order of 2 l/m/s on a prototype slope with CoastaLock armour units. This is significant already, as limits for overtopping can sometimes be set as low as 0.03 l/m/s (Besley and Michel, 2009), see Section 2.6.

However, the measured overtopping volume is very small and comes with a large amount of uncertainty for that reason. Moreover, only 2 to 4 data points of overtopping per test series are available, which increases uncertainty of the measurements and inaccuracy of a potential prediction. This, in combination with the fact that the overtopping discharge for armour spacings of 10% and more are of a different magnitude than other spacings suggests that overtopping does not play a dominant role in block spacings smaller than 10%, and that the armour layer fails due to other causes before the wave heights become large enough to induce problematic overtopping.

Large armour spacings

This is not the case for armour spacings of 10% and above, as more nonzero data points are available, overtopping volumes are larger and overtopping becomes a dominant mechanism (for spacings 10% and above, no failure was achieved. See Section 6.2). Therefore only overtopping values for armour spacings of 10% and above are considered from here on.

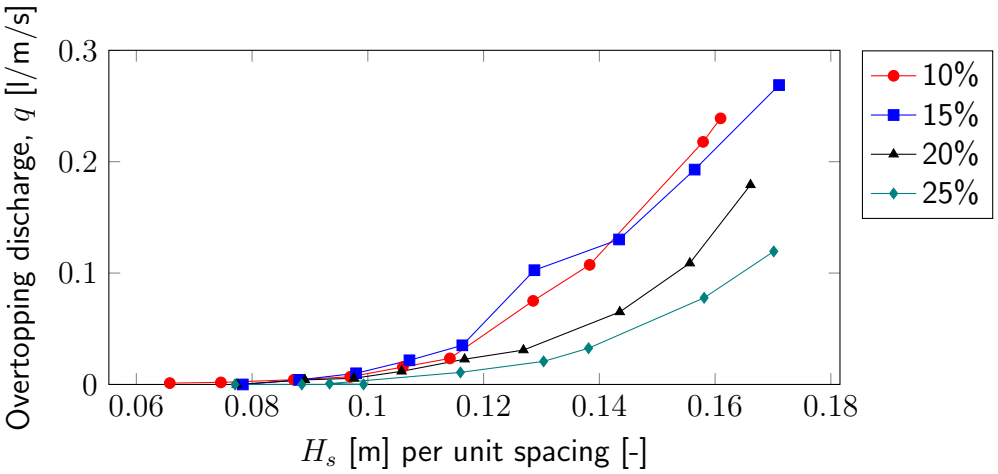

Figure 6.13: The influence of large armour unit spacings on the overtopping volumes of CoastaLock armour. The tests were executed with $s = 0.035$, under layer thickness 2 d_{n50} and orientation San Diego.

6.6.2 Derivation of roughness parameter

Finally Equation (2.11) from EurOtop (2018) is plotted against the overtopping results of CoastaLock and the roughness factor γ_f is derived. This is important as γ_f is an industry standard that will allow for an easy comparison with other armour units and practical application. In practice, due to the non-breaking nature of the waves used in this test, γ_f is solely derived using Equation (2.11b). γ_f is found with a Least Squares Error method and is applied to the data of every spacing individually with the roughness factor as only variable, producing the roughness factors as shown in Table 6.4.

Spacing	$\gamma_{f,CL}$
0.10	0.732
0.15	0.704
0.20	0.666
0.25	0.610

Table 6.4: Roughness factors for Equation (2.11) (EurOtop, 2018) from CoastaLock physical model testing.

Unfortunately, Table 6.4 only contains four data points on $\gamma_{f,CL}$ so no clear statement or equation that describes the behaviour of $\gamma_{f,CL}$ can be drawn up yet. When these roughness factors are applied to Equation (2.11) and plotted against the test data in Section 6.6.2, it must also be noted that either the test data on which it is based or $\gamma_{f,CL}$ itself does not seem to be very accurate for low wave heights and small wave spacings.

In other words, what can be seen in this figure is that Equation (2.11) with $\gamma_{f,CL}$ from Table 6.4 tends to underestimate the overtopping discharge for the smaller spacings and smaller wave heights, but that that effect decreases with increasing spacing or increasing wave heights. At the higher ends of those parameters the estimate even becomes slightly conservative.

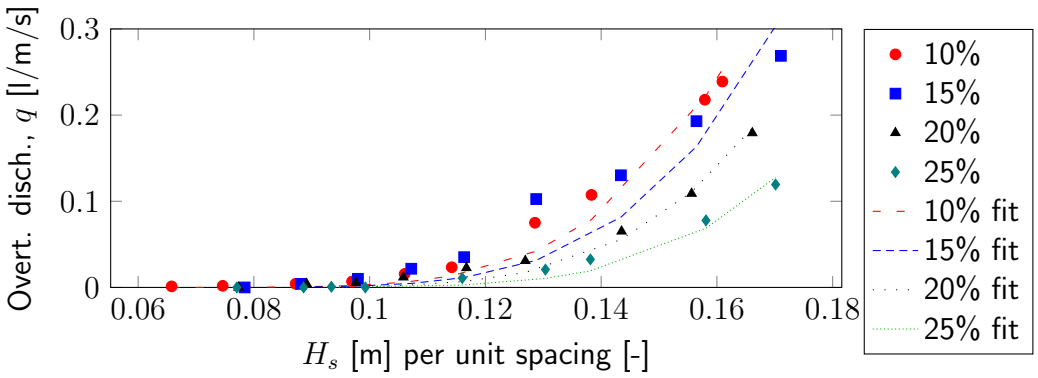

Figure 6.14: Fit of Equation (2.11)(EurOtop, 2018) to CoastaLock overtopping data with derived values for $\gamma_{f,CL}$. The tests were executed with $s = 0.035$, under layer thickness 2 d_{n50} and orientation San Diego.

Chapter 7

Discussion

The results and conclusions presented in this report should be interpreted as indicative rather than definitive. CoastaLock is a new concrete armour unit, with an unknown hydraulic behaviour. The research for this thesis consists of the first physical model tests done on the CoastaLock units and therefore aims to gather many different data sets on different parameters, in order to give a first indication on the general behaviour of CoastaLock armour units. The results and conclusions should therefore be interpreted as such.

7.1 Test programme

Due to the fact that these tests are the first, many factors around the CoastaLock units are still uncertain. An example of this is the failure modes of the CoastaLock armour layer. These have now been tested for deep water conditions without any berm effects, without construction of a realistic crest, on an impermeable core, on a straight slope and with normally incident waves. Therefore, the behaviour of CoastaLock elements under those conditions is still unknown. Other failure mechanisms might be possible, and may even be dominant, in different settings. Therefore the results of this research should be interpreted as an indication towards the behaviour of CoastaLock armour, and not as a definitive answer thereof.

7.2 Data collection

As stated in Section 5.2.4, the decomposition of the wave gauge signal is done according to two different methods, Mansard and Funke 3a (MF3a) and Goda and Suzuki (GS). MF3a uses three wave gauges for its spectral analysis, GS uses two. MF3a is widely regarded as the better, more accurate method to do this, and GS was intended to serve as a validation method.

However, as stated in Section 5.2.4, approximately 10% of the data generated with MF3a showed physically impossible values, with either reflection coefficients $C_{ref} > 1$, or significant wave heights of several metres.

Another 15% of the data showed improbable values, with reflection coefficients $0.85 \leq c_{ref} \leq 1$ or significant wave heights around a factor 10 higher than visual estimates of the significant wave height from the test videos. It can therefore already be assumed that at least 25% of the MF3a results do not resemble reality.

Inspection of the data generated with the Goda and Suzuki method did not reveal any such anomalies. Therefore, only the GS data was used to produce the results. This leads to a larger uncertainty concerning the test results, which is another reason why the results of this thesis must be interpreted as indicative rather than definitive.

7.3 Test results

The test results themselves also contain some discussion points. These are elaborated on below.

7.3.1 Overtopping

For example, the overtopping discharge for armour spacings below 10% is very uncertain. The wave generator needs to be switched of manually after the test duration has elapsed, which means that there can be a slight variation in the number of waves per test. Additionally, the measured discharges are so low for spacings below 10% (in the order of 2 or 3 litres per test) that this single extra overtopping wave can already alter the result. The overtopping test results for armour spacings below 10% are therefore not considered in the analysis in Section 6.6 and should be approached with a large degree of uncertainty.

7.3.2 Under layer thickness and block orientations

Secondly, very few data points are available to support any conclusions on the effects of under layer thickness and the influence of the block orientations on the hydraulic performance of CoastaLock armour units. As can be seen in Chapter 6, only three data points for the under layer thickness are available for every hydraulic parameter. This is not enough to accurately approach the behaviour of the CoastaLock units with an equation, and is therefore not done. The reader must therefore also be careful with drawing conclusions on the behaviour of the units as a result of under layer thickness.

Similarly, only one test was executed for every block orientation, and the results were not always as expected. An example of this is the results for reflection, where the rough cavity forward orientation has a higher coefficient of reflection than the smooth cavity sideways orientation. The combination of the two, the San Diego orientation, was even measured to yield the largest coefficient of reflection. An explanation of this could be that the influence of the orientation of the units could be very small and that variations of other parameters between those tests skewed the result. With only one test per orientation, there is not enough data to draw a solid conclusion on the influence of those orientations on the coefficient of reflection.

7.3.3 Predictive equation for the coefficient of reflection

The predictive equation for the coefficient of reflection should be approached with caution too. As can be seen in Figure 6.10, Equation (6.8) makes a jump between a wave steepness s of 3.5% and 4%, whereas the expectations, the theory and the data would predict something that would resemble a straight line. This can be explained by the fact that the measured wave length was used to fit and plot Equation (6.8) to the data rather than the theoretical deep-water wave length. An anomaly in the wave length due to the variation in the wave generator, the random wave generator script or a measurement error could therefore be the cause of this jump in Equation (6.8). It must therefore be approached with caution, and regarded as an indication rather than a definitive prediction of the behaviour of CoastaLock units.

7.4 Test analysis

The test analysis also shows some flaws on a few points. These are elaborated on below.

7.4.1 Leakage length for armour spacings above 10%

Firstly, Table 6.2 shows porosities and leakage lengths for armour spacings, whereas armour spacings of 15% and over never achieved failure. Therefore their stability number N_s is not known and, per definition, their porosity and leakage length are not known according to Pilarczyk (2003). These values are presented in Table 6.2, but the fact that they represent nothing more than a minimum porosity $k^{'}$ and a maximum leakage length Λ cannot be stressed enough.

Secondly, the theoretical prediction of stability displays many caveats as well. The simplification of the wave front on the armour layer in Figure 6.4 is very general and might therefore not accurately represent reality. Also, derivation of the parameters for the Darcy equation from the physical model tests might be inaccurate, and the method might need a different approach in order to link the leakage length to the armour spacing.

7.4.2 Validation against other research

Secondly, no literature is currently available to validate the approximations of the behaviour of CoastaLock based armour spacing. Van der Meer (1992) is actually not really applicable to the situation of large CoastaLock armour spacings; Van der Meer (1992) assumes empirical layer porosities of standard placed block revetments. Therefore Equation (6.8) can also not be validated, describing the data set obtained by this research but not being compared to any points outside of it.

Similarly, the new equation for reflection, Equation (6.8) is not validated against any points outside the data set. It can therefore not be used to predict the behaviour of other blocks than the CoastaLock armour units, nor can it be used to predict the CoastaLock behaviour outside the data set. Equation (6.8) really is only fitted to the data set obtained with this research and should be treated as such.

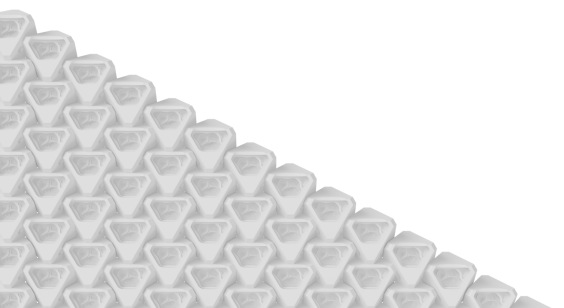

Chapter 8

Conclusion

With the growing urbanisation in coastal regions over the last decades comes an increase of shoreline alteration and (concrete) armouring of coastal areas, with a destruction of natural habitats as a result. ECOncrete Tech Ltd. have developed nature-enhancing quay walls, pile encasings, bed protections and tidal pool additions to rip-rap rock armour. Recently, they introduced a new single-layer interlocking concrete armour unit, the CoastaLock , for breakwaters, dykes and other slopes that require protection against incoming waves. However, little information is currently available about the hydraulic performance of these armour units. The objective of this thesis was therefore to answer the following research question:

> What is the hydraulic performance with respect to stability, overtopping and wave reflection of CoastaLock armour on a deep water impermeable slope?

This research question was subdivided into the four following sub-questions to aid with the answering of the main question.

1. What are the failure mechanisms of CoastaLock concrete armour units on a deep water impermeable slope, and when do they occur?

2. What is the influence of wave steepness, block spacing, under layer thickness and block orientation on the wave reflection of CoastaLock units?

3. What is the influence of wave steepness, block spacing, under layer thickness and block orientation on the stability of CoastaLock units?

4. What is the influence of wave steepness, block spacing, under layer thickness and block orientation on the overtopping of CoastaLock units?

This thesis used a literature study to breakwaters and revetments in combination with physical model testing to find answers to the research questions listed below. Those answers are presented in this chapter.

8.1 Failure mechanisms of CoastaLock

The CoastaLock armour units display a chain of failure mechanisms with the same root cause being large pressure differences over the armour layer. When CoastaLock armour units are packed tightly against each other, the lack of porosity in the armour layer causes the leakage length to be large, which 'traps' the water pressure in the filter. The difference in pressure over the armour then reaches its maximum when the wave run-down is maximum, causing a chain of failure mechanisms.

Firstly, the mechanism of breathing of the armour layer is observed. It describes the repetitive up-and-down movement perpendicular to the slope of the entire armour layer. Due to the interlocking nature of the layer, the pressure differences over the armour at maximum wave run-down cause for the whole layer to be lifted up before being put back down on the under layer by the next incoming wave. This process is then repeated as waves run-down and come in, and the movement of the layer resembles that of a human chest when breathing, hence the name for this mechanism.

This mechanism is not specific for CoastaLock, it is rather common for placed block revetments. However, it should be classified as a failure mechanism for a number of reasons. Firstly, because the repetitive up-and-down movement of the layer exposes the tightly interlocking armour units to large forces when rubbing against one another and making contact with the under layer. This behaviour can cause damage or breakage to the armour units and erosion in the under layer. Breathing also causes a deformation in the under layer, as during the cyclic up-and-down movement of the armour the under layer slides down and forms a concave S-curve, sometimes even exposing the core or filter material of the breakwater. The formation of a concave S-curve has previously been defined as a failure mechanism itself (Van den Berg et al., 2020). Moreover, deformations in the under layer should be prevented at all costs, as repairing them will require removal of the entire interlocking armour layer before repair, and reconstruction of it afterwards. Therefore, for all reasons mentioned above, the breathing behaviour of the CoastaLock layer should be classified as a failure mechanism.

The state of the armour layer consecutively deteriorates due to breathing, until extraction of an armour unit is reached. Once one armour unit has been displaced, the interlocking capabilities of the layer are lost and the hole in the armour layer quickly expands. Once initial extraction has been witnessed, damage increases exponentially and the layer collapses.

In conclusion, CoastaLock armour starts with exhibiting breathing, causing deformations in the under layer and dislocations of armour units, before finally showing extraction of armour units and collapse of the layer.

8.2 Stability of CoastaLock

In this thesis, the stability of CoastaLock is defined both by its breathing failure mechanism and its extraction point, with breathing occurring just before extraction does.

The stability of CoastaLock majorly depends on the porosity of the layer, which is controlled by the spacing of the armour units across the layer. For spacings (surface area of the under layer not covered by armour units) between 0% and 25% a clear distinction can be made. Spacings below 10% show insufficient stability of CoastaLock armour units when compared to other armour units in use today. However, for spacings of 10% and above, large stability numbers are reached. For spacings 15% and above, no failure of the armour units could be reached in this thesis.

When calculated with Pilarczyk (2003), test data yields the armour permeabilities and leakage lengths for the model tests as shown in Table 8.1 below. The values for spacings of 10% and higher could not be derived with this method, as the leakage lengths become smaller than the block size. For spacings of 10% and above it can therefore only be concluded that $k' > 0.221$ and $\Lambda < 0.034$m.

Spacing	k'	Λ	
0.00	0.023	0.106	$(\approx 3D)$
0.05	0.043	0.077	
0.075	0.060	0.065	$(\approx 2D)$
0.10			
0.15	>0.221	<0.34	$(< D)$
0.20			
0.25			

Table 8.1: Derived values for top layer porosity and leakage length.

Other factors have a minor influence on the stability of the blocks. The stability increases with wave steepness, but this effect is minor. The under layer thickness seems to have a negligible influence on the stability of the block, as long as there is one. No failure was reached for blocks placed directly on the impermeable core. However, very few data points are available to draw a concrete conclusion here. Similarly, the results suggest that the cavity forward orientation might be slightly more stable than the cavity sideways one, but very few data points are available here to draw a strong conclusion.

It is possible to predict the stability of high spacings of CoastaLock armour units from leakage length theory from data gathered during physical model tests. It is also possible to measure under layer deformations digitally using photographs. However, both methods still show caveats with respect to their accuracy.

8.3 Reflection of CoastaLock

The reflection of CoastaLock is mainly dependent on the steepness of the incident waves, showing reflection coefficients of up to 0.78 for waves with a steepness of 1.6%, and a reflection as low as 0.48 for a steepness of 4.6%. The reflection values for CoastaLock follow the trend of Muttray et al. (2006), but lie closer to those of Muttray and Oumeraci (2003).

Another factor that is of influence on the reflection of CoastaLock armour units, is the spacing of those units. As the spacing of armour units (at a wave steepness of 3.5%) increases from 0% to 25%, the reflection of those units decreases from 0.57 to 0.49. This is as a result of the increased porosity of the layer, which allows for more wave energy to penetrate the armour and be absorbed in the structure, rather than being reflected. The reflection coefficients as a function of armour spacing correspond with their expectation, but correlate poorly with existing literature such as Van der Meer (1992).

The wave steepness and armour spacing factors can be combined into a new single equation that describes both data sets accurately. This equation for the reflection coefficient of CoastaLock is based on the reflection coefficient by Muttray et al. (2006), $C_{r,M}$, and the spacing of CoastaLock armour units, S, and is shown in Equation (8.1).

$$C_{r,CoastaLock} = 0.2 + 2.34 \cdot C_{r,M} - 0.25 \cdot S \tag{8.1}$$

Furthermore, the under layer thickness and orientation of the units show minor influences on the reflection coefficient of CoastaLock armour. For example, the data suggests that CoastaLock armour placed directly on an impermeable slope yields a 10.5% increase in reflection coefficient compared to the situations where there is an under layer present. Nevertheless, the effects related to under layer thickness and orientation of the units are only minor compared to those of wave steepness and armour spacing, and not enough data points were available in order to draw concrete conclusions.

8.4 Overtopping of CoastaLock

The overtopping discharge of CoastaLock for all tests with armour spacings smaller than 10% is in the order of 10^{-2} l/m/s. Even though this could already be significant for the prototype CoastaLock units by ECOncrete, as this would scale up to an order of 2 l/m/s, the physical volume of overtopped water during the model tests was too small in order to draw a conclusion on the influence of wave steepness, unit spacing, under layer thickness or unit orientation on the overtopping reduction capabilities of the units. However, the conclusion can be drawn that for armour spacings lower than 10%, overtopping is not dominant for the overall behaviour of the layer with the crest height used in the physical model tests. This means that a CoastaLock armour layer will fail due to wave loading before overtopping becomes a problem.

For armour spacings of 10% and above, however, very large stability numbers were reached and overtopping became a dominant factor in the tests. Discharges in the order of 10^{-1} l/m/s were measured and therefore, for armour spacings of 10% and larger, relations between the unit spacings and the overtopping volumes could be derived. The data shows that the overtopping discharge has an exponential relation to the incoming significant wave height, but that the discharge is reduced as the unit spacing increases.

The relation between unit spacings of 10% and above and overtopping discharge can be expressed as described by EurOtop (2018). This is the most practical application as it allows for comparison with other armour units, but since this formula is applied to many armour units its accuracy to the data and CoastaLock in general is still uncertain. From EurOtop (2018), the following roughness factors for CoastaLock as shown in Table 8.2 have been derived.

Spacing	$\gamma_{f,CL}$
0.10	0.732
0.15	0.704
0.20	0.666
0.25	0.610

Table 8.2: Roughness factors for Equation (2.11) (EurOtop, 2018) from CoastaLock physical model testing.

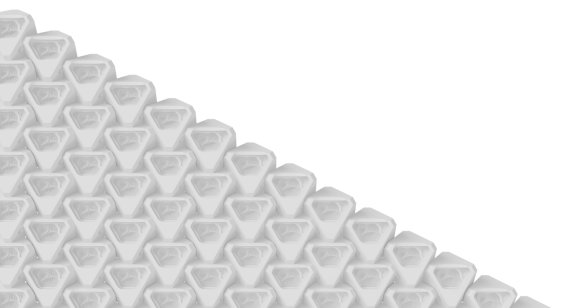

Chapter 9

Recommendations

For a new concrete armour unit that has just been subjected to its first exploratory research, naturally a lot of recommendations can be made. These concern an update of the design of CoastaLock armour units, further testing of these units, but also recommendations on improvements to the current tests based on Chapter 7 and research on placed block revetments in general. All of these recommendations are listed below.

9.1 Improvements to the current tests

Chapter 7 discusses multiple flaws of the executed physical model tests in detail. Some of these flaws can be addressed by introducing changes to the test programme and set up as used in this thesis. These are listed briefly below.

Predictive equation for CoastaLock armour behaviour Repeat the current tests to gather more data for the fitting of Equation (8.1), as it will increase its accuracy with respect to the behaviour of CoastaLock armour units in this setting.

Data collection Review or redesign the `decomp.m` MATLAB wave signal decomposition file so that the Mansard and Funke 3a method can be used reliably, or look into different decomposition software as a whole.

Overtopping To improve the accuracy of the measurements to small overtopping volumes, develop a method to extract the increase in water volume in the basin using a single wave gauge in the overtopping basin. Also, update the wave generator such that it stops automatically when the exact duration of the test has elapsed.

Uncertainty around under layer thickness and block orientations Repeat the tests on under layer variations and block orientations for greater accuracy. More different under layer thicknesses can also be used to gain a better understanding of the behaviour of CoastaLock units. The area of interest here would mainly be between an under layer thickness of 1 and 2 d_{n50}.

9.2 Further testing of CoastaLock

With the recommendations from Section 9.1, the tests as performed for this thesis can be improved upon. However, suggestions for future tests can also be made based on this thesis.

Different under layer sizes Firstly, more tests should be done with different under layer material sizes. With smaller under layer gradings, the under layer itself becomes thinner and therefore requires less and cheaper material. This means that the construction of the prototype under layer will become faster, cheaper and more environmentally friendly. A thinner under layer is also smoother, which reduces the micro-irregularities in the under layer, making it easier and more efficient to place CoastaLock units in a stable way. On the scale used for this thesis, smaller under layers were not possible due to scale effects in the under layer. Therefore, for smaller under layers relative to the CoastaLock armour units, larger scale tests should be used.

Overtopping Larger scale tests will also help quantify the smaller overtopping volumes with greater accuracy. With tests on a larger scale, the overtopping discharges are also larger, reducing the relative error and creating a more accurate view of the overtopping behaviour of CoastaLock armour units with small armour spacings.

Spacings The influence of armour spacing can also be researched further in the future. Tests would include more intermediate armour spacings (step sizes of 1% or 2% instead of 5%) to better assess the behaviour of CoastaLock units and generate a more accurate representation of the roughness parameter γ_f as a function of armour spacing.

Other test scenarios As stated in Section 7.1, CoastaLock armour might behave differently or even exhibit different failure modes under other conditions than tested for this thesis. Therefore it is recommended to also perform physical model tests with CoastaLock armour units on a breakwater with a permeable core, breakwaters with a berm or toe structure, or in shallow water conditions.

Crest Special attention for future tests must go to the performance of CoastaLock crest elements in future tests as well. No crest was constructed in the physical model tests for this thesis, but crest elements might have a reduced stability due to a lack of weight from blocks above them. Seperate crest elements might even need to be designed too. An example of this can be found in Ruwiel (2020), where crest elements for the XblocPlus were designed and tested. Ruwiel (2020) tests crest elements for low-crested breakwaters, so it is also recommended to look into the behaviour of CoastaLock crest elements on both high and low-crested breakwaters.

3D model tests and oblique incident waves 3D model tests are recommended to give some insight into the effect of obliquely incident waves on the CoastaLock armour units. Especially any potential extra uplifting effects around sideways placed elements in wave direction are interesting to research, as well as the potential loss in interlocking capabilities and stability around curved slopes such as breakwater heads.

Stability prediction from leakage length theory Predicting the stability of CoastaLock armour units from the theory of the leakage length is possible, but in this thesis a lot of simplifications and assumptions are made, and the method for determining the parameters for the Darcy equation has not been tested. It is therefore recommended to launch a full separate research focusing on two areas, one being a less simplified model and one being improving the link between the leakage length and armour spacing. A solid theoretical model, once accurate, can provide very valuable predictions on the behaviour of the units.

9.3 Design of CoastaLock

The findings of this thesis are also cause for recommendations towards redesigning the CoastaLock armour unit itself. The main lesson learned from the physical model tests is that the CoastaLock armour units are greatly sensitive towards the pressure differences over the top layer, and that these can be reduced by introducing a larger porosity or block spacing into the armour layer. In order to achieve this, two options can be entertained.

Option 1 Option 1 was designed by Holtzman and Bezner (2022), who were Industrial Designer and Head of Design at ECOncrete Tech Ltd. at the time. This concept was developed after consulting with the author of this thesis during the test phase of the project. Their solution to introduce more porosity to the armour layer was to introduce triangular cut outs in the side of the CoastaLock blocks.

The advantage of this is that the required amount of material per block is reduced, and that a large surface area of the blocks is still left over for interlocking and creating friction with other blocks. However, the shape of the block becomes more complicated and the amount of blocks required is not reduced. Moreover, larger armour spacings[1], say in the order of 25%, might be difficult to achieve with this method.

Option 2 Option 2 was entertained by Gutiérrez Martínez (2021), where external concrete components are added on to the blocks in order to keep them apart. This will require more material to be used per block, but less blocks to be placed per unit surface area of the slope. This will possibly reduce the overall material usage, project duration and labour cost. Option 2 also has a potential for achieving larger layer porosities than Option 1.

The disadvantages of Option 2 are that the armour units might have complicated shapes to produce, or that the external components are vulnerable and prone to breaking off. Option 2 is also likely to have a smaller contact area with other units, which will reduce its interlocking capabilities or friction.

[1]The term armour spacing was defined as the share of surface area of the under layer that is not directly covered by armour units. For this design option the amount of spacing will therefore indicate the surface area of the under layer exposed by making the cut outs in the side of the units, rather than the surface area exposed by moving the units apart.

Recommendation Both Option 1 and Option 2 seem to have some theoretical and technical feasibility and should therefore be explored. It is clear that the main issue with CoastaLock armour units now is the fact that they create large pressure differences over the top layer, and both options seem to address that. The recommendation towards ECOncrete is to mainly focus on this issue when updating their design and to discuss the choice for Option 1 or Option 2 with their technical staff, operational staff and biologists. These experts should be able to give a recommendation not only on the technical feasibility of the design of the unit, but also on the biological, practical and economical feasibility thereof.

Note on the practical application of armour spacing For updating the design of CoastaLock armour units, designers must realise that the leakage length over the top layer is a measure for the resistance to flow through the top layer, and that this should be kept small. Armour spacings were used in this thesis to give a quick approximation of the potential of a (semi) permeable CoastaLock armour layer. What this means in practice is that the channel shape and direction between the units also influences the leakage length. A horizontal channel, vertical channel or diagonal channel in between armour units all have different path or leakage lengths over the armour layer, and could therefore perform differently too. Similarly, channels that are smooth and straight will introduce less resistance to the flow between the blocks than rough channels with a lot of turns. The extent of these effects is expected to be minor, but unknown. Research into different design concepts is therefore advised.

Also, CoastaLock blocks with ECOncrete Admix are designed to enhance bio-growth on the blocks itself. A designer must realise that once bio growth occurs on the CoastaLock blocks, the effective diameter of the channel between two blocks will decrease, or the channel might even close up completely. A design team is advised to include or consult a marine biologist, to gain expert knowledge on the expected bio growth in the channels between armour units.

9.4 Research on placed block revetments in general

Finally, a common mechanism called breathing has been described in this thesis, that has not been described before. This thesis also advocates for the fact that breathing should be listed as a failure mechanism. For the general understanding of failure mechanisms of single layer interlocking placed block revetments, and this failure mode in specific, it is recommended to perform research focused on breathing of the armour layer with other single layer interlocking placed block revetments too. A range of tests with a variation in unit selection in terms of types and sizes would highlight the differences between these revetments, and could potentially offer more insight into the thresholds as well as the damage development for this failure mechanism.

Bibliography

Abankwa, N., Ossont, S., Scott, M., and Cox, S. (2015). Ship motion measurement using an inertial measurement unit. In *IEEE 2nd World Forum on Internet of Things (WF-IoT)*.

Acrystal Matériaux Composites (s.d.). *Datasheet Acrystal Aqua*. Accessed via polyester-shoppen.nl.

Airoildi, L. and Beck, M. W. (2007). Loss, status and trends for coastal marine habitats of Europe. *Oceanography and Marine Biology: An annual review 45*.

al Hanati, S. (2022). Ecological breakwater elements. Bachelor's thesis, Delft University of Technology.

Allaway, R. (2011). Marine Drive - Sea Wall, Rip-Rap and Accropodes. Via flickr.com.

Atangana, A. (2018). Chapter 2 - Principle of Groundwater Flow. In Atangana, A., editor, *Fractional Operators with Constant and Variable Order with Application to Geo-Hydrology*, pages 15–47. Academic Press.

Bakkenes, H. J. (2002). Observation and separation of bound and free low-frequency waves in the nearshore zone. Master's thesis, Delft University of Technology and Delft Hydraulics.

Barends, F. B. J. and Hölscher, P. (1988). Modelling interior process in a breakwater. In *Design of Breakwater, Proceedings of the Conference: Breakwater '88, Institution of Civil Engineers, Eastbourne*, pages 49–80.

Battjes, J. A. (1974). *Computation of set-up, longshore currents, rum-up and overtopping due to wind-generated waves.* PhD thesis, Delft University of Technology.

Besley, P. and Michel, D. (2009). *Single layer armour systems - toe, crest and roundhead details*, pages 128–141. Institution of Civil Engineers.

Bosch, A., Angremond, K., Verhagen, H., and Olthof, J. (2002). Influence of the density of placement on the stability of armour layers on breakwaters. *Coastal Engineering 2002: Proceedings of the 28th International Conference*.

Bulleri, F. and Chapman, M. G. (2010). The introduction of coastal infrastructure as a driver of change in marine environments. *Journal of Applied Ecology*, 47:26–35.

Burcharth, H. (1987). The lessons from recent breakwater failures. Developements in breakwater design. In *World Federation of Engineering Organizations Technical Congress, Vancouver 1987*.

Burcharth, H. (1997). *Reliability-Based Design of Coastal Structures*, volume 3, pages 145–214. World Scientific. print pages 37.

Burcharth, H. F. and Andersen, T. L. (2009). Scale effects related to small physical modelling of overtopping of rubble mound breakwaters. In *Coastal Structures 2007: Proceedings of the 5th international conference: Venice, Italy*, pages 1532–1541.

CIRIA, CUR and CETMEF (2007). *The Rock Manual. The use of rock in hydraulic engineering*. C683, CIRIA, London, 2 edition.

CLAS Certification (2018). clascertification.com. Accessed on October 20, 2021.

Copernicus Marine Service (s.d.). How to compute the mean wave period (mwp)? marine.copernicus.eu. accessed on may 25, 2022.

Creel, L. (2003). Ripple Effects: Population and Coastal Regions. *United States Population Reference Bureau*.

Dorst, K., Provoost, Y., and Verhagen, H. J. (2012). Stability of pattern placed revetment elements. In *8th international conference on coastal and port engineering in developing countries*.

ECOncrete Tech Ltd. (2021). CoastaLock Technical Product Information.

EurOtop (2018). *Manual on wave overtopping of sea defences and related structures. An overtopping manual largely based on European research, but for worldwide application*. Van der Meer, J.W.; Allsop, N.W.H.; Bruce, T.; De Rouck, J.; Kortenhaus, A.; Pullen, T.; Schüttrumpf, H.; Troch, P. and Zanuttigh, B.

Frostick, L., McLelland, S., and Mercer, T., editors (2011). *Users Guide to Physical Modelling and Experimentation: Experience of the HYDRALAB Network*. CRC Press/Balkema, leiden, The Netherlands.

Garcia, N., Richardson, S., and Rigden, T. (2013). *Physical Model Testing of the Hydraulic Stability of Single-layer Armour Units*, pages 122–130. Institution of Civil Engineers.

Gutiérrez Martínez, J. (2021). Discussions on CoastaLock model testing. ECOncrete Tech Ltd.

Hald, T. (1998). *Wave Induced Loading and Stability of Rubble Mound Breakwaters*. PhD thesis, Aalborg University.

Hasselmann, K., Barnett, T., Bouws, E., Carlson, H., Cartwright, D., Enke, K., Ewing, J., Gienapp, H., Hasselmann, D., Kruseman, P., Meerburg, A., Müller, P., Olbers, D., Richter, K., Sell, W., and Walden, H. (1973). Measurements of wind-wave growth and swell decay during the Joint North Sea Wave Project (JONSWAP). Technical report, Deutsches Hydrographisches Institut.

Holtzman, N. and Bezner, M. (2022). Conceptual design of CoastaLock armour units incorporating.

Kamali, B. and Hashim, R. (2009). Recent Advances in Stability Formulae and Damage Description of Breakwater Armour Layer. *Australian Journal of Basic and Applied Sciences*, 3(3):2717–2827.

Klaasman, H. (2005). Wave signal decomposition using MATLAB, the use of decomp.m in the TU Delft wave flume.

Klein Breteler, M. (2007). *Documentatie Steentoets 2007*. Onderzoeksprogramma Kennisleemtes Steenbekledingen: Rijkswaterstaat and Delft Hydraulics.

Klein Breteler, M., Mourik, G., and Provoost, Y. (2014). Stability of placed block revetments in the wave run-up zone. *Coastal Engineering Proceedings*, 1(34):structures.24.

Maia, A., Rodrigues, A., Lemos, R., Capitão, R., and Fortes, C. (2017). A web platform for the systematic monitoring of coastal structures. In *3rd International Conference on Geographical Information Systems Theory, Applications and Management*, pages 102–111.

Medina, J. R., Pardo, V., Molines, J., and Gomez-Martin, M. E. (2014). Armor porosity and hydraulic stability of mound breakwaters. *Coastal Engineering Proceedings*, 1(34):structures.11.

Moghim, M. and Lykke Andersen, T. (2015). Armor stability of hardly (or partly) reshaping berm breakwaters. *Coastal Engineering*, 104:1–12.

Muttray, M. and Oumeraci, H. (2003). Wave transformation at sloping perforated walls. In *Proceedings of the International Conference on Coastal Engineering*, volume 28, pages 2031–2043.

Muttray, M., Oumeraci, H., and ten Oever, E. (2006). Wave reflection and wave run-up at rubble mound breakwaters. In *International Conference of Coastal Engineering*.

Oxford University (2018). Urbanization over the past 500 years, 1500 to 2016.

Perkol-Finkel, S. and Sella, I. (2014). Ecologically Active Concrete for Coastal and Marine Infrastructure: Innovative Matrices and Designs. *Proceedings of the Institution of Civil Engineers*.

Perkol-Finkel, S. and Sella, I. (2015). Harnessing urban coastal infrastructure for ecological enhancement. *Proceedings of the Institution of Civil Engineers*.

Perkol-Finkel, S. and Sella, I. (2019). Blue Is the New Green: Eco-engineering for Climate Change. *Marine Technology Society Journal*, 53(4):7–10.

Pilarczyk, K. (2003). Design of revetments. Technical report, Rijkswaterstaat, Dienst Weg- en Waterbouwkunde.

Pilarczyk, K. and Klein Breteler, M. (1998). *Dikes and Revetments; Design alternative revetments + gabions*, chapter 16. Balkema, A.A.

Port of San Diego (2021). Port of San Diego and ECOncrete begin pilot project to boost coastal infrastructure and ecosystems on Harbor Island. Technical report, Port of San Diego.

Reedijk, B., Eggeling, T., Bakker, P., Jacobs, R., and Muttray, M. (2018). Hydraulic stability and overtopping performance of a new type of regular placed armor unit. *Coastal Engineering Proceedings*, 1(36):papers.111.

Reedijk, B. and Muttray, M. (2009). Design of Concrete Armour Layers. *Hansa International Maritime Journal*, 6:111–118.

Reedijk, B., Muttray, M., Vos-Rovers, I., and Bakker, P. (2005). Placement and Structural Strength of Xbloc and other Single Layer Armour Units. In *Proceedings of the conference of the Institution of Civil Engineers (ICE) on Coastlines, Structures and Breakwaters*.

Rijkswaterstaat and Stichting Toegepast Onderzoek Waterbeheer (2019). Publicaties Onderzoeksprogramma Asfaltdijkbekledingen. Technical report, inspectiewaterkeringen.nl.

Ruwiel, T. (2020). Crest stability of XblocPlus armoured breakwaters. Master's thesis, Delft University of Technology.

Schiereck, G. J. and Verhagen, H. J. (2019). *Introduction to bed, bank and shore protection*. Delft Academic Press / VSSD, second edition.

Sumer, B. and Fredsøe, J. (2000). Experimental study of 2d scour and its protection at a rubble-mound breakwater. *Coastal Engineering*, 40(1):59–87.

Van Alboom, W., Martínez, D., Correa, M., Fossati, M., Pedocchi, F., and Solari, S. (2018). Design of the scour protection layer for a breakwater in an estuarine environment. In *PIANC-World Congress Panama City*.

Van den Berg, I., Hofland, B., and Reedijk, B. (2020). Influence of irregularities in the rock underlayer on the stability of XblocPlus. *Coastal Engineering*, 157.

Van den Bos, J. P. and Verhagen, H. J. (2018). *Breakwater design*. Delft University of Technology.

Van den Bosch, I., Ten Oever, E., Bakker, P., and Muttray, M. (2012). Stability of interlocking armour units on a breakwater crest. *Coastal Engineering Proceedings*, 1(33):structures.11.

Van der Meer, J., van Hoven, A., and Steendam, G. (2010). Guidance on erosion resistance of inner slopes of dikes from three years of testing with the Wave Overtopping Simulator. *Coasts, Marine Structures and Breakwaters: Adapting to Change - Proceedings of the 9th International Conference*, 2.

Van der Meer, J. W. (1992). Conceptual design of rubble mound breakwaters. In *Proc. of the Short Course on Design and Reliability of Coastal Structures*, pages 447–510.

Van der Meer, J. W. and Bruce, T. (2014). New physical insights and design formulas on wave overtopping at sloping and vertical structures. *Journal of Waterway, Port, Coastal and Ocean Engineering*, 140(6).

Van Gent, M. and Van der Werf, I. (2017). Single layer cubes in a berm. In *Short Course and Conference on Applied Coastal Research (SCACR), Santander 2017*.

Vanneste, D. and Troch, P. (2013). A revision of the scaling method for core material in rubble-mound breakwaters. In *10th coasts, marine structures and breakwaters conference 2013: from sea to shore - meeting the challenges of the sea*, pages 112–121.

Vieira, F., Taveira-Pinto, F., and Rosa-Santos, P. (2020). Single-layer cube armoured breakwaters: Critical review and technical challenges. *Ocean Engineering*, 216:108042.

Wenneker, I. and Hofland, B. (2014). Optimal wave gauge spacings for separation of incoming and reflected waves. In *Coastlab 2014*.

Wolters, G., van Gent, M., ad Luc Hamm, W. A., and Muhlestein, D. (2009). Hydralab iii: guidelines for physical model testing of rubble mound breakwaters. In *Coasts, marine structures and breakwaters: Adapting to change: Proceedings of the 9th international conference organised by the Institution of Civil Engineers, Edinburgh*, pages 2–559.

Yagci, O. and Kapdasli, S. (2003). Alternative placement technique for Antifer blocks used on breakwaters. *Australian Journal of Basic and Applied Sciences*, 30(11):1433–1451.

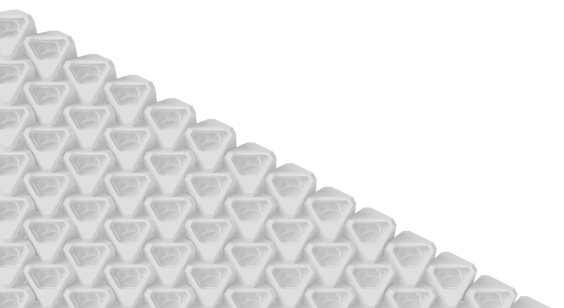

Appendix A

Revetment theory

Revetments are the protection layers on man-made slopes such as breakwaters in a coastal zone. They can be found in many different shapes and sizes on breakwaters, dykes, barrier islands, or on any other man-made slope on structures that protect a coast, beach or port.

A.1 Breakwater types

The fact that, slopes and revetments can be found on all kinds of structures, with different purposes and in different environments also means that they take on many different shapes and sizes. This is why background knowledge on different breakwater types is required for this thesis. Some different breakwater parameters are defined below.

A.1.1 Mound breakwaters

Mound breakwaters are among the most used breakwater types in Europe and North America, as they are easily applicable in shallow waters. A sketch of a standard mound breakwater is shown in Figure A.1. A few key differences between mound breakwaters are briefly highlighted below.

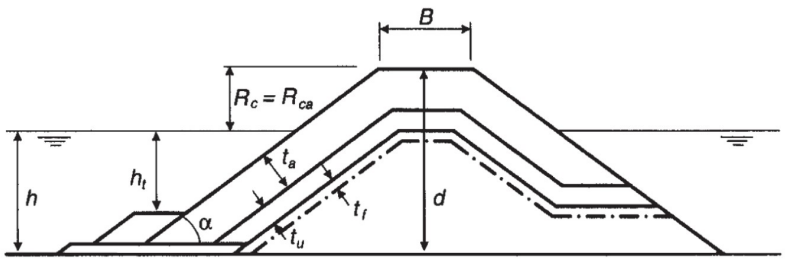

Figure A.1: A cross-section of a standard breakwater.

Permeability of breakwater cores

Breakwater cores can be constructed with either permeable (quarry run) or impermeable (sand or clay) core material. Impermeable defences either dissipate or reflect all incoming wave energy, they do not let anything through as opposed to permeable ones. Permeable defences block the short incoming wind waves, but will let long waves transfer energy through the structure. Permeable breakwaters are often found at port entrances, whereas impermeable breakwaters can be found in land reclamations.

Breakwater crest height

High crested defences have a crest height that is larger than the significant wave height ($\frac{R_c}{H_s} > 1$). In low crested structures this is not the case. As a result they come with a lot of wave overtopping, which exerts extra forces on the top rows of the armour. Low-crested breakwaters are usually used for situations where large overtopping volumes are allowed and are therefore mostly found offshore.

Definition of water depths

A slope situated in deep water will experience waves that are unaffected by bottom friction, shoaling, offshore wave breaking or other depth-related effects. It also means that the water is deep enough so that the incoming waves are unaffected by the toe of the structure. All of this is not the case for shallow water depths.

Deep water conditions occur when the local water depth is larger than half of the deep-water wave length, and shallow water depths occurs when the local water depth is smaller than a twentieth of the wave length (Schiereck and Verhagen, 2019). In between those, an intermediate or transitional water depth occurs. This is shown in Equations (A.1a) to (A.1c).

$$d > \frac{L_0}{2} \quad \text{(deep water)} \tag{A.1a}$$

$$\frac{L}{20} < d < \frac{L_0}{2} \quad \text{(transitional water depth)} \tag{A.1b}$$

$$d > \frac{L}{20} \quad \text{(shallow water)} \tag{A.1c}$$

The deep-water wave length, L_0, is defined by Equation (A.2).

$$L_0 = \frac{gT^2}{2\pi} \tag{A.2}$$

A.1.2 Monolithic breakwaters

Vertical, monolithic or caisson breakwaters are breakwaters that are constructed using caissons and are traditional in countries like Japan, where steep rocky coasts are the standard. These breakwaters are well suited for deep waters and their vertical impermeable walls are often cause for large overtopping discharges, so they are sometimes complemented with a so-called bullnose wall, which redirects splashing water back outwards. An example of a monolithic breakwater is shown in Figure A.2.

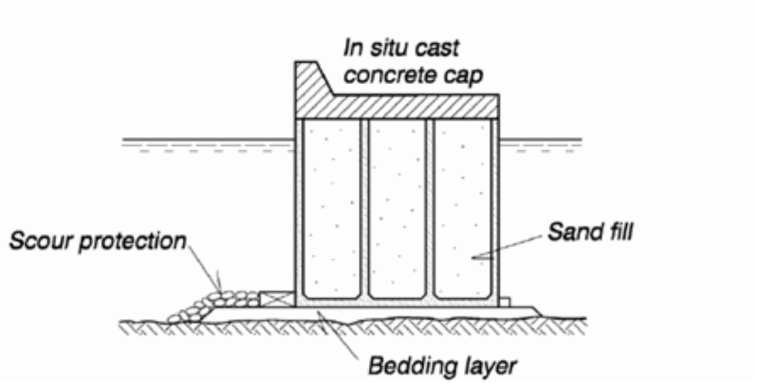

Figure A.2: Sketch of a simple monolithic breakwater (Maia et al., 2017).

A.1.3 Reshaping breakwaters

Reshaping, or Icelandic, breakwaters are breakwaters that change shape over their lifetime. When constructed, they might look somewhat like conventional rubble mound breakwaters, but the hydraulic loads on them will gradually move them into a stable concave S-shape. A sketch of such a reshaping breakwater is shown in Figure A.3.

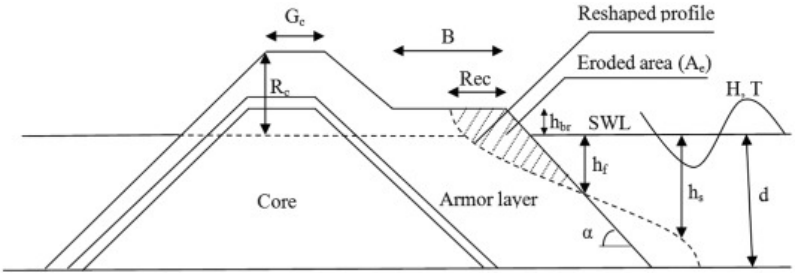

Figure A.3: Sketch of a standard reshaping or Icelandic breakwater (Moghim and Lykke Andersen, 2015).

A.2 Under and filter layers for mound breakwaters

As shown in Figure A.4, an under and filter layer are present in between the armour layer and the core material of a standard mound breakwater. This under layer provides drainage, and should consist of grains large enough to not be washed out from underneath the armour layer, but also small enough to keep the filter layer below in its place. Sometimes multiple layers are required, each one smaller than the next, until a proper size gradation through the layers is reached. However, more layers require more material and effort during construction, so an efficient balance needs to be found for the design of these layers. More information on the calculation of the under and filter layer for the physical model used for this thesis can be found in Chapter 3.

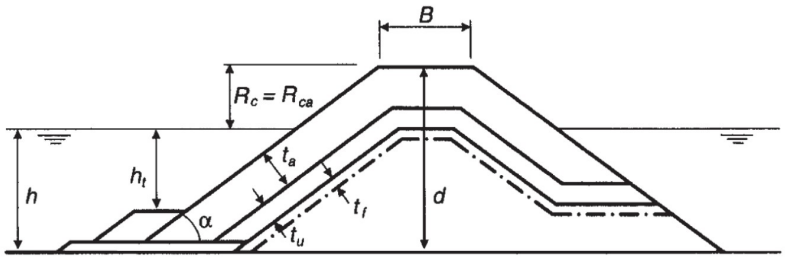

Figure A.4: A cross-section of a standard breakwater.

A.3 Stability

The forces on armour units can be classified into two categories: stabilising and destabilising forces. These are elaborated on in Appendices A.3.1 and A.3.2. In order for a block to be stable, i.e. in order for the block not to move, the forces on the block need to be in balance. The forces can be summarised in the three-dimensional balance equations as shown in Equations (A.3a) to (A.3f). These equations say that the summation of all forces on individual units in x (horizontal), y (horizontal, perpendicular to x) and z (vertical) and the rotational forces around these axes must all be equal to zero.

$$\Sigma F_x = 0 \quad \text{(A.3a)} \qquad \Sigma F_y = 0 \quad \text{(A.3b)} \qquad \Sigma F_z = 0 \quad \text{(A.3c)}$$

$$\Sigma T_x = 0 \quad \text{(A.3d)} \qquad \Sigma T_y = 0 \quad \text{(A.3e)} \qquad \Sigma T_z = 0 \quad \text{(A.3f)}$$

A.3.1 Stabilising forces

The stabilising forces working on CoastaLock are gravitational forces, surface friction and interlocking. In general, these stabilising forces depend on the slope angle and mass of the block.

Gravitational forces

Gravitational forces are the forces caused by gravity and the mass of the block, that pull the block down. The contribution of these forces are maximum for block placement on a horizontal surface, and zero for the placement of the blocks on a vertical one. In other words, the steeper the slope, the less gravity pulls the blocks into the slope. For normal breakwaters, gravitational forces are the main contributing factor to stabilising the blocks (Hald, 1998).

Friction

Another stabilising force is the surface friction between the blocks. A major contributing factor in placed block revetments such as Basalton or Hydroblocks (Dorst et al. (2012), see Figure A.5), surface friction between units is of a much smaller influence in rubble mound breakwaters. Surface friction depends on the contact area between them and the force that pushes the blocks together. Therefore, friction increases with the number of rows of blocks above a certain unit, as the total mass above the unit increases. Surface friction also increases with the angle of the slope, as the gravitational forces are more and more directed towards the lower blocks.

(a) Basalton (b) Hydroblocks

Figure A.5: Different types of placed block revetments (Dorst et al., 2012).

Interlocking

Armour units such as the Accropode (Figure A.6a) or the Xbloc (Figure A.6b) have as added advantage that they interlock, which means that they weigh each other down. This way, the weight of the blocks around a single unit contribute to the stability of that unit, resulting in the fact that the layer starts to behave more as a whole, instead of individual blocks.

CoastaLock armour units do this too, as can be seen in Figure A.7. The faces of the block that go from an edge of the top face to the point of the bottom face (marked in yellow) are used by other blocks to hold this one down. The sides going from a point of the top face to an edge of the bottom face (marked in blue) are used to hold other blocks down.

(a) Accropodes (b) Xblocs

Figure A.6: Different types of single-layer concrete armour units (CLAS Certification, 2018).

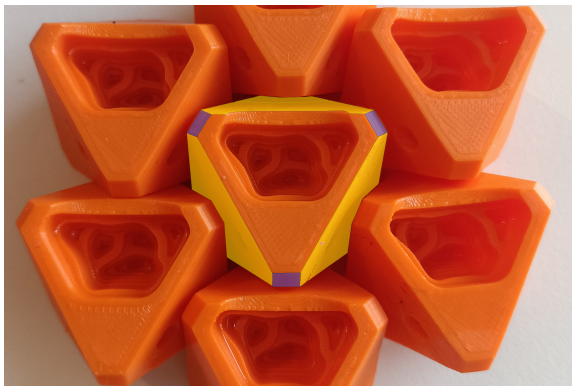

Figure A.7: Interlocking CoastaLock units, with highlighted faces. Blue faces hold other blocks down, yellow faces are used by other blocks to hold the centre block down.

A.3.2 Destabilising forces

Next to stabilising forces, there are also destabilising forces that act on the block. These forces are caused by the flow of water around and over the armour units and can be subdivided into internal and external forces. An overview of all the forces acting on a block is shown in Figure A.8.

External forces

The external destabilising forces working on the armour unit in Figure A.8 can be split up in three, and summarised in the Morris equations shown below (Hald, 1998). The drag force F_D, which is caused by the flow of water around the object. This can be either upwards parallel to the slope right after a wave impact, or downwards parallel to the slope right before a wave impact and is calculated according to Equation (A.4). For the definition of the symbols, please refer to the List of Symbols. Equation (A.4) shows that the drag force mainly depends on the flow velocity v and the cross-sectional area of the block A.

$$F_D \approx C_D \cdot \rho_w \cdot A_b \cdot v|v| \tag{A.4}$$

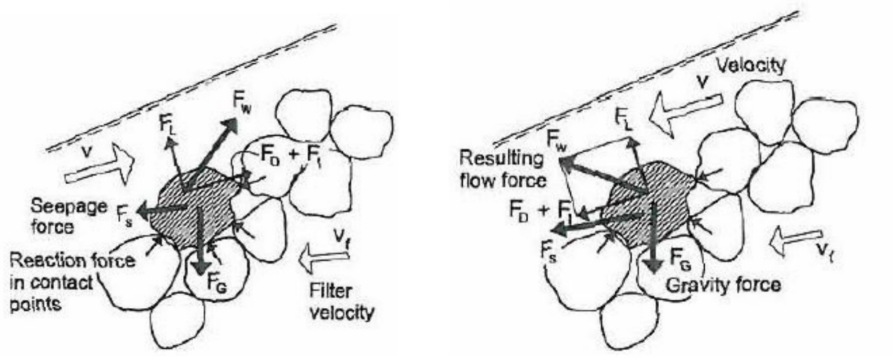

(a) During wave run-up (b) During wave run-down

Figure A.8: Forces acting on an armour unit (Hald, 1998).

The second external force is the lift force on the block. This is caused by the curvature of the flow around the armour unit (Schiereck and Verhagen, 2019) and also mainly depends on the cross-sectional area A and flow velocity v. Whereas drag forces act parallel to the slope, lift forces act perpendicular on the slope. Lift forces are defined as shown in Equation (A.5).

$$F_L \approx C_L \cdot \rho_w \cdot A_b \cdot v|v| \tag{A.5}$$

The final external force is the inertia force, which is caused by acceleration or deceleration of the flow (variation in speed over time), and is defined according to Equation (A.6).

$$F_I \approx C_I \cdot \rho_w \cdot V_b \cdot \frac{dv}{dt} \tag{A.6}$$

The combination of the drag, inertia and lift forces yields the total external forces acting on this armour unit. These forces depend on their coefficients C_D, C_I and C_L. These coefficients in their turn depend on the shape of the unit, as more streamlined units will experience less external forces, as well as the Reynolds number of the flow. The Reynolds number indicates whether a flow is laminar or turbulent, and since more laminar flows tend to increase the force on a unit, this affects the coefficients as well. Finally, the coefficients also depend on the Keulegan-Carpenter number K_C, which compares the length scale of the incoming wave to the length scale of the unit. Waves that are long tend to cause a steady current whilst passing the block, increasing the forces on it, whereas short waves exert relatively small forces on the unit.

Internal forces

Next to forces acting on the structure externally, internal forces are also present. According to Barends and Hölscher (1988), internal forces are the main driver of element displacement, as these forces cause the lifting up of armour units, only after which they are carried away by other forces. Internal forces, or seepage forces (F_s, as shown in Figure A.8) are mainly caused by the combination of pressure differences between the core material and the outside of the breakwater F_p and internal flow forces F_f (Hald, 1998). The more impermeable a core is, the larger the pressure differences between the inside and outside are, as pressure cannot flow out. This means that for (nearly) impermeable cores F_p is high, but F_f is low. For very permeable cores, this is the exact opposite, as there is a lot of flow but a very small pressure difference present. According to Hald (1998), the Forchheimer equation (Equation (A.9)) to determine the hydraulic gradient (pressure difference), after which the forces can be calculated according to Equations (A.7) and (A.8).

$$F_p \approx \frac{V_b}{1-n} \cdot \frac{dp}{dx} \tag{A.7}$$

$$F_f \approx \rho_w \cdot g \cdot \frac{V_b}{1-n} \cdot i \tag{A.8}$$

$$i = C_a \cdot v_f + C_b \cdot v_f|v_f| + C_c \cdot \frac{\delta v_f}{\delta t} \tag{A.9}$$

Appendix B

Wave theory

B.1 Definitions

For understanding this thesis, a few simple but key definitions of a wave signal need to be repeated. These are illustrated in Figure B.1 below.

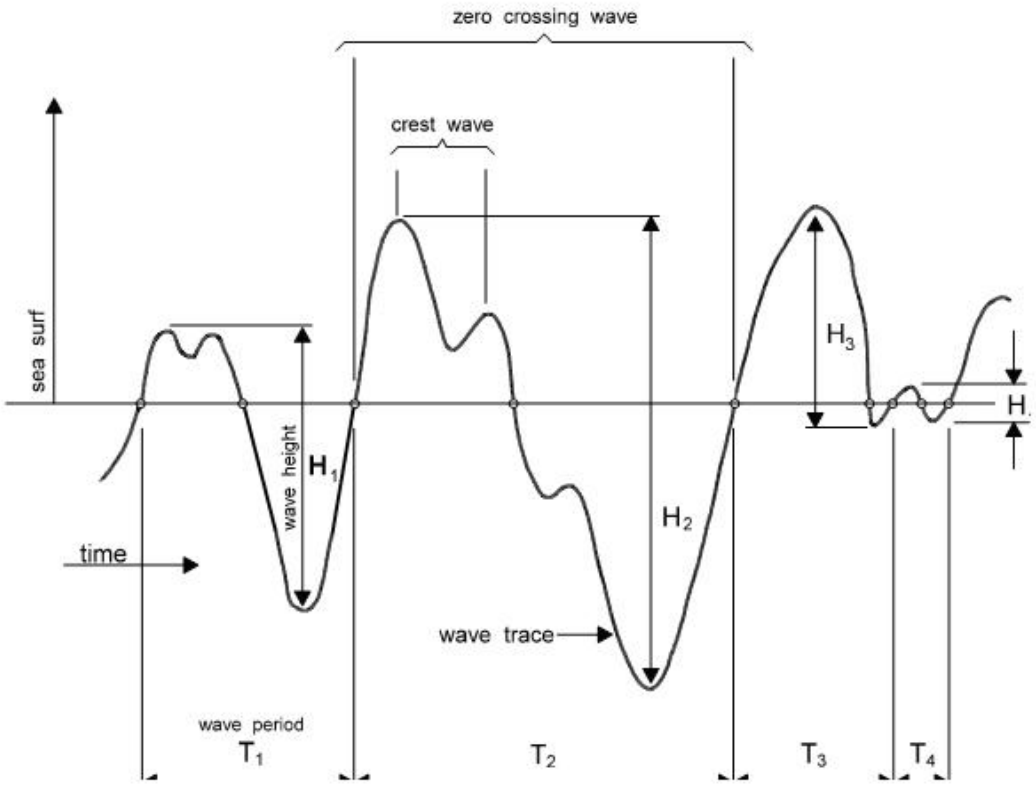

Figure B.1: Sketch of signal of a wave and its parameters (Copernicus Marine Service, sd).

In short, a wave is the elevation change of water in between two upwards (zero-up) or downwards (zero-down) crossings of the still water level (SWL). The time between these crossings is denoted with wave period T, and the wave height H is defined as the difference between the highest and lowest point of that wave.

B.1.1 Significant wave height and peak period

The significant wave height is widely used in the industry as a standard measure for wave heights of random or irregular waves. It is defined as the mean wave height of the largest one third of the measured waves, and corresponds quite well with visual estimates of irregular wave heights. The significant wave height is denoted with H_s or $H_{1/3}$ and can be expressed mathematically for a dataset with wave heights H_i ranked from highest to lowest as shown in Equation (B.1).

$$H_s = \frac{1}{\frac{N}{3}} \Sigma_{i=1}^{\frac{N}{3}} H_i \tag{B.1}$$

The significant wave height derived from a spectral analysis is based on the zero moment, which equals the area under the energy density spectrum. It is defined as shown in Equation (B.2).

$$H_{m,0} = 4\sqrt{m_0} \tag{B.2}$$

The peak period T_p or $T_{p,0}$ is the wave period associated to the respective significant wave heights and is used together with the significant wave height in calculations.

B.2 Wave attack

Next to the armour theory from Appendix A, wave theory also has an influence on the stability of armour units. How and where waves break has a significant impact on the behaviour and stability on the armour layer.

B.2.1 Breaker types

Waves can break on a slope or structure in different ways. According to Battjes (1974), five different breaker types can be distinguished, based on their Irbarren parameter ξ. The breaker types, together with their respective Irbarren parameters, are visualised in Figure B.2. The transition between breaking and non-breaking waves lies around $\xi \approx 2.5 - 3$ (Schiereck and Verhagen, 2019). The slope of a breakwater is limited by technical and economical requirements, as steeper breakwaters require less material, but shallow breakwaters are more stable. It is because of this limitation that often the major contribution to the breaker type on breakwaters is the steepness of the wave. The steepness of an individual wave ($s = \frac{H}{L}$) is limited to a maximum of 0.142 in deep water (Schiereck and Verhagen, 2019).

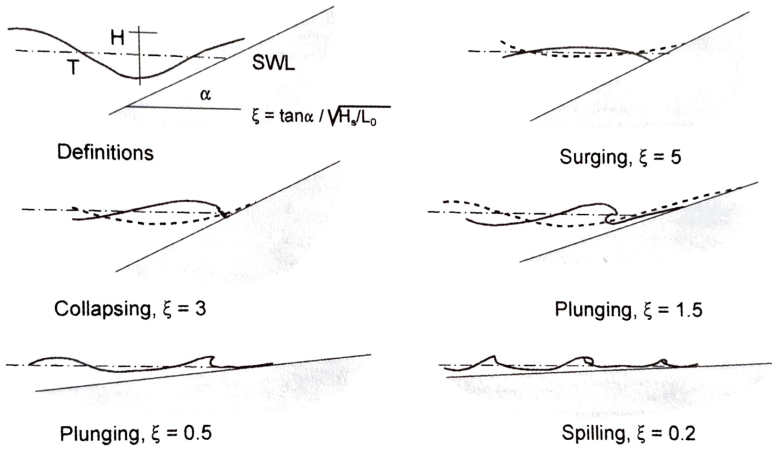

Figure B.2: Wave breaker types and their Irbarren numbers ξ (Schiereck and Verhagen, 2019).

B.2.2 Wave attack zone

For H_s in deep water, the wave steepness is about half of the value mentioned before, since H_{max} in deep water is about $2H_s$ (Schiereck and Verhagen, 2019). Most sea observations do not even exceed a steepness of 0.05 (Schiereck and Verhagen, 2019). The zone in which the maximum waves impact on the structure, the so-called wave attack zone, is therefore equal to $2H_s$, as the wave impact zone is of the same size as the maximum wave height (Schiereck and Verhagen, 2019).

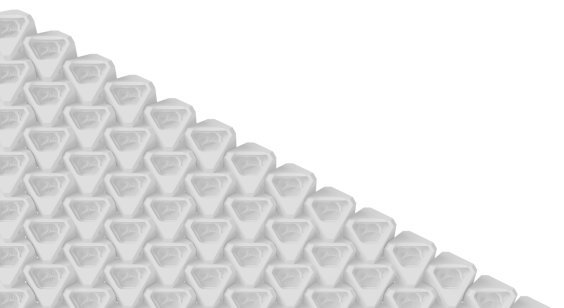

Appendix C

JONSWAP spectrum

The JONSWAP wave spectrum is a wave spectrum derived during research for the Joint North Sea Wave Project (JONSWAP) by Hasselmann et al. (1973). It is a spectrum that describes young sea states that are not fully developed and is one of the main wave spectra used worldwide for generating random realistic waves. It is an evolution on the Pierson-Moskowitz spectrum, which assumes fully developed sea states. A developed sea state is a sea state where the fetch of a constant wind is sufficiently long in order for the wind to not put any more energy into the sea state. Hasselmann et al. (1973) found that sea states are never fully developed and introduced a peak enhancement factor γ^{τ} into the Pierson-Moskowitz spectrum to create the JONSWAP spectrum. This peak enhancement factor can be varied, but is widely used with a value of 3.3, which also goes for this thesis.

A sketch of the JONSWAP and Pierson-Moskowitz spectra can be seen in Figure C.1.

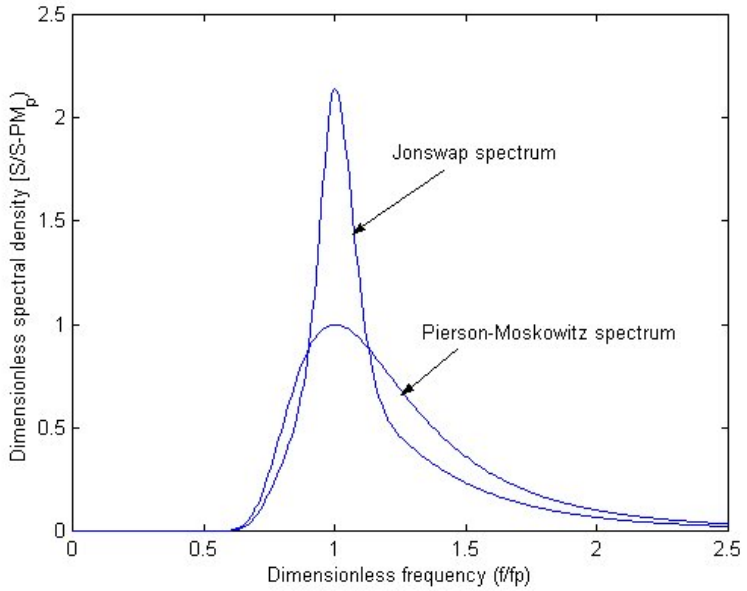

Figure C.1: The Pierson-Moskowitz and JONSWAP spectra (Abankwa et al., 2015).

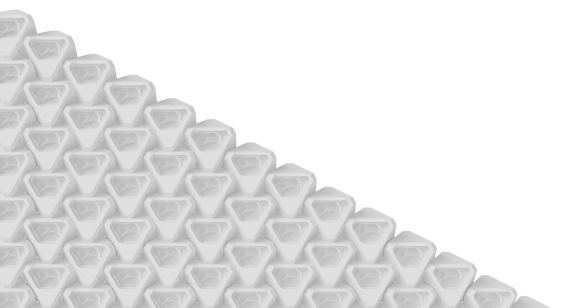

Appendix D

Scaling effects

When performing physical model tests, all objects need to be scaled properly to get reproducible results. As stated in Section 2.2.2, the strength of concrete is already something that cannot be properly scaled, and that therefore other parameters such as rocking must be monitored. Scaling, when not done properly, can cause results from physical model tests not to correspond with the prototype situation. Physical model tests need to be scaled according to geometric similarity, dynamic similarity and kinematic similarity. A correct kinematic (time scale) similarity follows from correct geometric and dynamic similarity (Wolters et al., 2009).

D.1 Geometric similarity

Keeping geometric similarity means that the length, width and height of the armour units must be kept to the same ratio as the full-scale objects. This means that all sizes and measures must be scaled by the constant scale factor λ. Therefore the dimensions in metres of the model (L_m) are defined by Equation (D.1).

$$L_m = \frac{L_p}{\lambda} \tag{D.1}$$

According to the Froude scaling laws discussed in Appendix D.2, not all units can be scaled linearly like in Equation (D.1). For example, time is scaled with a factor $\lambda^{\frac{1}{2}}$ and volume with a factor λ^3, as it consists of three length dimensions (Frostick et al., 2011).

D.2 Dynamic similarity

In order to maintain dynamic similarity, flow properties in the model must be kept the same. This means that the Froude, Reynolds, Cauchy and Weber numbers must be constant whilst scaling (Burcharth and Andersen, 2009). The numbers and their relation to the forces is displayed in Figure D.1.

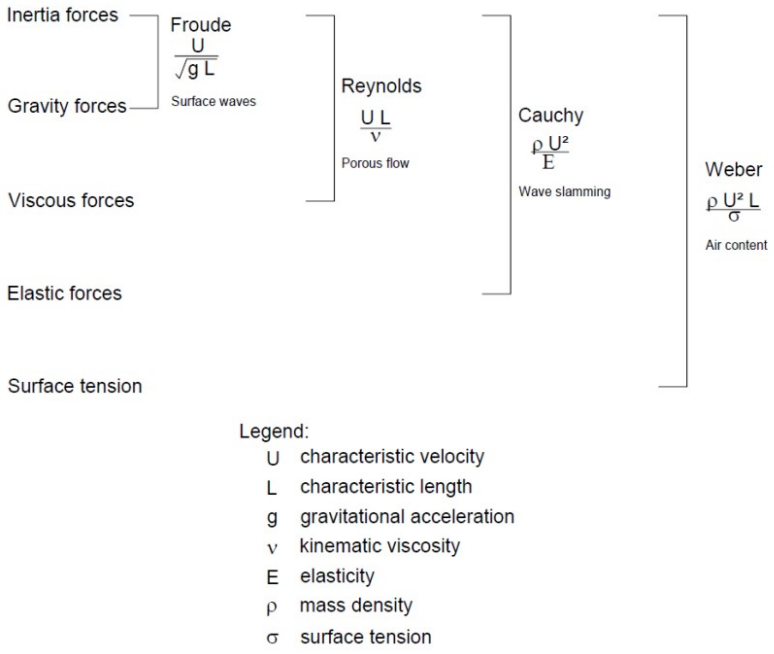

Figure D.1: Relation between flow properties and forces when scaling (Burcharth and Andersen, 2009).

As can be seen from the contradicting formulae for the Reynolds ($\frac{U \cdot L}{\nu}$) and Froude ($\frac{U}{\sqrt{g \cdot L}}$) numbers, perfect dynamic scaling is not possible. When using Froude scaling, inertia and gravity forces are correctly scaled, but errors may occur in the viscous and elastic forces and surface tension representation (Wolters et al., 2009). However, with certain limits to the Reynolds and Weber numbers, the errors become acceptable. The first limit is set on the Reynolds number, which makes sure that the flow through the primary armour layer remains turbulent (Wolters et al., 2009). This condition is displayed in Equation (D.2).

$$Re_{armour} = \frac{\sqrt{g \cdot H_s} \cdot D_n}{\nu} > 30000 \tag{D.2}$$

The second condition involves the surface tension. For very small waves, the impact of the surface tension on the wave cannot be neglected. When the Weber number meets the criteria specified in Equation (D.3), the waves are large enough to neglect surface tension effects (EurOtop, 2018).

$$h > 2cm \tag{D.3a}$$

$$H_s > 5cm \tag{D.3b}$$

$$L >> 2cm \tag{D.3c}$$

$$T > 0.35s \tag{D.3d}$$

D.3 Stability scaling

In order to obtain data from physical model testing that is applicable in the real world, the stability numbers (N_s) of both the prototype and the model should be the same. This can be achieved by keeping the relative density Δ of the model unit and prototype the same as well.

D.4 Permeability scaling

As stated in Appendix D.1, the dimensions of the breakwater material must be scaled geometrically with scale factor λ. However, this might induce problems in the filter layers or core material of the breakwater. If the core material of the prototype breakwater is permeable sand, but will be scaled to impermeable clay, the hydrodynamic conditions will still not be the same between the model and the prototype. In other words, if the filter layer or core material becomes too impermeable, the water that would otherwise flow in here will now be diverted. As a result, wave run-up height and velocity increase, which will negatively impact the stability of the armour layer (Vanneste and Troch, 2013). This phenomenon can be prevented by scaling such that the filter velocities in the model and prototype have a Froudian similarity, which will introduce similar hydraulic gradients in both cases.

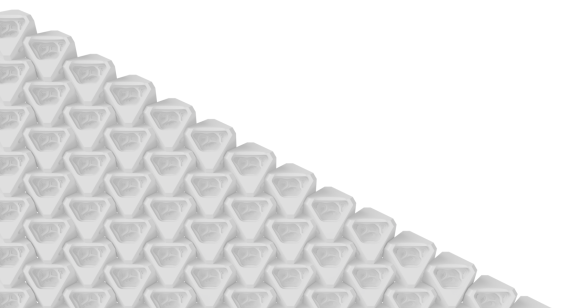

Appendix E

Construction of CoastaLock model units

The CoastaLock concrete armour units used in the tests for this thesis were constructed by hand between October and December 2021. They were produced with a scale factor $\lambda = 0.02675$ as compared to the dimensions as defined in the Technical Product Information (ECOncrete Tech Ltd., 2021). The steps to making these blocks are listed below.

E.1 Printing

The construction process started with 3D printing 10 CoastaLock units with the Ultimaker S5 Pro in the Hydraulic Engineering Laboratory of the TU Delft. The plastic used was regular PLA printing plastic with PVA supports. The blocks were removed from the printer, excess plastic was filed down with some sandpaper, and the blocks were submerged in room temperature water for 48 hours for the PVA supports to dissolve.

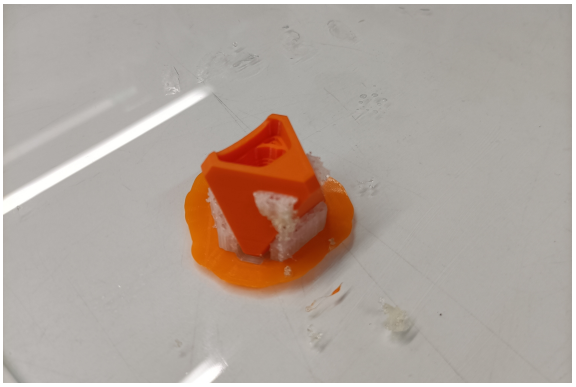

Figure E.1: 3D printed CoastaLock armour unit, right after printing with orange PLA and seethrough PVA.

E.2 Mould production

Once the plastic units had been produced, casting moulds were made out of concrete plywood. They had the internal dimensions (length by width by height) 500mm by 50mm by 40mm. A silicone mix of strength Shore 25 (medium flexible) was used to create the internal moulds.

First, the wooden moulds were filled halfway with silicone, and then the light plastic units were pushed down in the silicone. With weights on top of the plastic units floating of the units was prevented, whilst simultaneously not disturbing the silicone. Next, once the silicone had hardened over a period of 24 hours, the other half of the mould was filled with freshly mixed Shore 25 silicone, see Figure E.2a. The blocks were positioned with their cavities facing upwards to prevent any air bubbles from getting trapped in the cavities. Right after pouring the silicone, the moulds were also gently vibrated to release any excess air bubbles.

(a) After curing of the first half of silicone.

(b) After completion and removal of the units. Please note that the silicone mould has been turned upside down and that the blocks have been extracted from the bottom.

Figure E.2: Creation of silicone moulds for CoastaLock armour units.

After the entire mould had hardened, again over a period of 24 hours, the silicone was taken out of the wooden boxes, turned upside down and any excess silicone or thin silicone films were cut away. The moulds were then cut open from what previously was the bottom and the plastic armour units were removed. Whilst removing the armour units, the flexible silicone allowed for the channels through the blocks to be stretched and to easily be cut through at the centre of this canal. The silicone always returned to its original shape after this initial stretch.

The moulds were cut open from the bottom (see Figure E.2b), since the armour units were at the surface there, and now the armour units could be cast with their cavities facing downwards, again so that air bubbles would not be trapped in the casting mix and so that the silicone moulds were less prone to being damaged in the process. In total, five silicone moulds of 10 blocks were made.

E.3 Block casting

Consecutively, the units were cast into the finished silicone moulds. The casting material is Acrystal Aqua, as used before for the physical model testing of the XblocPlus crest elements by Ruwiel (2020). Acrystal Aqua is a cement and epoxy resin blend particularly designed for prolonged use in wet environments and has a density around 2275 kg/m^3 (Acrystal Matériaux Composites, sd). In order to raise this density towards the required 2330 kg/m^3, small lead weights were added into the centre of gravity of the blocks during casting. This reduces the moment of inertia of a single block, but this is considered to be negligible due to the fact that typical rubble mound behaviour like rocking or single unit failure does not occur in this thesis.

The mix was mixed using a mixer mounted to an electrical drill and once liquid enough poured into the silicone moulds, see Figure E.3a. Excess casting material was removed with a metal spoon, as shown in Figure E.3b. The moulds were then placed on a Vibro Shaper fitness vibration machine in order to allow air bubbles to escape the mix. Finally, the filled moulds resembled Figure E.3c.

(a) Pouring (b) Finishing (c) Final product

Figure E.3: Three steps out of the casting process of the CoastaLock scale model units.

E.3.1 Technical data

The mix for two moulds (20 CoastaLock units) consisted of 1050 grams of Acrystal Aqua powder, 150 grams of Acrystal Aqua liquid, around 5 millilitres of Colorex mixing colours (either blue or yellow) and anywhere between 15ml to 25ml of water in order to achieve the desired viscosity of the mix. Per unit 6 grams of lead was used.

The blocks were measured to have a nominal density ρ_{cl} of 2299.44 kg/m^3, which leads to a slightly more conservative but still realistic estimate to the behaviour of prototype CoastaLock blocks. The standard deviation σ of the block weight is 1.53 grams and the standard deviation of the volume is 0.35 millilitres. The standard deviation of the final density is 61.61 kg/m^3.

E.4 Curing

After casting, the moulds were covered and placed in a room temperature environment for 24 hours. After this, the blocks were removed from the moulds and cured in room temperature water for 72 hours. Finally, they were washed and ready for use in the physical model tests executed for this thesis. A picture of the first finished batch of CoastaLock model units is shown in Figure E.4.

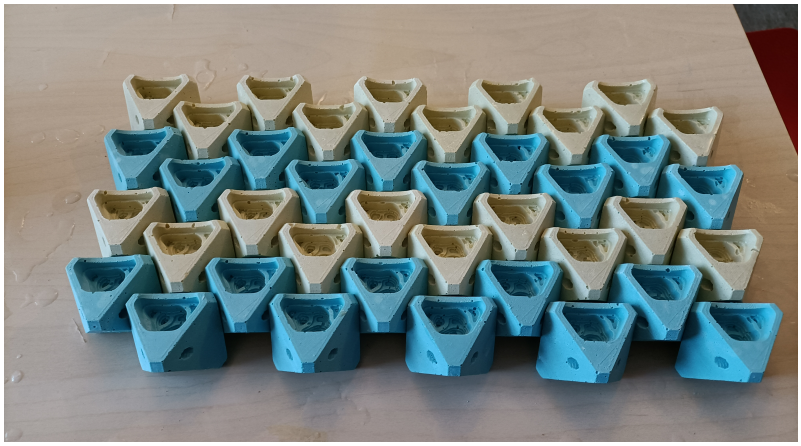

Figure E.4: The first batch of finished CoastaLock model concrete armour units, right after curing.

Appendix F

Theoretical relation between leakage length and stability

This section shows the derivation from the second order differential equation for the pressure differences over the top layer to an expression for those based on the leakage length, as referred to from Section 6.3.1.

F.1 Derivation of expression for pressure difference

According to Schiereck and Verhagen (2019), the pressure differences over the armour layer of a breakwater can be expressed as show in Equation (F.1).

$$\phi_F - \phi_T = \Lambda^2 \frac{d^2\phi_F}{dx^2} \tag{F.1}$$

It can then be rewritten as:

$$\frac{d^2\phi_F}{dx^2} - \phi_F = -\phi_T \tag{F.2}$$

Homogeneous solution
For the homogeneous solution to this equation, the assumption is made that $\phi_{F,hom} = e^{rx}$ in Equation (F.2). It then follows that:

$$\begin{aligned} r^2\ e^{rx}\ \Lambda^2 - e^{rx} &= 0 \\ e^{rx}\ (r^2\Lambda^2 - 1) &= 0 \\ r^2\Lambda^2 &= 1 \\ r^2 &= \frac{1}{\Lambda^2} \end{aligned}$$

And therefore:

$$r = \pm\frac{1}{\Lambda}, \quad \text{for} \quad \Lambda > 0 \quad \wedge \quad \Lambda \in \mathbb{R} \tag{F.3}$$

Inhomogeneous solution
For the inhomogeneous solution to this equation, the assumption is made that $\phi_{F,inhom} = C$ in Equation (F.2). It then follows that:

$$-C = -\phi_T$$
$$C = \phi_T$$

General solution
The total solution for Equation (F.2) then becomes Equation (F.4).

$$\phi_F = Ae^{\frac{x}{\Lambda}} + Be^{-\frac{x}{\Lambda}} + \phi_T \tag{F.4}$$

The general solution for pressure differences over the top layer can then be described according to Equation (F.5).

$$\phi_F - \phi_T = Ae^{\frac{x}{\Lambda}} + Be^{-\frac{x}{\Lambda}} \tag{F.5}$$

For $x \geq 0$
When solving for $x = \infty$, $\phi_F - \phi_T = 0$:

$$0 = Ae^{\frac{\infty}{\Lambda}} + Be^{-\frac{\infty}{\Lambda}}$$
$$0 = Ae^{\infty}$$

So therefore $A = 0$ and:

$$\phi_F - \phi_T = Be^{-\frac{x}{\Lambda}} \tag{F.6}$$

When solving for $x = 0$, $\phi_F - \phi_T = \frac{1}{2}H_{max} = H_s$:

$$H_s = Be^{-\frac{0}{\Lambda}}$$
$$H_s = Be^{0}$$

And therefore $B = H_s$ and the final relation for the pressure differential for $x \geq 0$ becomes:

$$\phi_F - \phi_T = H_s\, e^{-\frac{x}{\Lambda}} \tag{F.7}$$

Appendix G

Example of DASYlab file

The first two seconds of `010.ASC`.

```
DASYLab - V 13.00.00
Worksheet name:  Auke
Recording date      :  17-1-2022, 13:46:34
Block length        :  4
Delta               :  0.1 sec.
Number of channels  :  7
Measurement time[s];Write 0 [V];Write 1 [V];Write 2 [V];Write 3 [V];Write
4 [V];Write 5 [V];Write 6 [V];
0.0;0.33;-0.43;-0.49;-0.43;-0.14;-0.74;0.34;
0.1;0.33;-0.44;-0.48;-0.39;-0.17;-0.73;0.34;
0.2;0.28;-0.44;-0.50;-0.33;-0.16;-0.71;0.33;
0.3;0.23;-0.44;-0.52;-0.33;-0.16;-0.71;0.33;
0.4;0.24;-0.45;-0.54;-0.33;-0.16;-0.72;0.34;
0.5;0.26;-0.47;-0.55;-0.35;-0.15;-0.74;0.35;
0.6;0.29;-0.47;-0.55;-0.38;-0.15;-0.74;0.34;
0.7;0.31;-0.44;-0.52;-0.41;-0.15;-0.72;0.33;
0.8;0.32;-0.41;-0.49;-0.39;-0.15;-0.70;0.34;
0.9;0.30;-0.42;-0.51;-0.32;-0.16;-0.71;0.36;
1.0;0.27;-0.46;-0.55;-0.30;-0.16;-0.73;0.35;
1.1;0.25;-0.49;-0.57;-0.35;-0.15;-0.72;0.34;
1.2;0.26;-0.49;-0.54;-0.39;-0.16;-0.72;0.34;
1.3;0.27;-0.46;-0.49;-0.40;-0.16;-0.75;0.34;
1.4;0.28;-0.43;-0.50;-0.38;-0.15;-0.73;0.34;
1.5;0.28;-0.40;-0.53;-0.34;-0.14;-0.70;0.33;
1.6;0.27;-0.40;-0.53;-0.31;-0.16;-0.71;0.32;
1.7;0.27;-0.44;-0.51;-0.34;-0.18;-0.74;0.33;
1.8;0.29;-0.49;-0.49;-0.38;-0.15;-0.74;0.35;
1.9;0.31;-0.51;-0.53;-0.40;-0.12;-0.72;0.35;
```

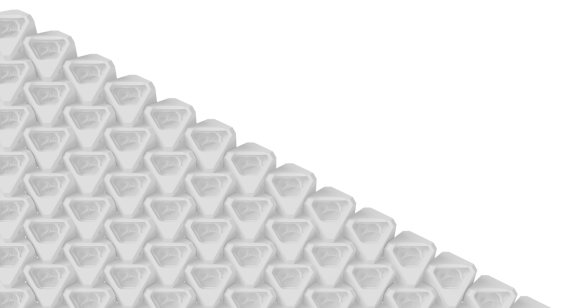

Appendix H

Python script used for DASYlab file conversion

```
# -*- coding:  utf-8 -*-
from datetime import date
import os


print('DASYlab file conversion')
print('MSc thesis')
print('Auke Molenkamp')
print('4548000')
print(date.today().strftime("%d-%m-%Y"))
print('\n')


### Open and list filenames ###
files = os.listdir('H:\\Wave gauge data\\raw data')
files.sort()


### Replace commas, replace unit of time, place comma back after year ###
for l in range(len(files)):
    with open('H:\\Wave gauge data\\raw data\\'+str(files[l]), 'r')
    as f:
        filedata = f.read()


    filedata = filedata.replace(',', '.')
    filedata = filedata.replace('[hh:mm:ss]', '[s]')
    filedata = filedata.replace('2022.', '2022,')


    k = -1
```

```
### Calculate time values in seconds and rewrite time column ###
    for i in range(45):
        for j in range(60):
            k = k+1
            if i < 10:
                if j < 10:
                    filedata = filedata.replace('00:0'+str(i)+':0'+str(j),str(k))
                elif j >=10:
                    filedata = filedata.replace('00:0'+str(i)+':'+str(j),str(k))
            elif i >= 10:
                if j < 10:
                    filedata = filedata.replace('00:'+str(i)+':0'+str(j),str(k))
                elif j >=10:
                    filedata = filedata.replace('00:'+str(i)+':'+str(j),str(k))


    ascii = filedata.encode('ascii')


    with open('H:\\Wave gauge data\\converted data\\'+str(files[l]), 'wb')
    as f:
        f.write(ascii)
```

Appendix I

Template parameter files for decomp.m

Template parameter file for wave gauge set 1 (.txt)

```
time step used in data file
0.1
Tp (s),  f-resol/Tp  fmin (Hz),  fmax (Hz),  thresh
1.06,    0.025,      0.25,       -1,         0.01
column with time (0 if none)
1
columno gauge,  pos (m),  scale fact to m
2,              0,        0.021287
3,              0.5,      0.020716
4,              0.75      0.021069
```

Template parameter file for wave gauge set 2 (.txt)

```
time step used in data file
0.1
Tp (s),  f-resol/Tp  fmin (Hz),  fmax (Hz),  thresh
1.06,    0.025,      0.25,       -1,         0.01
column with time (0 if none)
1
columno gauge,  pos (m),  scale fact to m
2,              0,        0.021413
3,              0.5,      0.025203
4,              0.75      0.025206
```

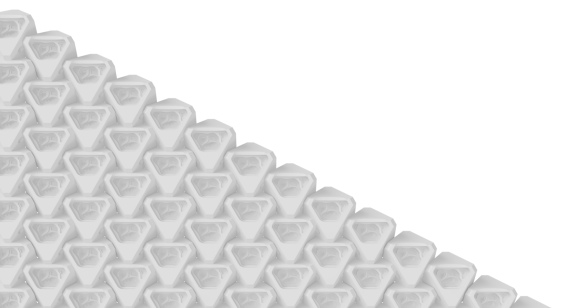

Appendix J

Python script for creating parameter files

```
# -*- coding:  utf-8 -*-
from datetime import date
import os


print('Parameter file creation')
print('MSc thesis')
print('Auke Molenkamp')
print('4548000')
print(date.today().strftime("%d-%m-%Y"))
print('\n')

### Open filenames and sort them ###
testlist = os.listdir('H:\\Wave gauge data\\raw data')

for i in range(len(testlist)):
    testlist[i] = testlist[i].removesuffix('.ASC')

testlist.sort()


### Create array with all wave periods per test ###
T01 = [1.06, 1.13, 1.20, 1.27, 1.33]
T02 = [0.89, 1.23, 1.27]
T03 = [0.98, 1.27, 1.33, 1.39, 1.44, 1.52, 1.60, 1.67, 1.74]
T04 = [0.98, 1.74]
T05 = [0.98, 1.20, 1.27]
T06 = [0.89, 1.20, 1.23]
T07 = [0.89, 0.92, 0.98, 1.03, 1.08, 1.13]
T08 = [0.89, 1.06, 1.08]
T09 = [0.89, 1.50, 1.60, 1.70]
T10 = [0.89, 1.06, 1.13, 1.20, 1.27, 1.33]
```

```
T11 = [0.89, 1.13, 1.20, 1.27, 1.33, 1.39, 1.44, 1.52, 1.60]
T12 = [1.67, 1.74]
T13 = [0.89, 1.20, 1.27, 1.33, 1.39, 1.44, 1.52, 1.60, 1.67, 1.74]
T14 = [0.89, 1.20, 1.27, 1.33, 1.39, 1.44, 1.52, 1.60, 1.67, 1.74]
T15 = [0.89, 1.20, 1.27, 1.33, 1.39, 1.44, 1.52, 1.60, 1.67, 1.74]
T16 = [0.89, 1.06, 1.13, 1.20]
T17 = [0.89, 1.06, 1.13, 1.20]
T18 = [0.89, 1.20, 1.27, 1.33, 1.39, 1.44]
T19 = [0.89, 1.06, 1.13, 1.20, 1.27]
T20 = [0.89, 1.06, 1.13, 1.20, 1.27]
T21 = [0.89, 1.06, 1.13, 1.20, 1.27, 1.33, 1.39, 1.44, 1.52]
T22 = [0.89, 1.13, 1.22, 1.31, 1.39]
T23 = [1.79, 1.88, 1.96, 2.04, 2.15, 2.26, 2.37]
T24 = [0.89, 1.01, 1.07, 1.13, 1.19]

Tps = T01 + T02 + T03 + T04 + T05 + T06 + T07 + T08 + T09 + T10 + T11 +
T12 + T13 + T14 + T15 + T16 + T17 + T18 + T19 + T20 + T21 + T22 + T23 +
T24

### Check if the number of wave periods matches the number of files ###
if len(Tps) > len(testlist):      excess = len(Tps) - len(testlist)
    print(excess, 'wave periods too many!')
elif len(Tps) < len(testlist):
    shortage = len(testlist) - len(Tps)
    print(shortage, 'wave periods short!')


### Generate the parameter files with the right data ###
with open('H:\\Wave gauge data\\converted data\\template_parameter1.txt',
'r') as f:
    template = f.read()

template = template.replace('1.06', str(Tps[0]))
with open('H:\\Wave gauge data\\converted data\\'+str(testlist[0])
+'_parameter1.txt', 'w') as f:
    f.write(template)

for i in range(1, len(Tps)):
    template = template.replace(str(Tps[i-1]), str(Tps[i]))
    with open('H:\\Wave gauge data\\converted data\\'+str(testlist[i])
    +'_parameter1.txt', 'w') as f:
        f.write(template)

with open('H:\\Wave gauge data\\converted data\\template_parameter2.txt',
'r') as f:
    template = f.read()
```

```
template = template.replace('1.06', str(Tps[0]))
with open('H:\\Wave gauge data\\converted data\\'+str(testlist[0])
+'_parameter2.txt', 'w') as f:
    f.write(template)

for i in range(1, len(Tps)):
    template = template.replace(str(Tps[i-1]), str(Tps[i]))
    with open('H:\\Wave gauge data\\converted data\\'+str(testlist[i])
    +'_parameter2.txt', 'w') as f:
        f.write(template)
```

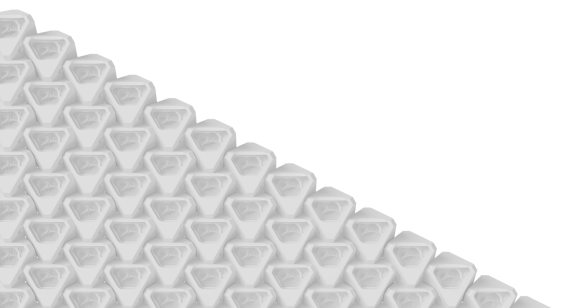

Appendix K

Python script for data collection after decomposition

```
# -*- coding:  utf-8 -*-
from datetime import date
import os
import csv
import numpy as np

print('Compile decompresults into .csv')
print('MSc thesis')
print('Auke Molenkamp')
print('4548000')
print(date.today().strftime("%d-%m-%Y"))
print('\n')

### Open output files and sort them ###
files = os.listdir('C:\\Users\\aukem\\Desktop\\Wave gauge maths\\results')
files.sort()

### Create header of results.csv ###
header = ['Test', 'Hm0 incident 1 [m]', 'Hm0 reflected 1 [m]', 'Coeff.
refl.  1', 'Tpmean 1', 'Hm0 incident 2 [m]', 'Hm0 reflected 2 [m]', 'Coeff.
refl.  2', 'Tpmean2']
data = np.empty((0, len(header)))

### Check if an even number of files has been processed ###
if (len(files) % 2) != 0:
    print('No even number of files')

### Extract required data from the output files ###
for i in range(len(files)):
    with open('C:\\Users\\aukem\\Desktop\\Wave gauge maths\\results\\
    '+str(files[i]), 'r') as f:
        waveheights = f.readlines()[-4:-2]
```

```
    with open('C:\\Users\\aukem\\Desktop\\Wave gauge maths\\results\\
    '+str(files[i]), 'r') as f:
        inputfile = f.readlines()[4]

    with open('C:\\Users\\aukem\\Desktop\\Wave gauge maths\\results\\
    '+str(files[i]), 'r') as f:
        Tp = f.readlines()[-18:-16]

    Tps = [0,0]
    Tps[0] = float(Tp[0][-8:-2])
    Tps[1] = float(Tp[1][-8:-2])

### Check if the right input files have been opened ###
    if inputfile[12:15] != files[i][0:3]:
        print('ERROR: input file not corresponding with output file name
    in', files[i][0:4])

### Generate lines of results.csv ###
    if (i % 2) == 0:
        a = float(waveheights[0][-10:-3])
        b = float(waveheights[1][-10:-3])
        c = round(b/a, 5)
        d = np.mean(Tps)
        nextline = np.array([[files[i][0:3], a, b, c, d]])

    if (i % 2) != 0:
        a = float(waveheights[0][-10:-3])
        b = float(waveheights[1][-10:-3])
        c = round(b/a, 5)
        d = np.mean(Tps)
        nextline = np.append(nextline, [a, b, c, d])
        data = np.append(data, [nextline], axis=0)
        if nextline[1] == nextline[5] and nextline[2] == nextline[6]:
            print('ERROR: two identical outputs in', nextline[0])

### Write results.csv ###
with open('results.csv', 'w', encoding='UTF8', newline='') as f:
    writer = csv.writer(f)
    writer.writerow(header)
    writer.writerows(data)
```


TU Delft
Auke Molenkamp
ECONCRETE